Received: 7 January 2021 | Revised: 9 February 2021 | Accepted: 10 February 2021

DOI: 10.1002/ntls.10005

Natural Sciences

REVIEW

Chemical dynamics from the gas-phase to surfaces

Daniel J. Auerbach[1,2] | **John C. Tully**[3] | **Alec M. Wodtke**[1,2]

[1] Institut für physikalische Chemie, Georg-August Universität Göttingen, Göttingen, Germany

[2] Abteilung für Dynamik an Oberflächen, Max-Planck-Institut für biophysikalische Chemie, Göttingen, Germany

[3] Department of Chemistry, Yale University, New Haven, Connecticut, USA

Correspondence
Alec M. Wodtke, Institute for Physical Chemistry, University of Göttingen, Tammannstr. 6, 37077 Göttingen, Germany.
Email: alec.wodtke@mpibpc.mpg.de

This Review has elicited Commentaries https://doi.org/10.1002/ntls.10006 and https://doi.org/10.1002/ntls.10007

[Correction added on 25 June 2021, after publication in Early View: permission statements have been added to the captions of all relevant figures.]

Abstract: The field of gas-phase chemical dynamics has developed superb experimental methods to probe the detailed outcome of gas-phase chemical reactions. These experiments inspired and benchmarked first principles dynamics simulations giving access to an atomic scale picture of the motions that underlie these reactions. This fruitful interplay of experiment and theory is the essence of a *dynamical approach* perfected on gas-phase reactions, the culmination of which is a standard model of chemical reactivity involving classical trajectories or quantum wave packets moving on a Born–Oppenheimer potential energy surface. Extending the dynamical approach to chemical reactions at surfaces presents challenges of complexity not found in gas-phase study as reactive processes often involve multiple steps, such as inelastic molecule-surface scattering and dissipation, leading to adsorption and subsequent thermal desorption and or bond breaking and making. This paper reviews progress toward understanding the elementary processes involved in surface chemistry using the dynamical approach.

Key points:

- The fruitful interplay between chemistry and physics leads to an atomic scale view of reactions taking places at catalytically active surfaces.
- Improved observations of chemical reactions taking place in complex environments drive the development of new approaches to theoretical chemistry.
- Complex reaction networks from real catalysts are boiled down to their elementary steps and examined from first principles.

KEYWORDS
dynamics, catalysis, graphene, lasers, surface science

GLOSSARY OF ACRONYMS AND ABBREVIATIONS: AIMD, *ab initio* molecular dynamics; DFT, density function theory; EHP, electron–hole pair; EMT, effective medium theory; ER, Eley–Rideal; FGR, Fermi golden rule; GGA, generalized gradient approximation; HDNN, high-dimensional neural network; IESH, independent electron surface hopping; LIF, laser-induced fluorescence; LDFA, local-density friction approximation; LH, Langmuir–Hinshelwood; MBRS, molecular beam relaxation spectrometry; MDEF, molecular dynamics with electron friction; ML, monolayer; ODF, orbital-dependent friction; PES, potential energy surface; QBS, quantum bottleneck states; QCT, quasi-classical trajectories; RAIRS, reflection/absorption infrared spectroscopy; REMPI, resonance-enhanced multiphoton ionization; SEP, stimulated emission pumping; SRP, specific reaction parameter; TOF, time-of-flight; TST, transition state theory; UHV, ultrahigh vacuum

Many of the individual topics of gas phase and surface chemical dynamics addressed by this paper have been treated in Nobel lectures,[1–5] *reviewed previously*[6–23] *or discussed in excellent book by leaders in these fields.*[24–28] *In this paper, we stress the linkages between gas phase and surface chemical dynamics, emphasizing the development, application, and extension of experimental and theoretical methods, first developed for gas-phase problems that have led to improved understanding of surface chemistry via a fruitful interplay of theory and experiment. An aim of this paper is to enable those working in gas-phase chemical dynamics to make the jump to*

problems in surface chemistry, which may often seem impenetrably complex and challenging.

THE ORIGINS OF CHEMICAL DYNAMICS

Seeds leading to the emergence of the field of chemical dynamics were clearly sown during the whirlwind of progress ushered in by the discovery of quantum mechanics,[29] which stirred the pot of physical chemistry with the prospect for a vastly improved understanding of microscopic objects. In 1928, the then dominant journal of physical chemistry, *Zeitschrift für physikalische Chemie*, split into two. The editors declared their intent to foster the research energy of physics and chemistry necessary to solve the difficult interdisciplinary problems posed by *der Chemie Der Elementarprozesse Aufbau Der Materie (the chemistry of elementary processes and the structure of matter*), the name of the new journal. In what would become a defining aspect of chemical dynamics, the editors ardently sought contributions from theoretical physicists. And the physicists were eager to contribute.

Dirac set the tone in a seminal paper declaring that "…the underlying physical laws necessary for the mathematical theory of… …the whole of chemistry are thus completely known."[30] He emphasized that "approximate practical methods of applying quantum mechanics should be developed" as the fundamental equations were too difficult to solve. Born and Oppenheimer successfully reduced the molecular Schrödinger equation to a nuclear wave equation governed by an effective electronic potential,[31] the potential energy surface (PES). This set the stage for Henry Eyring and Michael Polanyi in 1931 to produce the first PES for a chemical reaction[32,33]—see Figure 1. Theoretical chemistry was well underway as a burgeoning field reaching perhaps its most important milestone, the so-called absolute theory of reaction rates.[34] Chemists now had not only the mathematical theory of chemistry, but in addition, new chemical concepts—for example, *PESs and transition states*—defined in terms of fundamental physics.

Despite this profound conceptual progress, a cloud hung over this field for decades to come, as only limited means existed to test the approximations introduced by theorists, tests that would be needed to prove that the theories had practical value. By 1933, the *Journal of Chemical Physics* (JCP) had published its first issue and, reflecting the tentative nature of the young field, its first editor Harold Urey wrote, "…The methods of investigation used are, to a large extent, not those of classical chemistry and the field is not of primary interest to the main body of physicists…".[35] The fact was that methods of experimental verification and numerical simulation lagged dramatically behind the conceptual breakthroughs of the quantum era. This was to change soon and JCP would become the vanguard forum showing the successes of converging the methods of physics with problems of chemistry.

THE EXPERIMENTAL BASIS FOR MODERN CHEMICAL DYNAMICS

The second half of the 20th century witnessed a revolution for the atomic scale viewpoint of chemistry, as molecular spectroscopy,[36] the laser,[37,38] molecular beams,[39] and high-power computing[40] established themselves as critical tools for probing molecular motions.

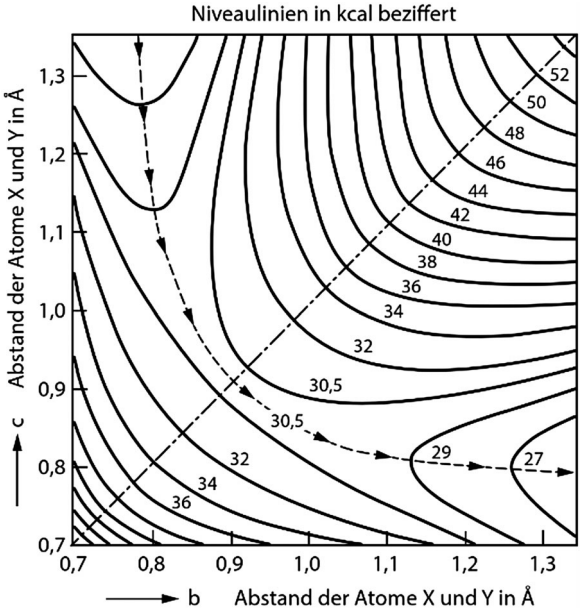

FIGURE 1 The first potential energy surface ever calculated for a simplified chemical reaction: the H-exchange reaction occurring along a line: $H_a + H_bH_c \rightarrow H_aH_b + H_c$. In the figure, the x-axis is the distance between H_b and H_c, while the y-axis is the distance between H_a and H_b. The contour lines represent equipotentials with energies denoted in kcal/mol. The reaction proceeds from upper left to bottom right along a reaction path (dashed arrow). The saddle point reached at about 30.25 kcal/mole is the reaction's transition state.[32] Reprinted from Eyring H, Polanyi M. Concerning simple gas reactions. Z Phys Chem B-Chem Elem Aufbau Mater. 1931;12(4):279-311, Copyright 2021, with permission from De Gruyter

Infrared emission spectroscopy

Even before masers[37] and lasers[38] introduced the concept of a population inversion, scientists had evidence of molecules in the atmosphere and in the laboratory with quantum state population distributions far from thermal equilibrium, a glittering signpost for the importance of dynamical processes. Emission spectra from the night sky which could be recorded on photographic plates showed OH(v =6–9)[41]—the same spectra were seen using flash photolysis[36] to drive the reaction $H + O_3 \rightarrow OH(v) + O_2$.[42] Similar methods revealed reactions that produced highly vibrationally excited O_2[43,44] and N_2.[45] This field accelerated dramatically with the advent of infrared chemiluminescence,[4] which revealed vibrationally excited HCl produced in the reaction of $H+Cl_2$.[46]

New dynamical concepts also emerged, notably the "Polanyi Rules"—see Figure 2. These state that for exothermic reactions, an energy barrier located early along the reaction path will preferentially produce vibrationally excited products, whereas a late barrier will likely lead to higher product translational energy and require reactant vibration to proceed efficiently.[4,48] Work in this direction also led to clear ideas about how chemical reactions can produce population inversions and a prediction that a chemical laser could work based on a "partial" population inversion.[49] This prediction was realized only a few years later, exploiting the $H + Cl_2 \rightarrow Cl + HCl(v > 0)$ reaction to produce a vibrational population inversion.[47]

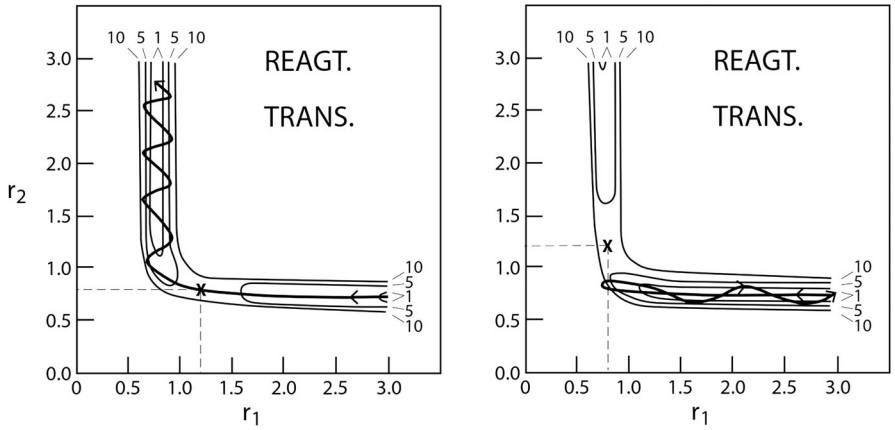

FIGURE 2 The (John) Polanyi Rules: The reaction $H + Cl_2 \rightarrow Cl + HCl(v > 0)$ produces vibrationally hot HCl, which emits in the infrared. In fact, this reaction formed the basis of the first chemical laser.[47] The PES on the left exhibits an early transition state; one that resembles the $H + Cl_2$ reactants, where r_1 would represent the H–Cl distance and r_2 the Cl–Cl distance. Reagent translation allows efficient access to the transition state, where a large energy release occurs before the HCl bond is fully formed, snapping the two atoms together and producing HCl vibrational excitation with a bobsled-like trajectory. The late barrier shown on the right requires reagent vibration to be efficient—with reagent translation, the reaction fails as shown.[4,48] Equipotential lines are shown with their energy values in kcal/mol. Reprinted from Polanyi JC. Some concepts in reaction dynamics. Acc Chem Res. 1972;5(5):161, Copyright 2021, with permission from ACS Publications

Laser-induced fluorescence and resonance-enhanced multiphoton ionization

The inventor of the ruby laser[38] once described the laser as "a solution seeking a problem."[50] Chemical dynamics had the problems! Due to the ease of constructing gas discharges, c. w. and pulsed "line tunable" lasers using He, Ne,[51,52] Ar or Kr,[53] and N_2/CO_2[54,55] were the first sources of laser light used in this field. Their application quickly led to a new technique that marked a sea change in chemical dynamics, laser-induced fluorescence (LIF).[56] This technique enabled quantum-state resolved studies that quickly became a major focus of experimentalists. While LIF was first detected as spontaneous infrared emission produced after infrared laser excitation,[57–59] its true potential became evident only after a HeNe-laser was used to excite K_2 and this molecule's emission spectrum was photographically recorded behind the Berkeley 21-foot concave grating.[60] Soon after, LIF was detected by a photomultiplier[61] and lifetimes of excited electronic states were derived with a phase shift method.[62] By observing LIF while tuning a dye laser,[63,64] background-free laser excitation spectra were demonstrated—this method was so sensitive that it could be exploited to probe the internal state distribution of reaction products[65] and later even to obtain state-resolved angular distributions of reaction products.[66,67]

The pulsed ruby laser provided such high peak powers that multiphoton ionization of atoms[68–70] could be demonstrated including resonance enhancement.[71] Applied first to molecules as a 1+1 resonance enhanced multiphoton neutralization of a 1-keV beam of C_2^-, a spectrum was obtained by detecting neutral C_2 as a function of the laser wavelength.[72] Resonance enhanced multiphoton ionization (REMPI) was first demonstrated using Cs_2.[73] Soon thereafter, the 3+1 REMPI spectrum of NO[74] and the 2+1 REMPI spectrum of I_2[75] were reported followed by REMPI spectra of larger polyatomics.[76,77]

Molecular beams

Molecular beams became another vital piece of the experimental tool-box of chemical dynamics—the high-energy physicists' scattering experiments using charged particles and accelerators were being transitioned to the study of ion–molecule[79,80] and even molecule–molecule[39] reactions at low, chemically relevant energies. Reactions could now be studied by crossed molecular beams methods.[81] Figure 3 shows an instrument that detects reaction products resulting from the collisions between molecules in two different beams. The densities of the two beams ensured that within the crossing volume of the beams, at most, one collision could occur and the products could escape collision free.

The data observed with this instrument provided the product flux–map in the center-of-mass frame of the reacting molecules. Figure 4 shows an experimentally derived flux map for the $F + H_2 \rightarrow HF(v) + H$ reaction.[82] Several vibrational states of HF could be resolved and their flux-maps obtained. Experimental observations like these provided attractive targets for the developing field of theoretical chemical dynamics.

Applying external electric fields to polar molecules in low J-states produced molecular beams of oriented molecules and observations of steric effects in chemistry.[83] Using pulsed electric fields, deceleration of molecular beams also proved possible,[84,85] improving our ability to study quantum effects in collisions between molecules.[86] But REMPI detection in combination with the power of molecular beams proved pivotal,[87] setting the stage for what was to become one of the most important tools for chemical reaction dynamics, ion imaging.[88]

Ion imaging

Ion imaging became possible by applying REMPI to reaction products and detecting them with position sensitive (electron multiplier

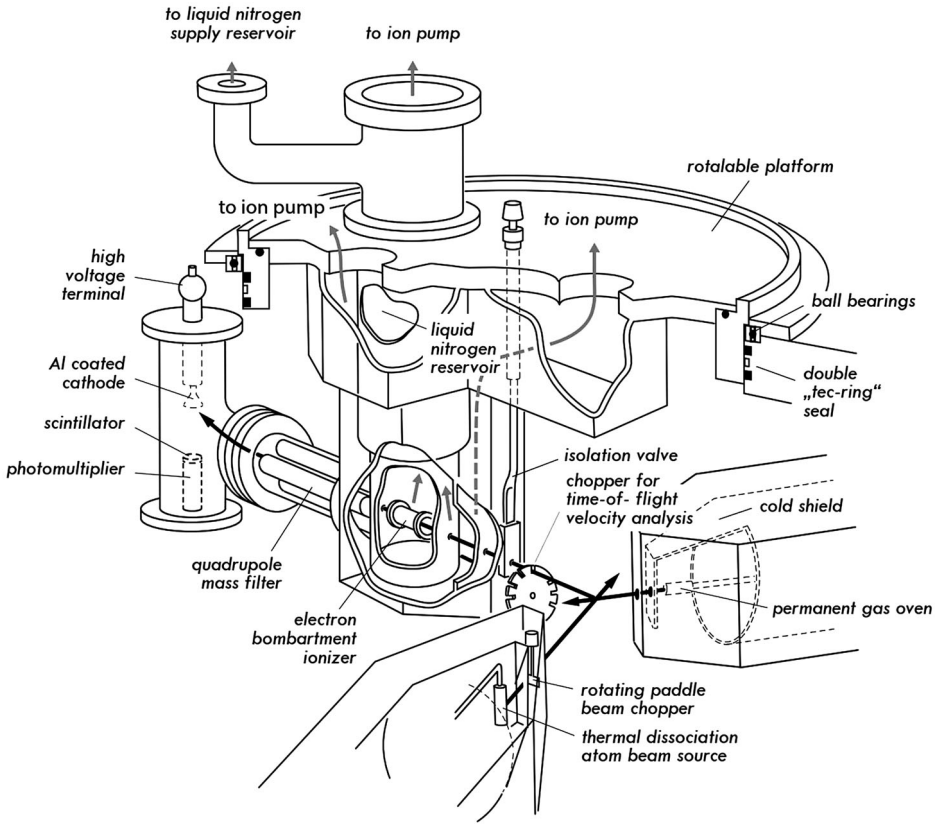

FIGURE 3 The universal crossed molecular beam machine––nicknamed "Hope." The reaction $H + Cl_2 \rightarrow Cl + HCl(v)$ [2,3,78] as well as many others was observed under "single collision conditions" with this instrument. Laboratory frame scattering data yield the center-of-mass frame product flux-map. See Figure 4. The use of electron bombardment ionization with quadrupole mass spectrometry made product detection "universal," opening the field to the diversity of phenomena that defines chemistry. Reprinted from McDonald JD, Lebreton PR, Lee YT, Herschbach DR. Molecular Beam Kinetics: reactions of deuterium atoms with halogen molecules. J Chem Phys. 1972;56(2):769-788, Copyright 2021, with permission from the AIP Publishing

like) detectors. Ion imaging is a method that provides sensitivity to product angular and speed distributions that had previously only been possible using molecular beam machines with rotating mass spectrometers. It not only represented a dramatic simplification over the universal crossed molecular beam machine, it provided entirely new capability. The method was quickly applied to both products of photodissociation[89] as well as bimolecular reactions[90,91] and became even more attractive when velocity map imaging[92] demonstrated that speed and angular distributions could be obtained with high resolution. In its initial incarnations, analyzing ion images required that the plane of the ion camera be parallel to a cylindrical symmetry axis of the three-dimensional product distribution, a requirement that is often difficult to fulfill. With the advent of "slice imaging" in 2001,[93] this requirement was relaxed and has over time become the method of choice for problems in chemical dynamics.[94,95]

COMPUTATION COMPLETES THE DYNAMICAL APPROACH

With these new experimental tools, exquisite observations of elementary chemical reactions became available,[96] but it was only with the advent of high power computing that the field could reach its potential, as cooperation between experiment and theory became increasingly valuable.

The extraordinary growth in the capabilities of computers has thoroughly transformed theoretical chemistry; however, the development of efficient and accurate algorithms has been at least as important. The calculation of PESs has evolved from empirical and semi-empirical models, to Hartree–Fock theory,[97] to wavefunction-based methods that include electron–electron correlation, such as valence-bond,[98] Møller–Plesset perturbation,[99] coupled-cluster,[100] and configuration interaction theories.[101] In parallel, density functional theory (DFT)[102] has emerged within a "sweet spot," balancing accuracy with affordability for larger molecular systems. Machine learning algorithms now provide efficient and accurate fitting of high-dimensional PESs to *ab initio* energies.[103]

Methods for tracing out the atomic motions governed by PESs have also advanced, from classical mechanics,[104,105] to time-independent quantum scattering theory,[106,107] to time-dependent wave-packet motion.[108,109] Classical mechanics remains the workhorse, especially on-the-fly methods that compute the classical forces as the trajectory proceeds, usually by DFT.[110] The design of algorithms has adapted to hardware advances like parallel computing and the use of graphical processing units as computational engines.[111] Widely available

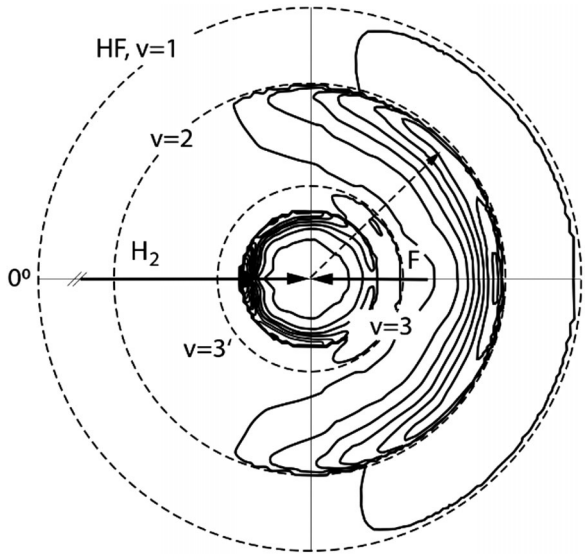

FIGURE 4 The product flux map in the center of mass frame for the $F + H_2 \rightarrow HF(v) + H$ reaction. The contour plot reflects the probability for product HF to appear with a specific velocity vector (e.g., dashed arrow). The velocity vectors of the reactants are also shown as vectors, labeled F and H_2. The dashed line of smallest radius produces $HF(v = 3)$ from both $F(^2P_{3/2})$—mainly forward scattered—and $F(^2P_{3/2})$ labeled $v = 3'$, which is mainly backward scattered and appears with slightly higher speed. $HF(v = 2)$ appears within a larger radius (dashed) circle and is mainly formed in a rebound reaction, where the HF recoils in the opposite (backward) direction of the incident F-atoms.[82] Reprinted with permission from Neumark DM, Wodtke AM, Robinson GN, Hayden CC, Lee YT. Experimental investigation of resonances in reactive scattering—the $F+H_2$ reaction. Phys Rev Lett. 1984;53(3):226-229. Copyright 2021 by the American Physical Society

computational chemistry packages allow nontheorists to make use of these tools. These refined theoretical methods have proven to be extremely important; but even more important is the fact that an intimate interplay between experiment and theory has developed, propelling impressive advances in achieving molecular-level insights in chemical dynamics. We now turn to some illustrative examples.

The quantum $H+H_2 \rightarrow H_2+H$ reaction and the standard model of reactivity

The simplest chemical reaction—$H + H_2 \rightarrow H_2 + H$—became the test system for detailed and quantitative comparisons between theory and experiment[112,113] three decades after Eyring and Polanyi's PES (Figure 1). The first modern dynamical calculations used a computer with 2800 vacuum tubes and weighing five tons[40,114] to solve Newton's equations on Eyring and Polanyi's 1931 semi-empirical PES. They found that both reactant translation and vibration promoted reaction. The first successful crossed-beam experiments for $D + H_2 \rightarrow HD + H$ reaction[115] stimulated further theoretical advances: the reaction cross-section versus energy was calculated with classical mechanics[105] using an improved semi-empirical PES.[116] Soon, quantum dynamics calculations using time-independent scattering theory on semi-empirical PESs appeared, first with approximations[106,117] and then with numerically exact solutions.[107,118] Quantum mechanical resonances were predicted[119]—peculiar oscillations in the reaction probability's dependence on collision energy that arise because a piece of the wave packet becomes stalled at the transition state. Theory also predicted quantized bottleneck states (QBS),[120] where wave-packet motion through the quantized transition state produces interferences.

Experiments, however, turned out to be tremendously challenging—one group used beams of tritium to investigate $H + T_2 \rightarrow HT + T$ capturing the T-atom products on MoO_3 "buttons" arranged around the reaction zone. By later scraping off the MoO_3 and analyzing the samples with a scintillation counter, angular distributions could be derived.[121] Eventually, angular distributions of scattered products could be seen using electron bombardment ionization detection.[122] This showed that the transition state was short lived and products formed by a rebound mechanism. Soon, nascent low-resolution product speed distributions were obtained.[123,124] Resolution was dramatically improved by photolyzing D_2S, providing D atom beams with relatively narrow speed distributions. When reacted with H_2, angular and speed distributions exhibited multiple peaks, corresponding to individual vibrational states of the HD product.[125,126] Photolyzing DI led the first CM contour plot of scattered product flux for the $D + H_2 \rightarrow HD + H$ reaction and a comparison to theoretical predictions could be made.[127] This work also suggested how quantum resonances might be detected.[128]

The Rydberg-atom tagging method was the next experimental advance. Here, H or D atom products are pumped with two laser pulses to a high Rydberg state only a smidge below the ionization limit, using a two-photon transition, for example, $1s \xrightarrow{h\nu_1} 2p \xrightarrow{h\nu_2} 45l$. The metastable neutral is immune to space charge and stray fields and can be easily ionized and detected after a long (~25 cm) flight distance, providing extraordinarily high-resolution measurements for obtaining H and D atom translational energies. When combined with photolytic D atom sources, Rydberg tagging provides an excellent experimental test of theory: the HD(v, J) ro-vibrationally state-resolved differential scattering angular distributions for the $D + H_2 \rightarrow HD + H$ reaction.[129] When compared to the best calculations then available, it could be seen that quasi-classical trajectory (QCT) simulations worked well at $E_i = 1.29$ eV, but not at $E_i = 0.53$ eV.[130] Also, some PESs worked better than others.[131]

The influence of quantum mechanics on the H_3 reaction is profound. Applying the Rydberg tagging approach led to direct observation[133,134] of the influence of the predicted QBS-states.[120] Perhaps most spectacular are observations of Berry's phase[135] influencing the reaction. When three H-atoms are arranged in an equilateral triangular geometry, the two lowest electronic states, φ_1 and φ_2, are degenerate as they are forbidden by symmetry to interact with one another, $\langle \varphi_1 | \hat{H} | \varphi_2 \rangle \equiv 0$. On the other hand, at all nonsymmetric structures, the two states mix and split. This gives rise to a "conical intersection" marked with an × in Figure 5(a). In fact, conical intersections are very important in chemistry.[136–139] For the DHH isotopologue shown in Figure 5, reaction can occur via two pathways: the red pathway is a simple abstraction of green H by brown H, while the green pathway involves

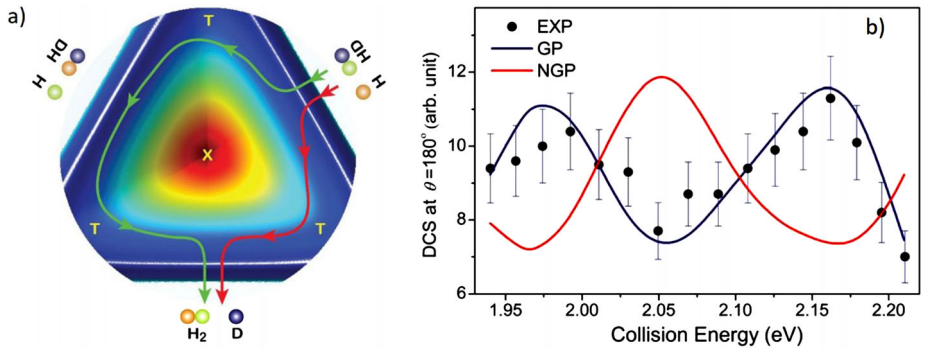

FIGURE 5 Quantum interference through a conical intersection: (a) a cut through the HHD PES showing the conical intersection (×) and three transition states (T) that connect three stable arrangements of the atoms. Note the color of the atoms. Direct abstraction visits one transition-state (RED ARROW), while the spiral or roaming reaction visits two (GREEN ARROW). Both paths lead to the same products. (b) The experiment (•) detects reactive flux arriving in the backward scattering direction producing $H_2(v' = 2, J' = 3)$ as the incidence energy is scanned. The oscillations are due to quantum interference between the two topological pathways. The red line shows quantum scattering calculations that neglect the phase-shift of π (geometric phase) introduced by traversal around a conical intersection. The blue curve accounts for the geometric phase.[132] Reprinted from Xie Y, Zhao H, Wang Y, et al. Quantum interference in H plus HD → H_2 + D between direct abstraction and roaming insertion pathways. Science. 2020; 368(6492):767, Copyright 2021, with permission from AAAS

a failed reactive attack of brown H on D followed by a complex internal rearrangement (sometimes called a spiral reaction) allowing abstraction of green H by brown H. Since the identical products, H_2 + D, formed via two pathways, interference arises.

But beyond this, quantum mechanics requires that when a conical intersection is traversed, the phase of the quantum flux passing on opposite sides of the conical intersection must be shifted by π with respect to one another—Berry's phase.[135] Obviously, this affects the interference.[132,140,141] These observations relied on Rydberg-atom tagging, but REMPI-based methods like ion imaging and Photoloc[142–151] have also been crucial to revealing the dynamics of this system.[142–153] The basis of this success and the others that space does not allow us to present is the concept that chemical reactivity involves quantum mechanical motion of nuclei on a Born–Oppenheimer PES. The remarkable agreement between the predictions of the theory and the observations from experiment earns this concept the name *the standard model of chemical reactivity.*[8]

Classical roaming reaction

The standard model affords the possibility of computing and illustrating the time-dependent motions of individual atoms through a chemically reactive encounter by following, for each atom, either the classical mechanical position or the quantum mechanical expectation value of position. It is even possible to make movies of reactions using calculated trajectories, effectively providing a microscope with time and space resolution far better than will ever be experimentally possible. One of the most inspiring examples of this is the gas-phase roaming reaction, first reported in the unimolecular decomposition of H_2CO.[154] Following up on suspicions that the reaction $H_2CO \rightarrow H_2 + CO$ may proceed by more than one mechanism,[155] ion imaging was applied to obtain speed and angular distributions of specific rotation-vibration states of $CO(v_{CO}, J_{CO})$. Figure 6 shows data revealing that when CO is produced with low rotational excitation, H_2 is produced with low speed and high vibrational excitation, and vice versa. Using a six-dimensional

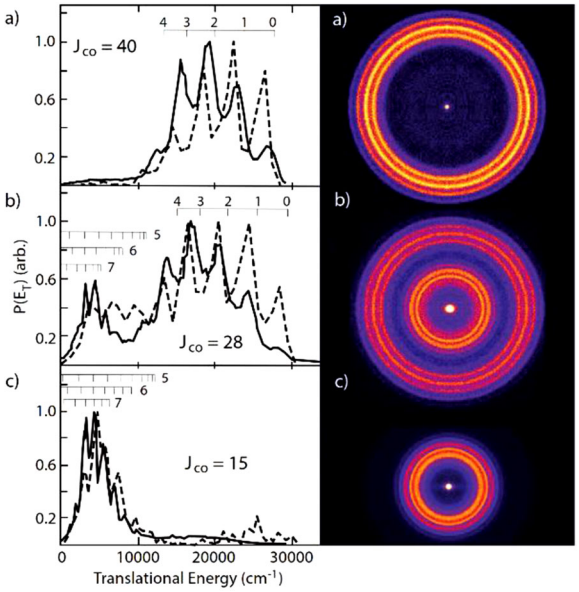

FIGURE 6 The roaming reaction in formaldehyde. Ion images (right) and CO translational energy distributions (left) for selected rotational states of CO, J_{CO}, formed in formaldehyde photodissociation. (a) $J_{CO} = 40$; (b) $J_{CO} = 28$; and (c) $J_{CO} = 15$. The rings correspond to different quantum states of H_2 produced in coincidence with these states of CO. The peaks in the CO translational energy distributions show assignments to specific $H_2(v)$ vibrational states—integers in the left panels show v, where experimental results are solid lines and results from QCT calculations on a full-dimensional PES are the dashed lines.[154] In (b) and (c), some H_2 rotational assignments are indicated by combs. Reprinted from Townsend D, Lahankar SA, Lee SK, et al. The roaming atom: straying from the reaction path in formaldehyde decomposition. Science. 2004; 306(5699):1158-1161, Copyright 2021, with permission from AAAS

Born–Oppenheimer PES to calculate classical trajectories, theory reproduced the experimental observations—compare blue and black curves. There are two classes of trajectories; one reveals a concerted molecular elimination of H_2 achieved by passing over a barrier. This

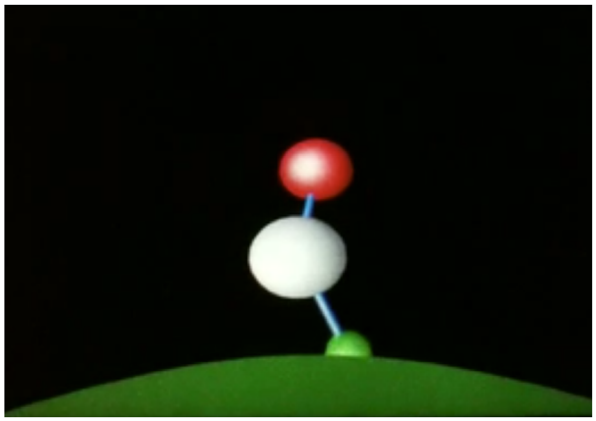

FIGURE 7 Animation of a classical trajectory of the roaming reaction in CH_2O decomposition with H (green), C (white), and O (red).[154] Note the high vibrational excitation of H_2 products seen also experimentally. Used with permission of Arthur Suits and Joel Bowman

channel leads to low vibrational states of H_2 and high rotational states of CO.

The second class of reactions is shown in Figure 7. Here, a highly excited formaldehyde molecule breaks one of its C-H bonds, but with insufficient energy for the H atom to escape. It orbits about the HCO fragment until it finds an attack angle toward the other H-atom—$H + HCO \rightarrow H_2 + CO$. This is an exoergic early barrier reaction that, just as predicted by the Polanyi rules, leads to highly vibrationally excited H_2.

This example fulfills the childhood fantasy that drove some of us to become chemists, the wish to be able watch the atoms while they are reacting. Remarkably, this is no fantasy—the classical approximation is highly accurate for many examples in chemistry and we use it often to understand the motion of atoms in reactions. Despite the successes of classical mechanics, it is impossible to avoid the quantum nature of electrons when two (or more) quantized electronic states are involved.

Electronically nonadiabatic dynamics

The reaction of $H^+ + H_2 \rightarrow H_2^+ + H$ appears superficially simpler than the H_3 reaction—H_3^+ has one less electron. However, looks may deceive—this reaction may occur in three ways. Isotopic labeling helps illustrate this. Reacting $H^+$with D_2 may involve ion exchange, producing $HD + D^+$, electron transfer, producing $H + D_2^+$, or ion exchange with electron transfer, forming $HD^+ + D$. We need to extend the standard model to consider the quantum motion of protons influenced by an avoided intersection between the two lowest energy electronic states of H_3^+.

In a reactive encounter, the nonadiabatic coupling—Figure 8(d) —is defined as:

$$\overrightarrow{D_{12}} = \langle \varphi_2 | \vec{\nabla} \varphi_1 \rangle \tag{1}$$

and controls the probability of a transition between the two PESs. Here, φ_1 and φ_2 are the adiabatic wave functions and $\vec{R}$ defines the positions of the nuclei. $|\overrightarrow{D_{12}}|$ is a measure of how rapidly nuclear motion flips the electronic wavefunction from one electronic state to the other. $|\overrightarrow{D_{12}}|$ is large at the avoided crossing when the incident proton wavepacket is at a distance ~8Å, ensuring nearly unit probability of a change in adiabatic state (no electron transfer) as the system passes through the crossing. As the wavepacket moves closer, it may branch onto both PESs. Further branching can occur each time wavepackets enter regions of space where $|\overrightarrow{D_{12}}|$ is large.

The H_3^+ reaction inspired a successful approximate method, "trajectory surface hopping,"[158] a procedure for integrating the classical mechanical equations of motion of the nuclei on a single adiabatic PES, until a hop to a different PES occurs at random according to probabilities determined from the magnitude of $|\overrightarrow{D_{12}}|$. Application of this theory to the $H^+ + D_2$ reaction reproduced quite accurately the experimentally measured absolute cross sections[159] for the three reaction channels as a function of energy—see Figure 9.

In the initial version of surface hopping, transitions between PESs occurred only at positions of maximal nonadiabatic coupling. This is unrealistic. Nonadiabatic coupling can be significant over broad regions of space, meaning that wavepackets may enter into strong coupling regions without reaching an avoided crossing. Multiple transitions may occur leading to different pathways with different quantum mechanical phases, resulting in interference effects.[160] Well-defined avoided crossings may not even exist.[161]

Theoretical advances to address these issues are continually being developed. In Ehrenfest theory,[162] atoms evolve classically on a weighted average of the PESs—here, the weightings are computed by integrating the time-dependent Schrödinger equation for the electrons along the trajectory. In an improved surface hopping theory,[163] at every instant in time, the atoms evolve by classical mechanics on a single adiabatic PES, but with the possibility of a hop to a different PES at each time step. Hops occur probabilistically according to the electronic state amplitudes obtained from integration of the time-dependent electronic Schrödinger equation. Many variations of surface hopping have since evolved, including methods for introducing quantum decoherence.[164–170] An extension of Gaussian wavepacket propagation—multiple spawning[171,172]—allows new wavepackets to be spawned to account for bifurcation on different PESs. Semiclassical[173,174] and quantum mechanical methods, such as multiconfiguration time-dependent Hartree,[175] are becoming more widely used as well. A number of approaches for computing the required excited state PESs and nonadiabatic couplings are under development, but details are outside the scope of this review.

There have been many beautiful experimental studies of gas-phase nonadiabatic dynamics. Molecular beam studies have been performed on reactions of $O(^3P, ^1D)$ and $S(^3P,^1D)$ with H_2, employing Rydberg tagging to detect product H atoms.[154,176] Reactions of $O(^3P)$ with ethylene have employed soft electron-ionization mass-spectrometry to unravel the multiple product channels of this reaction.[177] Femtosecond soft X-ray spectroscopy of the electro-cyclic ring-opening reaction of 1,3-cyclohexadiene revealed the ultrafast time scales of the nonadiabatic events.[178] The conical intersection dynamics of the RNA base uracil was studied using a UV pump with stimulated-Raman probe.[179] All of these studies were successfully modeled by surface hopping calculations.

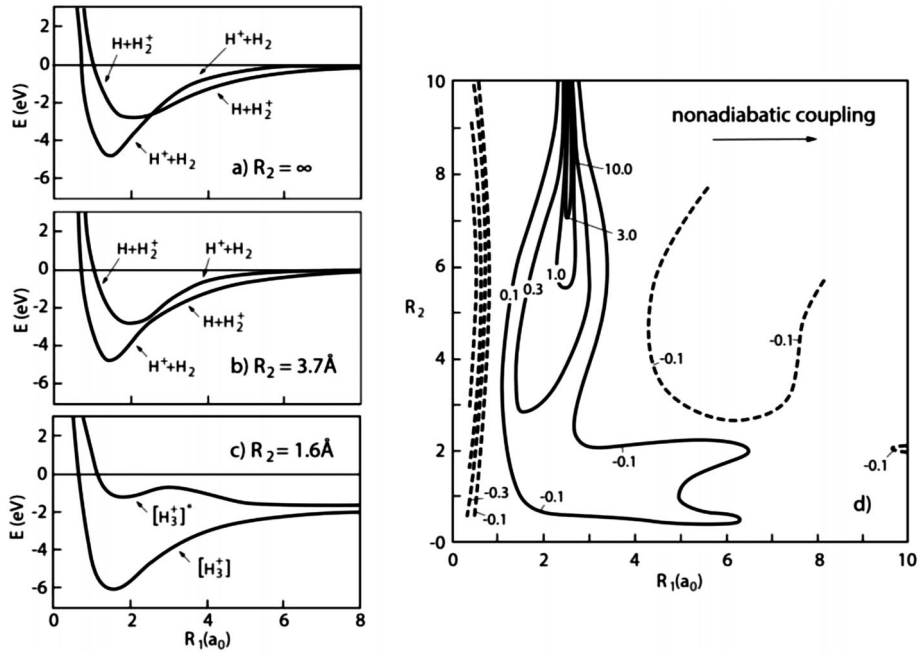

FIGURE 8 A simple charge transfer reaction. $H^+ + H_2 \rightarrow H_2^+ + H$ may proceed by three pathways involving electron transfer, proton exchange, or electron transfer with proton exchange.[156] R_1 and R_2 are the distances between atoms 1&2 and 2&3, respectively. Panel (a) shows the situation when one atom is far away. Two potentials are present describing the two possible choices of placing two electrons on two centers. Panels (b) and (c) show how these states interact at closer approach. Panel (d) shows the nonadiabatic coupling between the two states as a function of nuclear positions, more specifically, the magnitude of the component of the vector $\overrightarrow{D_{12}}$ for motion in the R_1 direction. Distances are in units of a_0

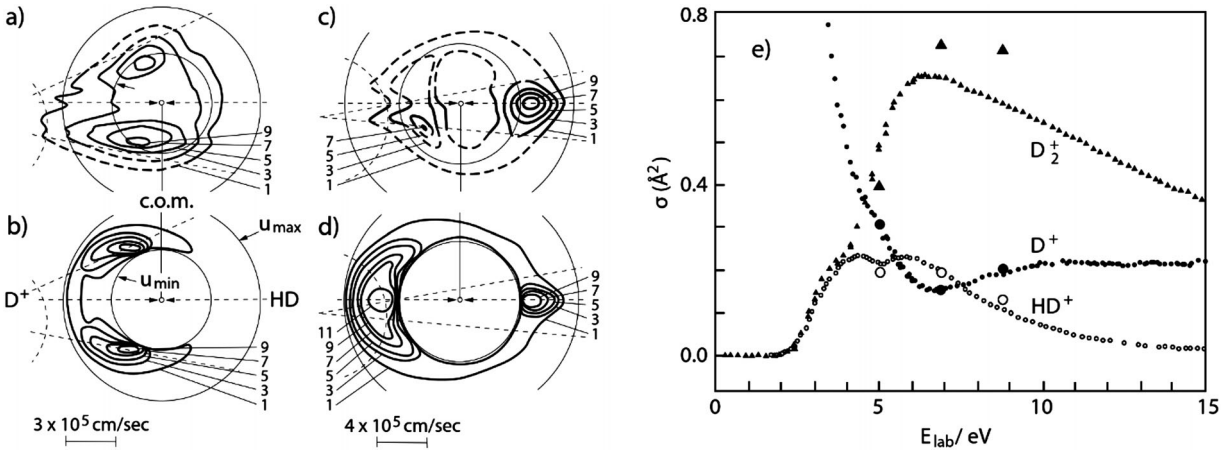

FIGURE 9 (a–d) Product flux contour maps for a simple charge transfer reaction. (a) Experimental and (b) trajectory surface hopping result for $D^+ + HD \rightarrow D_2^+ + H$. (c) Experimental and (d) trajectory surface hopping result for $D^+ + HD \rightarrow D + HD^+$. The collision energy in the center-of-mass frame was $E_{COM} = 5.5$ eV and the energy of the reactant ion was $E_{D^+} = 9.2\ eV$. (e) Integral cross sections as a function of laboratory collisional energy. Enlarged symbols represent results of trajectory surface hopping calculations. Small symbols are experimental results. Note the theory was performed prior to the experiments[157]

Transition state theory

Chemistry is the science of materials conversion and while thermodynamics tells us which reactions are fundamentally possible, to be of practical importance, we must design chemical pathways to reach the desired products using rapid reactions. This simple argument underlies the entire field of catalysis and drives much of synthetic chemistry. One of the major motivations to develop an atomic scale foundation of understanding in chemical dynamics is the desire for a predictive theory of chemical reaction rates. Transition state theory (TST) has filled this need, allowing us to exploit our understanding of chemical dynamics to make quantitative predictions about the speed of a reaction.

In its original formulation, Eyring postulated a special state of the system—the activated complex—that when formed, would with almost complete certainty, go on to products. In a remarkable leap of insight, he assumed that this species would be in thermal equilibrium with the reactants. If one could determine its energy and structure—necessary to obtain its entropy—the activated complex's concentration as well as the speed of passage on to products could be found with statistical mechanics.[34] At the time these ideas were developed, it was difficult to predict theoretically many of these quantities. However, the development of computational chemistry has provided all of the machinery necessary for making these calculations accurately for many gas-phase reactions.

The current formulation of TST prescribes a dividing plane that separates reactants from products such that every trajectory that originates in the reactant region of configuration space and evolves to the product region must pass through the dividing plane at least once. The TST thermal rate constant is equal to the equilibrium one-way flux through the dividing plane in the direction of reactant to product. Thus, TST provides an upper bound to the rate constant, since some trajectories might pass through the dividing plane more than once or pass through without leading to product—so, the equilibrium flux will include nonreactive events. The location of the dividing plane is usually chosen at the reaction barrier, but ways that are more sophisticated can be used, including variational TST,[180] in which the location of the dividing plane is chosen to minimize the TST rate. Improvement to TST can be obtained by running classical trajectories to count the number of recrossing events and reduce the TST rate accordingly.[181] This technique is particularly advantageous in cases where the reaction barrier height is high, perhaps many times kT. An effective way to simulate this is to initiate trajectories at the dividing plane, integrate forward and backward in time, and modify the TST rate constant by the fraction of trajectories that underwent recrossings.

TST has been extremely successful and many comparisons between measured and predicted rates have proven its validity. It has been particularly important in atmospheric[182] and combustion chemistry[183] and finds widespread use to predict reaction rates, especially where they are impossible to measure. It is also worth contemplating that TST has led to a deeper understanding of how enzymes work.[184] Many concepts of enzyme catalytic activity—correlated conformational fluctuations, dynamical and nonequilibrium effects, electrostatic preorganization, entropic guidance, fluctuating barrier height, near-attack configurations, reactant destabilization, and tunneling—can be understood within the language of modern TST. In this language, "the entire and sole source of the catalytic power of enzymes is due to the lowering of the free energy of activation and any increase in the generalized transmission coefficient„…."[184] These insights about some of the most complex catalysts in nature are a culmination of nearly a century of effort starting with the H_3 reaction and should make us optimistic that applying the dynamical approach to surface chemistry can lead to similar successes.

To summarize this section, "the dynamical approach" applied to gas-phase reactions has led to a standard model of chemical reactivity, involving quantum motion of nuclei on an electronically adiabatic Born–Oppenheimer PES. The classical approximation often holds and the standard model can be generalized to involve multiple electronic states. The standard model has allowed us to develop and validate a nearly exact predictive theory of gas-phase reaction rates derived from TST.

EXTENDING THE DYNAMICAL APPROACH TO SURFACES

Extending the dynamical approach to problems in surface chemistry may appear impenetrably complex and challenging. The remainder of this review breaks down the complexity and reveals the commonalties to gas-phase dynamics. Progress derives from adapting the basic concepts and many exquisite theoretical and experimental tools of gas-phase dynamics to problems at surfaces and inventing new ones based on the spirit of the dynamical approach.

The most obvious challenge facing the extension of the dynamical approach to surfaces is that surfaces are big and they are dense. In a crossed molecular beam experiment, most of the molecules in one beam pass through the other without colliding, ensuring single collision conditions where we can observe elementary reaction steps. In contrast, in a beam-surface scattering experiment, every molecule collides. While this contributes to strong signals, molecule-surface encounters may involve many collisions. Hence, the challenge of size is not just one of high-dimensionality; rather, we need to disentangle a sequence of elementary events and learn about each one individually. In this spirit, we have sections below on Dissipation and Inelastic Scattering (Section 5), Adsorption––Desorption (Section 6), and Dynamics of Reactions at Surfaces (Section 7). Inelastic encounters of atoms and molecules with surfaces determine whether adsorption takes place; likewise, adsorption is often the step preceding reactions, which must compete against reactant desorption.

The fact that multiple elementary processes typically occur even in the best-designed experiments makes cooperation with theory all the more important. On the other hand, theoretical tools for surface dynamics often require new approximations meaning they require testing against experiment. Most significantly, wave function-based methods for treating electron correlation are generally too computationally demanding to be applicable to molecule–surface interactions. As a result, DFT, with plane-wave basis functions, generalized gradient approximation (GGA) functionals,[185] and the inclusion of dispersion,[186] dominates the computation of PESs. The quantum mechanical methods for computing atomic motions that revealed such detailed and definitive behavior in gas-phase reactions are not often applicable for describing molecule–surface interactions, except in reduced dimensions, for example, under the extreme assumption that the surface atoms do not move. As a result, classical mechanics, sometimes augmented by dissipative or nonadiabatic features, remains the workhorse for simulating chemical dynamics at surfaces. On-the-fly dynamics calculations have made many contributions, but new machine learning algorithms[103] are slowly replacing them with full-dimensional analytical PESs constructed by fitting to DFT energies.

We also face new experimental challenges when making the leap from the gas phase to surfaces. Of course, we need ultra high vacuum (UHV) ($\sim 10^{-10}$ mbar) to establish conditions where surfaces remain clean and we need the tools of surface science for cleaning and characterizing the sample. Fortunately, these tools are now commercially available and offer no significant barrier to entering the field.

The truly daunting challenges include the following. We often do not know *a priori* the reactive site, as adsorption and diffusion as well as the surface heterogeneity are conditions not faced in the gas phase. A theoretician working to understand experiments in the gas phase takes comfort in knowing the stoichiometry of the transition state. In surface reactions, knowing which atoms to include in a model of reactivity may be the first puzzle to solve. Of course, the surface itself behaves like a reactant. Yet, there are few tools available to excite specific motions of the solid to investigate their influence on reactivity—most studies simply vary the temperature. More subtle problems also arise. Gas-phase experimentalists take for granted tools that offer detection sensitivities of as low as one molecule per cm^3; common methods in surface science offer adsorbate detection sensitivities of about 10^{13} molecules cm^{-2} or 0.01 of a monolayer (ML).

While the challenges and limitations described above present barriers, they also provide opportunities for great progress through a combination of ingenuity, advancing technology, and theory development. It is a common occurrence—in fact, many examples can be found in Section 2 of this review—that today's sensation or "miracle experiment" becomes tomorrow's routine calibration measurement. In experimental science, the more we learn, the more we are able to learn. This inevitable improvement of measurement methods should make us optimistic about meeting the challenges.

DISSIPATION AND INELASTIC SCATTERING

Breaking or making chemical bonds consumes or releases energy that, in gas-phase reactions, flows among the translation, vibrational, rotational, and electronic degrees of freedom of the species actively involved. In surface chemistry, energy can also flow between the reacting species and the substrate vibrational (phonon) and electronic degrees of freedom. Probing and understanding these energy transfer pathways are central topics in surface dynamics.

Lifetimes of vibrationally excited molecules adsorbed on surfaces (Section 5.1) reveal important mechanisms of dissipation; whereas, energy, angle, and quantum state resolved differential inelastic surface scattering experiments (Sections 5.2–5.6) reveal more directly the flow of energy among the degrees of freedom of the incident and scattered species and the flow of energy to and from the surface. An important aspect of this work is the large role played by nonadiabatic electronic excitation in certain energy transfer processes. The theory of these nonadiabatic effects is taken up in Section 5.7. Finally, we present high-resolution inelastic scattering experiments of H and D atoms (Section 5.8) together with molecular dynamics simulations that have proved to be an excellent testing ground of the dynamical approach in surface chemistry.

Vibrational relaxation rates of adsorbates

Lifetimes of vibrationally excited molecules on surfaces have been inferred from infrared lineshapes and measured directly using infrared pump-probe methods. Lifetimes range from milliseconds for $CO^*(v = 1)$ physisorbed on NaCl[187,188] to 2–3 ps for chemisorbed CO on metals.[189–193] The long lifetime of $CO^*(v = 1)$ on NaCl reflects the fact that more than thirteen phonons must be excited to relax the molecule—CO's vibrational frequency (~ 2100 cm^{-1}) is much higher than the highest frequency phonon of NaCl (~ 160 cm^{-1}). The anharmonicity of the PES is so small initially that excited CO vibration does not easily decay to other vibrational degrees of freedom. In fact, relaxation occurs via an electromagnetic interaction independent of the PES—the Sommerfeld ground wave limit.[188] When CO is chemisorbed on metals, the coupling to phonons is no more favorable; therefore, the ps vibrational lifetimes observed suggest that vibrational relaxation via excitation of electron–hole pairs (EHPs) in the metal is highly efficient.

The importance of vibrational relaxation to excite EHPs has been confirmed by a variety of theoretical methods. One of the first used is Fermi's golden rule (FGR) with the jellium approximation for the metallic conduction electrons to study H_2 relaxation near Al, Mg, and Na surfaces.[194,195] Similarly, CO on a Cu cluster was examined using FGR with DFT.[196] A Newns–Anderson Hamiltonian approach showed similar results for CO and CN adsorbed on Ag, Cu, Au, and Pt.[197] Electronic friction methods for CO on Cu(100) employed a local-density friction approximation (LDFA) and also yielded picosecond lifetimes.[198] Recently, pump-probe measurements of the vibrational relaxation of physisorbed CO on Au(111) showed a lifetime of ~ 50 ps, much longer than chemisorbed CO[199]—a recent theoretical treatment was consistent with this measurement.[200] Such long vibrational lifetimes for physisorbed species suggest that reactions of vibrationally excited adsorbates[201] may be more important than previously believed.

All of these studies investigated the high-frequency CO stretch. For other modes and lower frequency stretch modes, phonons can play a significant role in coupling to adsorbate vibrations, as shown by FGR calculations of vibrational lifetimes of all four vibrational modes of CO on Cu(100) using finite-sized Cu clusters at the Hartree–Fock level.[202–204] Here, EHP excitation entirely dominated the lifetime of the internal stretch (3.3 ps) and bend (2.3 ps) modes, while phonon excitation significantly contributed to the lifetimes of the CO-surface stretch (22 ps) and the frustrated translational modes (14 ps).[204] All four of these lifetimes are in reasonable accord with experiment.[189,192] The conclusions are that EHP excitations dominate the relaxation of the internal stretch and bending modes, whereas the molecule–surface stretch and frustrated translational modes relax mainly via phonons. It is not known whether these trends hold for other adsorbates or other metal surfaces.

Early molecular beam surface scattering experiments

The success of molecular beam scattering experiments in gas-phase dynamics created a lot of enthusiasm that similar success was possible

by the application of these techniques to surfaces. Early experiments faced limitations stemming from the difficulty of combining beam and surface science methods. High-performance molecular beam machines typically had poor vacuum and it was necessary to work with surfaces at elevated temperatures to prevent contamination or to use continuous epitaxial deposition to maintain a clean surface.[205,206] UHV surface science machines retrofitted with rotating detectors for beam surface scattering, usually using effusive beams,[207] did not have the full molecular beam performance as their gas-phase cousins. Angular distributions of scattered rare gas atoms and small diatomic molecules were an important focus of these studies.

Measured angular distributions often showed broad lobes centered near the direction of specular reflection of the incident beam. These lobes resulted from incident species striking the moving surface atoms, exchanging energy and momentum, and then returning to the gas phase. The angular position and width of the lobes provided information on momentum and energy exchange with the surface. Treating surface atoms as hard cubes moving with a thermal velocity distribution[208] had success in predicting observed trends. The hard cube model forces parallel momentum conservation and, hence, the normal momentum transfer could be determined by conservation of energy and momentum and knowledge of the masses and velocities of the incoming species and surface atom. Improved versions of the hard cube model included adding a spring to the hard cube to represent the lattice vibration (soft cube model),[209] and treating the substrate atoms as having truncated spherical caps[210] to allow modeling of parallel momentum transfer. This later refinement was particularly necessary to obtain agreement with measurements at hyperthermal incidence energies.[211]

Velocity distributions of molecules scattered from clean and well-characterized surfaces became available only after combining UHV surface science techniques with state-of-the art molecular beam methods. In one of the first instruments,[212] three differentially pumped supersonic beam sources were directed at the surface, producing molecules with narrow velocity distributions. A differentially pumped mass spectrometer and associated vacuum pumps mounted on a rotating platform sealed with Teflon "tec" seals[213] provided a rotatable detector, which, with the use of a chopper wheel, allowed for the measurement of scattering-angle resolved times of flight (TOF). Rotation of the solid target allowed variation of the incidence angle. The instrument was bakeable, used UHV compatible pumps, components, and materials of construction and had surface science equipment to clean and characterize the target surfaces. Figure 10 shows an example of measured velocity distribution data for Ar scattering from a Pt(111) surface.[214] The iso-flux contour plots shown combine results of TOF measurements at many scattering angles. Cuts of the iso-flux plots give the velocity distribution in the directions normal and parallel to the surface. The spread in velocities in the perpendicular direction (v_z) is clearly larger than that in the parallel direction (v_y) showing the coupling of normal momentum to the surface is larger than that of parallel momentum. The data show the "the law of parallel momentum conservation" that had emerged from interpretations of angular distribution measurements[215] is not correct, although there

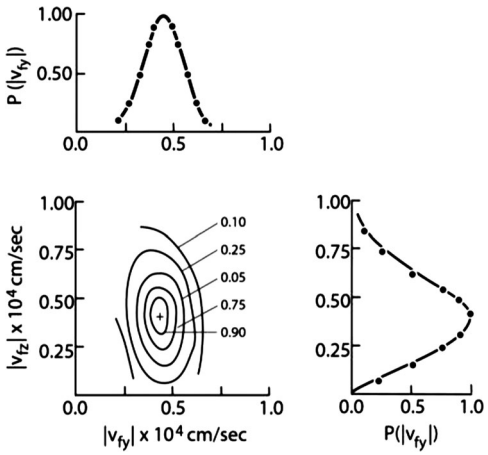

FIGURE 10 Velocity distribution measurements for in-plane Ar scattering from Pt(111). Iso-flux contours for Ar with an incidence energy $E_i = 94$ meV and angle $\theta_i = 45°$. Out-of-plane scattering data were also obtained by tilting the surface.[214] Reprinted from Hurst JE, Wharton L, Janda KC, Auerbach DJ. Direct inelastic scattering Ar from Pt(111). J Chem Phys. 1983;78(3):1559-1581, Copyright 2021, with the permission of AIP Publishing

is a clear propensity for parallel momentum conservation. Data of this type are also available for a range of incidence energies and angles and for scattering both in and out of the principal scattering plane. Very high-resolution experiments were also done with He atom scattering capable of resolving single phonon excitation of the solid. These experiments primarily probe the structure of the solid rather than reaction dynamics and we refer the interested reader to a recent book on the subject.[216]

The availability of accurate scattering data stimulated the development of methods to simulate gas-surface scattering. Even for scattering of rare gas atoms from clean, perfect surfaces, it is a challenge to employ an accurate gas–surface interaction potential, energy dissipation to phonons, and quantum mechanical effects. In principle, for metal surfaces, the effects of EHP transitions should also be included, but these appear to be relatively unimportant for rare gas atom scattering.

The first advance in theory beyond the cube models was to integrate the classical equations of motion numerically for the rare gas atom and a slab of surface atoms. These studies modeled the gas–surface interaction using empirical potentials with harmonic interactions among the surface atoms. It was found that, for metal surfaces, Lennard-Jones pairwise additive gas-surface potentials produced too much corrugation; presumably, the metallic electron cloud smooths out the corrugation. This problem was addressed by the addition of a background smoothing potential.[217] Initial simulations employed only a small number of surface atoms with frictions and fluctuating forces to define surface temperature, T_S and with memory chosen to approximately reproduce the phonon spectrum.[218] As more powerful computers became available, hundreds of surface atoms could be included, with or without frictions and random forces.[219,220] To date, however, there do not appear to be any simulations of the scattering of rare gas atoms from surfaces based on accurate *ab initio* PESs.

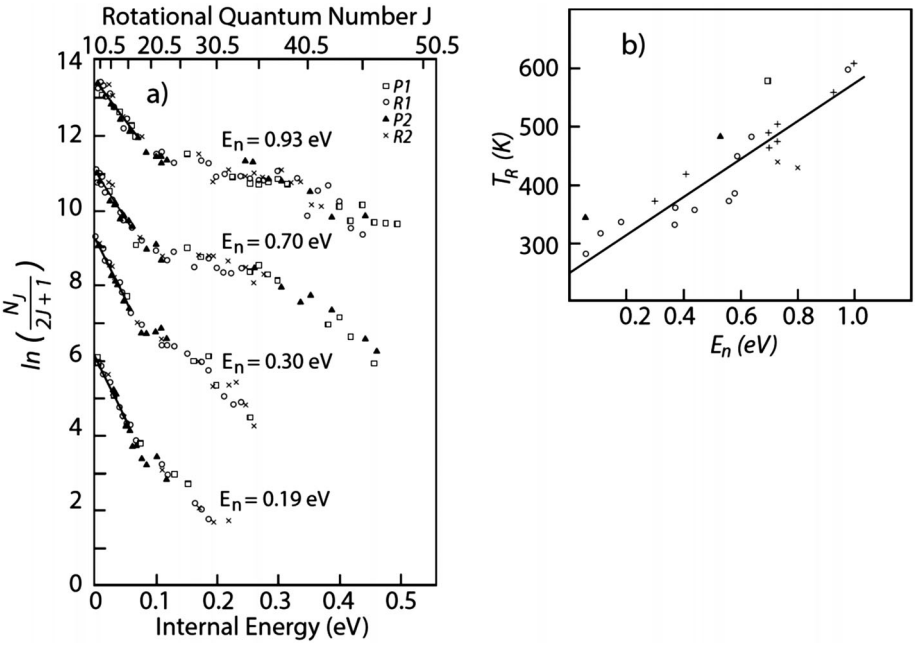

FIGURE 11 (a) Rotational state distributions normalized to degeneracy for NO scattering from Ag(111)[224] for $E_n = E_i \cos^2(\theta_i)$ as indicated. Note the emergence of a broad peak at high J as E_n is increased. (b) Rotational temperature, T_R of the low-J region of the spectrum as a function of E_n. The linear increase in T_R is evidence that the rotational excitation is the result of transfer of translational motion into molecular rotation (T→R coupling), a signature of direct scattering

Simulations based on classical adiabatic molecular dynamics using empirical potentials provide reasonable agreement with measured energy and angular distributions. An example for the direct inelastic scattering of Xe scattering from Pt(111) is shown in Figure 24(a)–(d). For this system, there are two peaks in the TOF spectrum; one resulting from direct "single bounce" inelastic scattering, and the other from molecules that trap on the surface and then desorb. The general agreement of measured rare gas atom scattered velocity distributions with calculations based on a single PES indicates that electronically adiabatic coupling to phonons dominates and that electronically nonadiabatic excitation of EHPs is not important. At higher energies where $E_i \cos(\theta_i) > 3$ eV, the measured energy loss is larger than that calculated from the adiabatic picture, suggesting that nonadiabatic excitation starts to become important, even for rare–gas metal interactions.[221]

State-resolved detection of scattered molecules, rotational effects

Probing transitions between a molecule's rotation-vibration states due to collisions at a surface required state-specific detection techniques. Here, molecular beams deliver rotationally cold molecules in their ground vibrational state moving with controlled and narrow speed distributions, while detecting scattered molecules with LIF or REMPI. Early experiments done with NO showed strong rotational excitation and no vibrational excitation.[222–224] Rotational excitation increased with incidence kinetic energy and a broad nonthermal peak in the rotational state distribution emerged[224]; see Figure 11(a). Increased rotational excitation in the scattered molecules arises from a loss of translation energy (T → R coupling), Figure 11(b). This conclusion was supported by independent measurements for NO scattered from Au(111) showing decreased translational energy of the scattered NO when produced in higher energy rotational states.[225–227]

The nonthermal rotational states populated at high incidence translational energy were interpreted as a "rotational rainbow," where a specific orientation angle of the molecule with respect to the surface leads to maximum rotational excitation. The rotational rainbow gets its name from the mathematically analogous optical rainbow, where a specific impact distance of a light ray from the center of a water droplet leads to a maximum scattering angle and an intensity maximum at that angle.[228] Classical trajectory and quantum wavepacket calculations based on empirical potentials provide support for this interpretation[229,230] and rotational rainbows have since been seen many times.[229,231–237] Since then, it was possible to see an N-side and an O-side rainbow for NO scattering using oriented beams of NO[238] and to witness a rainbow in formaldehyde, where the rotation about the CO bond axis exhibits a rainbow.[239]

Combining TOF with REMPI provides velocities of scattered, state-selected molecules. Knowing the initial and final translational and rotational energy, we can compute the energy transfer to the lattice. Interestingly, the energy going into the lattice depends on the degree of rotational excitation; molecules that undergo more rotational excitation transfer less energy into the phonons of the substrate, in good agreement with theoretical calculations.[225,240] This anticorrelation of rotational excitation and phonon excitation seems also to be a ubiquitous feature of molecular scattering from surfaces.[9,227,238,241]

State-resolved detection of scattered molecules, vibrational effects

Observations of vibrational excitation were reported for REMPI detected NH_3 after its collision with Au(111) surface—umbrella motion in NH_3 gives rise to low-lying vibrational levels that become increasingly populated with increased incidence transitional energy.[242] Observed thresholds tellingly close to the detected state's vibrational excitation energy showed that a minimum of incidence energy was needed to produce each new vibrational states (T→ *V* coupling). The excitation probability was, furthermore, insensitive to T_S. The authors concluded that vibrational excitation was occurring via a direct (single bounce) adiabatic ("mechanical") coupling of the incoming normal motion to the vibrational modes of the molecule.

Efficient vibrational excitation from $v = 0 \rightarrow 1$ was also observed in collisions of NO with a hot Ag(111)[243] surface. In contrast to the results for NH_3, the excitation probability increased exponentially with T_S, displaying an Arrhenius-like behavior with an activation energy equal to the NO vibrational spacing. Furthermore, no thresholds were seen in the incidence energy dependence. The authors argued that NO vibrational excitation resulted from an electronically nonadiabatic coupling of NO stretch motion to thermally excited EHPs in the metal and that the coupling increased at higher incidence energies as a closer approach was possible. This interpretation was supported by later measurements of the velocity distributions of scattered NO in the vibrationally elastic and inelastic channels showing the energy for vibrational excitation did not come from translational motion.[244]

Since this discovery, the literature has filled with reports of similar observations—systems where hot EHPs excite vibrations include: HCl on Au,[245] CO on Au,[246] and Ag.[247] For NO on Au, it was even possible to see $\Delta v = 1$, 2, and 3, each displaying an Arrhenius-like behavior with an activation energy equal to $\hbar\omega_{vib} \times \Delta v$.[248] In these experiments, the production of NO($v = 3$) with its vibrational energy of 0.687 eV occurred in collisions of NO ($v = 0$) with a hot Au(111) surface at incidence energies of only 0.4 eV.[248]

Figure 12 shows absolute measurements of excitation probabilities of NO($v = 1$) and NO($v = 2$) for NO($v = 0$) colliding with Au(111) over a wide range of incidence energies and surface temperatures.[249] These data are particularly valuable for comparison with theories of nonadiabatic energy transfer because the availability of absolute measurements for both single and multiquantum excitation helps distinguish different theoretical treatments of the nonadiabatic coupling. We will return to this topic in Section 5.7.

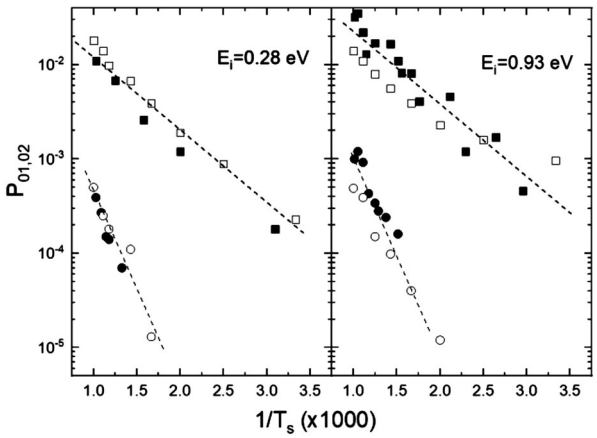

FIGURE 12 Excitation probabilities for NO($v = 0 \rightarrow 1, 2$) scattering from Au(111) as a function of surface temperature, T_S, for two translational incidence energies, E_i. Squares show results for NO($v = 0 \rightarrow 1$) and circles for NO($v = 0 \rightarrow 2$). The Arrhenius form possesses a prefactor, and an "activation energy" that is equal to the energy gap of the inelastic transition. Note that the prefactor increases with E_i, but that the activation energies are independent of E_i while being larger for NO($v = 0 \rightarrow 2$) compared to NO($v = 0 \rightarrow 1$). This reflects the stronger temperature dependence of the populations of higher energy thermally excited EHPs.[249] Note that the vibrational energy of NO($v = 2$), 0.462 eV, is substantially higher than the incidence energy of 0.28 eV seen in one of the experiments shown here, proving that the vibrational excitation does not originate as incidence translational energy

Vibrational state-to-state scattering

Improved observations of vibrationally inelastic scattering are possible using a state-to-state approach, combining optical pumping of molecular beams with REMPI detection of scattered molecules. While experimentally more complex, this set-up also provides improved TOF capability, simplifying the identification of direct scattering channels versus trapping followed by desorption. Simply by varying the delay between the two lasers and separating the laser beams from one another, state-to-state TOF can be performed.[226,227,250,251]

IR pumping allows for the production of beams with substantial populations in the $v = 1$–3 vibrational states[227] and with stimulated emission pumping (SEP), much higher vibrational states can be reached.[252] SEP is the conceptual child of microwave-optical double resonance [253–257] and optical-optical double resonance spectroscopies.[258,259] In SEP, molecules are excited or pumped by one laser to an excited electronic state—subsequently, emission is stimulated by a second laser, "dump"-ing the excited state population back to the ground electronic state. By tuning the lasers so that the stimulated emission goes to a vibrationally excited state, this "pump-dump" approach populates the beam with highly vibrationally excited molecules selected by the frequency difference of the two lasers. In surface scattering, SEP is most often performed with pulsed nanosecond lasers.[260]

The first application of SEP to surface dynamics[261] prepared NO($v = 15$) and used REMPI to determine the final vibrational state distributions after collision with Au(111)—see Figure 13(a). NO($v = 15$) hardly survives—the most probable state-to-state relaxation process loses eight vibrational quanta (~1.5 eV). Narrow angular distributions indicated single bounce dynamics. Coupling of high-frequency NO vibrations to the phonons of the Au(111) lattice is improbable due to the large energy mismatch between the vibrational energy change and the phonon energy. The remarkable vibrational relaxation was attributed to nonadiabatic electronic effects, specifically the excitation of EHPs of the substrate mediated by vibrational promotion of

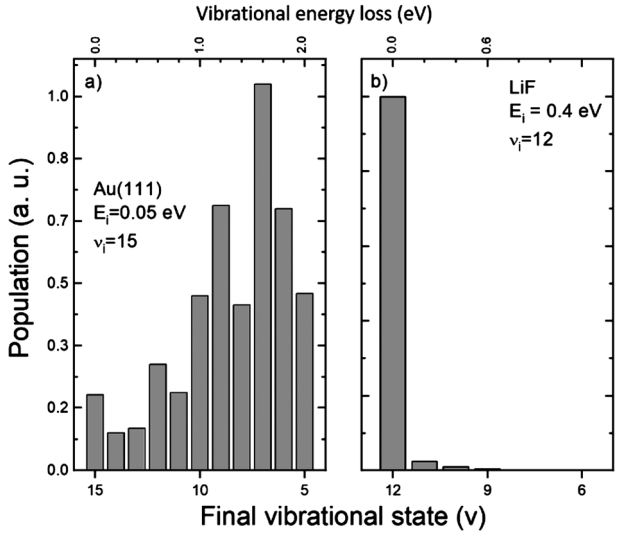

FIGURE 13 NO vibrational relaxation from a metal and an insulator. NO with indicated incidence vibrational quantum numbers, v_i, scatters from Au (a) and from LiF (b). The efficiency of vibrational energy transfer is much larger for Au than for LiF. This is due to Born–Oppenheimer failure, where NO vibrational energy is converted to electronic excitation in the metal. For Au, it was not possible to probe states lower than $v = 5$, but with little doubt, those states are also populated. Reprinted from Huang YH, Rettner CT, Auerbach DJ, Wodtke AM. Vibrational promotion of electron transfer. Science. 2000;290(5489):111-114, Copyright 2021, with permission from AAAS

electron transfer.[261] This conclusion was supported by a comparison with data on the scattering of NO(v = 12) from an LiF crystal shown in Figure 13(b), where little vibrational relaxation is observed. Unlike a metal, insulators like LiF have no continuum of low-lying electronic excitations. Nonadiabatic electronic excitations are thus not possible for LiF and vibrational relaxation occurs by the much weaker coupling to phonons.

Since that time, methods have continued to improve. Spontaneous emission from the intermediate "stepping-stone state" used in SEP produces vibrationally excited states indiscriminately, which is usually an unwanted background. The utility of pump-dump optical excitation improves dramatically when using a "sweep" laser that dissociates the stepping-stone state within a few ns after pump-dump has been performed, removing most of the spontaneous emission and concomitant background.[262] It also proved possible to develop a variant of SEP that was used to produce highly vibrationally excited CO exploiting perturbations.[263] Overtone pumping of HCl and NO to low lying vibrational states was another path to additional data.

We now have rich and extensive data on the inelastic scattering of vibrationally excited molecules colliding with metal surfaces—it is one of the best-studied examples of the failure of the Born–Oppenheimer approximation to describe molecular interactions at metal surfaces.[6–9] State-to-state data are now available for vibrational relaxation and excitation of HCl,[264–266] NO,[267–269] and CO[247,270] prepared with both low and high levels of initial vibrational excitation. Most work has been done on Au(111) and Ag(111). Remarkably, Ag(111) induces much larger vibrational relaxation probabilities[271] than Au(111)—see Figure 14(a).

While Ag and Au have many similarities, it is noteworthy that Ag possesses a substantially lower work function than Au (4.5 vs. 5.3 eV). NO vibrational relaxation is believed to occur by an electron transfer-mediated mechanism involving a transient anion, NO^-. If true, it would not be surprising that the work function plays an important role. Systematic control of the work function was achieved using atomically layered films of Ag grown on Au(111).[272] Silver grows layer by layer on Au, hence, only when the nth layer closes does the n+1th layer begin to grow. Evaporating Ag onto Au with a Ag-beam block moving continuously across the Au crystal allows fabrication of an atomically defined edge structure—see inset of Figure 14(b). Using this wedge in a molecular beam surface scattering experiment, one can examine the inelastic scattering seen when the beam of vibrationally excited molecules collides at different positions on the wedge.

Figure 14(b) shows the results of such measurements. The survival probability of NO(v = 2) decreases with increasing Ag coverage—furthermore, as each atomic layer closes, there is a discontinuity in the survival probability. Such discontinuities are also seen in the layer dependence of the surface work function—this is perhaps the strongest evidence that work function is central to the mechanism of nonadiabatic vibrational energy exchange between the molecule and the surface, consistent with a transient NO^- anion mechanism.[272]

A mechanism involving a transient negative ion formed by electron transfer to either NO or CO helps to explain many of the observations. Both the vertical electron binding energy at the outer turning point of vibration, $E_{v(v,\, r_{outer})}$, and the work function, Φ, determine if electron transfer is energetically possible. There is actually a very good correlation between vibrational relaxation probability and $E_{v(v,\, r_{outer})} - \Phi$ across a large number of systems as shown in Figure 15.

Experiments with oriented NO were also developed, where either N or O faces the surface upon collision.[238,273,274] Vibrational relaxation is more efficient when N is oriented toward the surface than away,[274,275] consistent with theoretical predictions that electron transfer is more labile for this orientation.[276]

Vibrationally promoted electron emission

Taken together, there is compelling evidence that vibrational relaxation of NO and CO molecules colliding with a metal surface occurs via an electron transfer process. If vibrational energy loss resulted in low energy excitations of many electrons, electron emission could not occur. However, if many quanta of vibrational energy can be channeled to a single electron giving it enough energy to overcome the work function, not only will emission be possible, but it also will be a strong sign that "one electron does all the work," a concept consistent with an electron transfer process. Thus, looking for electron emission and measuring its quantum yield can teach us something very important about the dynamics of the EHP excitation.

When highly vibrationally excited NO with variable incidence vibrational energy was scattered from a surface with 1.6 eV work function,[279] prepared by dosing a sub-ML amount of Cs on Au(111),

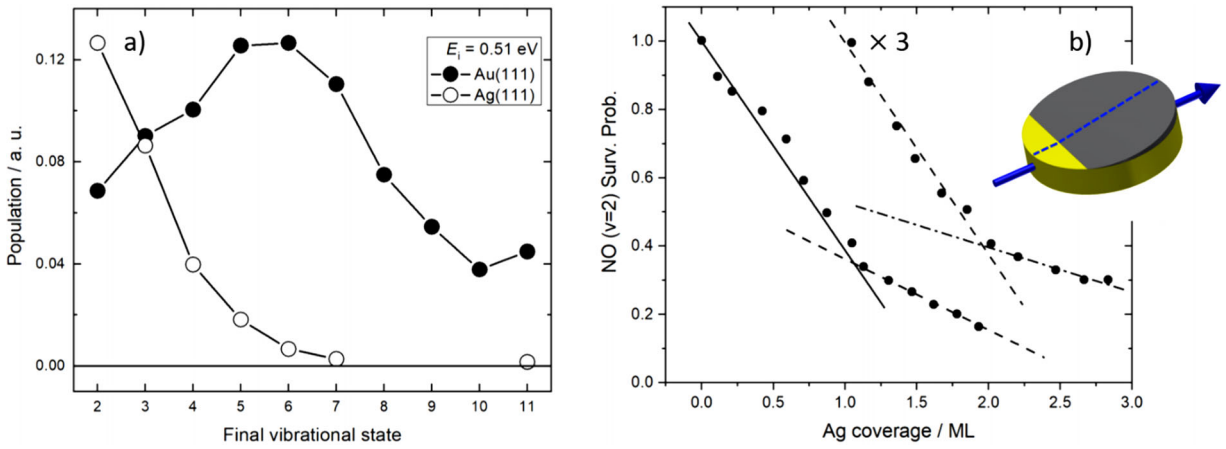

FIGURE 14 The influence of work function on electronically nonadiabatic vibrational relaxation. (a) NO(v_i= 11) colliding Au(111) and Ag(111). The multiquantum vibrational relaxation is much stronger on Ag, whose work function (4.5 eV) is substantially lower than that of Au (5.3 eV). (b) A wedged sample of atomically layered Ag on Au (inset) is translated through a molecular beam of NO(v = 2). The REMPI signal reports vibrational survival probability as a function of Ag layer thickness. Coverage dependence of the first (solid line), second (dashed line), and part of the third (dashed-dot line) ML of silver are shown. A discontinuity in the survival probability appears as the first and second atomic layers close. A similar discontinuity is seen in the coverage dependence of the work function[272]

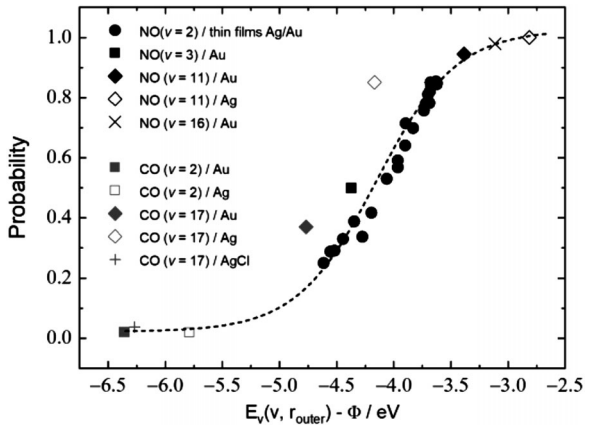

FIGURE 15 Vibrational relaxation probability in scattering as a function of the vertical electron binding energy minus the work function.[9] The incidence energy for all data is ~ 0.6 eV so the turning point is similar for all systems. AgCl denotes a monolayer of Cl on Ag(111). Au and Ag both refer to the (111) facet. Republished with permission of IOP Publishing, Ltd, from Park GB, Krüger BC, Borodin D, Kitsopoulos TN, Wodtke AM. Fundamental mechanisms for molecular energy conversion and chemical reactions at surfaces. Rep Prog Phys. 2019;82(9):096401; Copyright 2021, permission conveyed through Copyright Clearance Center, Inc.

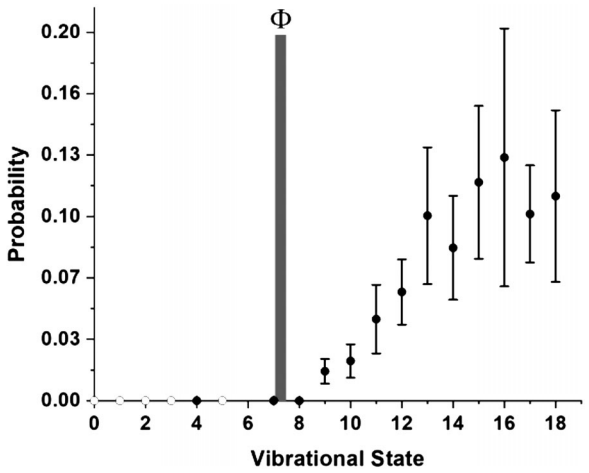

FIGURE 16 Probability of electron emission resulting from 29 meV NO (v = 18) incident upon a Au(111) surface dosed with a submonolayer of Cs to reduce the work function to 1.61 eV. The vertical bar shows the work function and the range of uncertainty.[277,278] Reprinted from White JD, Chen J, Matsiev D, Auerbach DJ, Wodtke AM. Conversion of large-amplitude vibration to electron excitation at a metal surface. Nature. 2005;433(7025):503-505

electron emission was readily observed as soon as the vibrational energy exceeded the work function.[277] See Figure 16. This directly shows that vibrational energy has been used to excite a single electron. Furthermore, this is not a rare or highly forbidden channel—the yield is large, reaching over 10% for v = 18.

An inverse velocity dependence gives further evidence of a transient negative ion formation, since, due to increasing image charge stabilization, a newly formed negative ion must emit its electron before getting too close the surface.[278] Measurements of the energy distributions of emitted electrons provided information on the number of quanta of vibration that go into exciting the emitted electrons.[280,281] The sum of the measured electron energy and the work function is simply the vibrational energy that couples into a single electron. The measurements showed that when NO(v = 16) collides at the surface, with highest probability, 10 vibrational quanta couple into a single electron.[281]

The results presented in this and the preceding five sections provide a rather complete experimental characterization of the electronically nonadiabatic dynamics of molecules interacting with metal surfaces. Key observations include vibrational excitation and de-excitation as well as multiquantum vibrational relaxation, vibrationally promoted electron emission, and strong orientation effects. These observations

provide strong evidence of an electron transfer-mediated mechanism involving transient anions. They remain, however, a challenge for electronically nonadiabatic theory of surface chemistry,[267] to which we now turn.

Theory of nonadiabatic coupling to EHP excitations

Vibrational lifetimes, vibrationally inelastic collisions, and vibrationally promoted electron emission all give strong evidence of the importance of the coupling of vibrational motion to EHP excitations. The theory of this coupling divides into two classes, weak coupling where the changes in vibrational state in a coupling event are small, and strong coupling where the changes can be large. The next two sections discuss these two approaches in turn.

Electronic friction

The introduction of an electronic friction in classical mechanical simulations to account for the dissipation of energy via EHP excitations arose first in calculations of the slowing of ions moving through metals[282–286] and was carried over to the interaction of atoms and molecules with metal surfaces.[287–291] There are two general strategies used to compute electronic friction.

The simplest and most often used is referred to as the LDFA and is based on the response of the free electron gas density at the position of the atom.[286] A number of methods have been employed to partition the local electron density computed by DFT into an atomic part and a free electron part, including carrying out a separate DFT calculation of the substrate without the adsorbate,[292,293] or adapting approximate models, such as embedded atom,[289,294] atoms in molecules,[198] or effective medium theory (EMT).[295–298] The sticking probability of H atoms on a number of transition metal surfaces is predicted to be dominated by EHP energy exchange.[289,292,296,298] LDFA calculations of the scattering of H atoms from Au(111) achieve good agreement with molecular beam results.[298] LDFA has also been employed to predict chemicurrents in the conduction electrons induced by scattering of H atoms from gold and silver surfaces.[297] In contrast to the dominance of EHP energy transfer in the interaction of H atoms with metal surfaces, calculations for H_2 on Cu(110),[299] H_2 on Ru(0001),[294] N_2 on W(110),[299] and N_2 on Fe(110)[300] indicate that EHP excitations appear to have little effect on molecular dissociative sticking probabilities. The LDFA has been applied to vibrational lifetimes of adsorbates as well.[198] There is controversy, however, about whether LDFA can accurately compute the full electronic friction tensor.[301,302]

The second strategy for incorporating electronic friction in molecular dynamics simulations of chemistry on metal surfaces is based on the Ehrenfest[162] mean-field theory of nonadiabatic dynamics. While Ehrenfest theory has been employed directly to describe nonadiabatic interactions of O atoms with graphite[303] and Li^+ ions with aluminum,[304] the computational time is substantial. However, in the weak coupling limit, the Ehrenfest equation can be transformed into a generalized Langevin equation: molecular dynamics with electronic friction,[305] with classical motion evolving on the ground state PES and subject to frictions and fluctuating forces arising from EHP transitions. The friction and random force satisfy the fluctuation-dissipation theorem,[306] such that the system properly approaches the desired temperature. In principle, the frictional terms include memory of the past evolution of the system. While memory effects may well be important to describe frequency-dependent friction due to, for example, electronic resonances or nonuniform densities of states, to our knowledge, memory effects have not been explored in this context. Rather, in practice, memory effects have been neglected. In this Markov limit, the equations that result for the electronic friction are given by FGR.[194–196,203] Note that the friction is a tensor of the components of the atomic velocity vectors, for example, for a diatomic molecule, it is a 6×6 tensor, and in general is not diagonal in either Cartesian or normal mode coordinates.[307] The implementation of FGR sometimes presents numerical difficulties, in part due to representing the electronic continuum by discrete levels. A DFT-based procedure, dubbed orbital-dependent friction (ODF), appears to overcome these issues and provides accurate and stable results.[308,309] ODF in the Markov approximation has been applied to compute lifetimes of the C-O stretch, CO-surface stretch, bend and frustrated translation vibrational modes of CO on Cu, Ag, Ni, and Pt surfaces, obtaining good agreement with experiment, where available.[308] One exception to this is CO on Au, where great care must be taken with electronic structure theory to ensure an accurate description of the physisorption binding in this system.[310] Importantly, the off-diagonal elements of the friction tensor are significant in some cases. ODF with electronic frictions computed on-the-fly for scattering and dissociative chemisorption of H_2 indicated that the major pathway for energy transfer was via the H-H stretching mode.[311,312] Moreover, they observed a dynamical steering due to tensorial friction that influenced the scattering. Overall, however, they observed a minor effect of nonadiabaticity on the probability of chemisorption,[313] in agreement with prior LDFA studies for H_2 on Cu(110)[299] and Ru(0001).[294] Recently, a symmetry-adapted neural network representation of the electronic friction tensor has been developed and promises to render ODF calculations quite practical.[314]

Independent electron surface hopping

The experiments shown in Figure 13 of the scattering of vibrationally excited NO ($v = 15$) from a gold surface[261] revealed huge amounts of energy transfer, with the vibrational distribution of scattered NO molecules peaking at $v = 7$ and 8. These results not only demonstrated unequivocally the importance of nonadiabatic EHP excitations, but also strongly implicated a mechanism of transient electron transfer from the surface to the NO molecule. Vibrationally promoted electron emission, discussed in the previous section, also implicates electron transfer. Electron transfer is clearly an example of strong coupling between the substrate electrons and the molecule, and casts doubt on the applicability of electronic friction theories of any sort, since they all rest on a weak coupling approximation. With a sufficiently large friction constant, a friction theory can account for large vibrational

energy transfer,[315] but it is not likely to be able to reproduce the detailed behavior that was observed in subsequent experiments (see Section 5.5 and Figure 15), and certainly cannot properly describe electron transfer. The observation of electron emission induced by impact of a highly vibrationally excited molecule on a low work surface (Section 5.6) is also clearly beyond the scope of friction theories, all of which would describe electronic excitation as a sequence of single vibrational quantum transitions.

Inspired by the NO/Au experiments, surface hopping theory[163] was extended[316] to treat nonadiabatic transitions among the continuum of electronic levels of a metal. This independent electron surface hopping (IESH) theory represents the metallic continuum by a coarse-grained set of N single electron levels, initially populated according to a Fermi function at the surface temperature. For the NO/Au system, application of IESH requires a diabatic $(N+1)\times(N+1)$ Hamiltonian matrix with the negative ion state of NO coupled to the N conduction electron states. The diabatic Hamiltonian was constructed as follows.[317] First, a 2×2 diabatic matrix was calculated. For a given nuclear geometry, the ground state energy and the charge on the NO molecule were computed by DFT. This produced two of the three pieces of information required to define a 2×2 matrix. The third piece of information was obtained by repeating the DFT calculation with a weak applied electric field in the direction of the normal to the surface plane. The approximation that the main result of the weak field was to lower or raise the energy of the negative ion state provided the third piece of information required to construct the 2×2 matrix. The 2×2 matrix was then expanded to the needed $(N+1)\times(N+1)$ diabatic matrix under two additional approximations: (1) the density of electronic states of the metal is assumed uniform, and (2) the coupling of the negative ion state to each conduction electron state was held constant. The diabatic Hamiltonian was then calculated for all relevant N, O, and Au positions and fit to analytical expressions. The IESH simulations were carried out by diagonalizing the diabatic Hamiltonian at every time step to obtain the $N+1$ energies as well as the nonadiabatic couplings, while integrating the time-dependent Schrödinger equation to obtain the instantaneous amplitudes of each excited state as required to determine stochastic hops between states. Simultaneously, the classical equations of motion were integrated for the atoms governed by the forces on the occupied electronic state. With $N = 60$–80 levels, the IESH simulations proved quite feasible.

The initial comparisons of the IESH simulations with the experimental results were quite encouraging. For example, Figure 12 shows a comparison of measurements (filled symbols) and IESH theory (open symbols) for multiquantum vibrational excitation for NO(v = 0) scattering from Au(111).[249] The agreement is good. In contrast, an electronic-friction calculation using the same Hamiltonian used in IESH severely underestimates the excitation probability.[249] However, later experiments revealed shortcomings of the IESH calculations,[267] notably that predicted sticking probabilities were too high due to an unrealistically attractive adiabatic PES.[318] This artificially enhanced IESH's predicted probabilities for multiquantum vibrational relaxation at low incidence energy and led to a fortuitous agreement with the experimental observations of Figure 13. When comparisons were made at high incidence energies, where trapping was absent in the theory, IESH predicted too little multiquantum vibrational relaxation. This is at least partly due to the fact that the adiabatic PES used here also has no dissociation channel. Since then, a more realistic PES has been developed, one that is less attractive and allows for dissociative adsorption of NO on Au(111).[319,320] Adiabatic calculations using this PES predict enhanced multiquantum vibrational relaxation, but still substantially less than seen in experiment. A renewed attempt to test IESH using this improved PES is warranted, but this will also require accurate calculations of excited and charge-transfer states. New electronic friction approaches have also been reported[315] and reproduce some of the data seen in the laboratory—but multiquantum vibrational relaxation is still not captured by friction theory as it predicts that only low energy EHPs can be excited.

IESH still appears to be the theory in front-runner status to eventually solve the problem of NO vibrationally inelastic scattering on noble metals and while it is tempting to assign much of the disagreement between simulation and experiment to the input PES used in IESH, other more fundamental issues may prove important. Specifically, the approximations invoked to construct the $(N+1)\times(N+1)$ diabatic Hamiltonian were relatively crude and remain untested. Further work to test IESH against available experimental results is clearly needed.

High-resolution inelastic scattering–Rydberg-atom tagging

Rydberg-atom tagging was a breakthrough for the experiments on the H_3 reaction—see Section 3.1—and it has proved similarly useful in surface scattering once the technical hurdles of implementing it for UHV were overcome.[321] Photolysis sources of H and D atoms provide atomic beams with narrow energy distributions and tunable hyperthermal energies, making possible many unique new experiments in surface reaction dynamics. Furthermore, the fact that the method excels for H atoms facilitates cooperation with theory.

H atom scattering from metals

The first experiments investigated inelastic scattering of H and D atoms from transition metal surfaces, aiming to observe the contribution of nonadiabatic electronic excitation to the energy loss. The mere fact that H atoms stick to metals with high probability is suggestive that there must be large contribution of EHP excitation to the energy loss, since otherwise, due to the mass disparity, it would not be possible for an incident H atom to lose enough energy to adsorb. Hence, it was long suspected that EHP excitation is needed for sticking of H at metals.[289,322] Furthermore, calculations of the energy loss by the best adiabatic methods predicted an energy loss of order 2%.[323] It appeared that Rydberg-atom tagging would easily provide the energy resolution necessary to detect any extra contributions to the energy loss due to nonadiabaticity.

Figure 17(a) shows the energy loss spectrum measured with Rydberg-atom tagging for H atoms incident on Au(111) with 2.76 eV

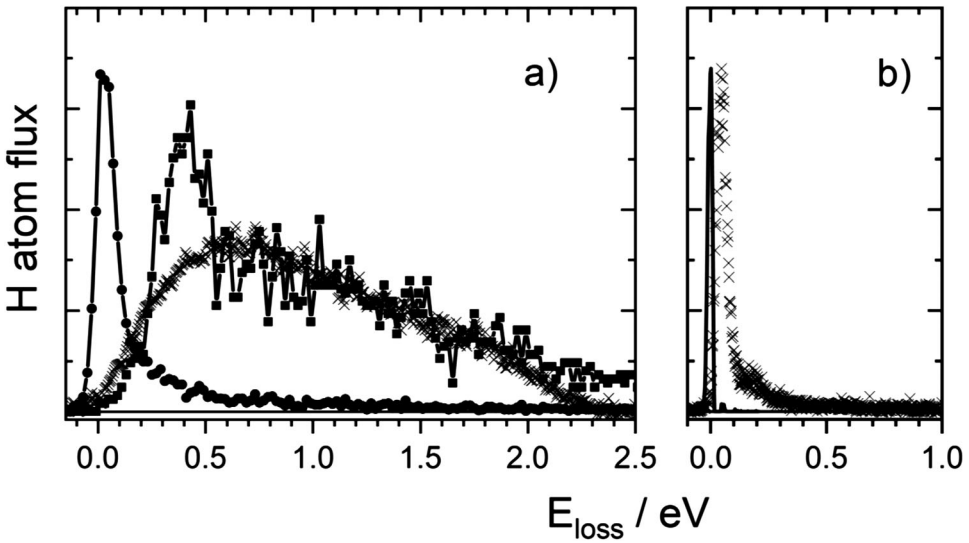

FIGURE 17 H atom scattering from Au(111) showing dominant participation of EHP excitation. (a) The experimentally derived energy loss for H scattered from Au(111) (×) compared to MD simulations carried out on an EMT PES and nonadiabatic electronic friction (squares)[295] and adiabatic MD simulations on the same PES (solid circles). (b) The experimentally derived energy loss for H scattered from solid Xe (×)—the black line shows the energy distribution of the incident H atom beam[298]

translational energy.[298] The energy loss peaks at 0.7 eV and extends to 2.3 eV, far higher than the energy loss derived from the best adiabatic models[323] and consistent with the idea that nonadiabatic excitation of EHPs dominates the energy loss. A comparison to scattering from an insulator (a multilayer Xe film adsorbed on Au), also shown in Figure 17(a), demonstrates the dramatically smaller energy loss when EHP excitations are eliminated. Figure 17(b) shows simulations of the scattering using a full-dimensional PES fitting an EMT function to DFT data, and a self-consistent treatment of adiabatic and nonadiabatic contributions at the level of the LDFA.[295] Calculations which include electronic friction (squares) agree well with the measurements (x's), while calculations done without nonadiabatic energy loss (closed circles) show far too little energy loss.

Both experiment and theory could be extended to H and D scattering from Pt, Ag, Pd, Cu, and Ni[296]. In each case, a PES was generated by fitting an EMT function to DFT data, using a genetic algorithm.[324] As with Au, there is excellent agreement between data and simulations for H and D atom scattering from these metals.[296] In all cases, EHP excitation dominates the energy loss—a small mass-dependent contribution to the energy loss from phonon excitation was also identified. Experimental and simulated angular distributions are also in good agreement—they are broad but clearly not due to trapping followed by thermal desorption. The results from metal to metal are so similar that one is tempted to conclude that there is a nearly universal behavior—the dynamics depend mainly on the metal's electron density and weakly on its mass.

Examination of the classical trajectories used for the simulations revealed that even at the high incidence energies of the Rydberg-atom tagging experiments, sticking is efficient. Analytic expressions were fitted to incidence energy, E_{in}, and angle, ϑ_{in}, dependent sticking coefficients, $S(E_{in}, \vartheta_{in}, M)$, derived from numerical simulations. This provides a practical way to estimate the sticking coefficient for H or D to any metal, by knowing only the metal's mass, M.

$$S\,(E_{in}, \vartheta_{in}, M) = (S_0 + a \cdot E_{in} + b \cdot M) \times \left[1 - h\,(\vartheta_{in} - c)\left(1 - \cos(\vartheta_{in} - c)^{d \cdot h(E_{in}-e)(E_{in}-e)}\right)\right] \quad (2)$$

where h is the Heaviside step function and the parameters for H are given by:

$$S_0 = 1.081,\ a = -0.125\ \text{eV}^{-1},\ b = -8.4 \times 10^{-4}\ \text{u}^{-1},\ c = 28.88°,\ d = 0.443\ \text{eV}^{-1},\ e = 1.166\ \text{eV};$$

and for D by:

$$S_0 = 1.12,\ a = -0.124\ \text{eV}^{-1},\ b = -1.2 \times 10^{-3}\ \text{u}^{-1},\ c = 28.62°,\ d = 1.196\ \text{eV}^{-1},\ e = 0.474\ \text{eV}.$$

We give these parameters in this review as an erratum[325] was published clarifying the parameters that might be overlooked in a perusal of the primary literature.

Similar to what was possible for formaldehyde roaming reactions (Section 3.2), animations of H atom trajectories reveal the atomic scale mechanisms of adsorption of H atoms on metals. Figure 18 shows such an animation. Remarkably, adsorption trajectories involve H-atom penetration to the first subsurface layer, where it remains trapped for ~250 fs until sufficient energy can be transferred to nearby surface gold atoms opening an "escape hatch." It then returns to the surface still with a substantial fraction of its initial translational energy and equilibrates over about 1 ps.[295] This should not be entirely surprising. Electronically adiabatic simulations show H atoms penetrating and even passing through a four-layer thick slab of *fcc* Au.

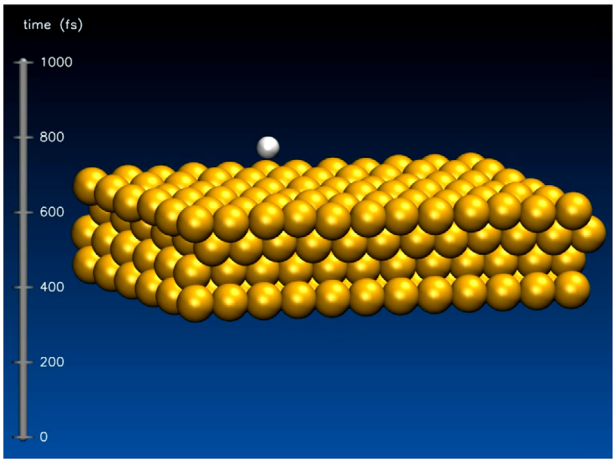

FIGURE 18 The dominant mechanism for H atom adsorption involves penetration and resurfacing. This animation shows a single MD trajectory, where an incident H atom moves under the influence of the Born–Oppenheimer PES and a drag force induced by electronic friction. The trajectory has an initial kinetic energy of 2.7 eV[295]

Imaging covalent bond formation: H atom scattering from graphene

H atom adsorption on graphite or graphene is quite different from its adsorption on metals—it is an activated process driven by covalent C-H bond formation and $sp^2 \rightarrow sp^3$ re-hybridization of the C-framework is required to make this happen.[326,327] Studying the scattering of H and D from graphene with tunable incidence energies above and below the barrier to adsorption thus presents an opportunity to probe the dynamics of transient bond formation. Experimentally, the H or D energy is tuned by varying the incidence angle, θ_i, while holding the incidence energy, E_i, constant, as only the normal component of the incidence kinetic energy, $E_n = E_i \cos^2(\theta_i)$, is effective in overcoming the barrier.

Figure 19(a–c) shows H atom scattering flux maps for $E_i = 1.9$ eV, where $E_n = 0.49$, 0.78, and 1.11 eV, respectively.[328] For the lowest value of E_n, H atoms lose little energy (quasi-elastic), but as E_n increases, a second peak appears exhibiting ~1 eV energy loss. At the highest E_n, almost no quasi-elastic scattering is seen. The narrow angular distributions seen under all conditions rule out trapping and raise the question of how a light H atom can lose so much energy in a sub-picosecond collision. Theoretical simulations of the scattering provide an answer to that question.[329]

Figure 19 panels(d–f) show the simulation results, which are a good example of the power of current computational techniques for surface reaction dynamics. Here, a high-dimensional neural network (HDNN) was used to provide a representation of the H-graphene PES. Importantly, the PES is a function of both H and C atom coordinates and accurately represents the potential for large displacements of the C atoms from their equilibrium positions in graphene. This was achieved by using machine learning algorithms to train the HDNN to energies calculated with DFT, including configurations of the H and C atoms from *ab initio* molecular dynamics (AIMD) (on the fly DFT) trajectory calculation.[329] The comparison between simulations, based on hundreds of thousands of trajectories, and the experimental results is remarkably good.

The success of the trajectory simulations allows us to learn more about the process of covalent C-H bond formation and other scattering phenomena seen in experiment. Figure 20 shows two animated trajectories representative of the quasi-elastic channel and transient chemical bond formation, respectively. For the quasi-elastic channel, one sees little change to the C-C motion, while the H-atom is scattered in a plane near the specular direction. For transient chemical bond formation, the H-atom scattering on average remains close to the specular angle, but there is a high probability for the trajectory to emerge in a plane

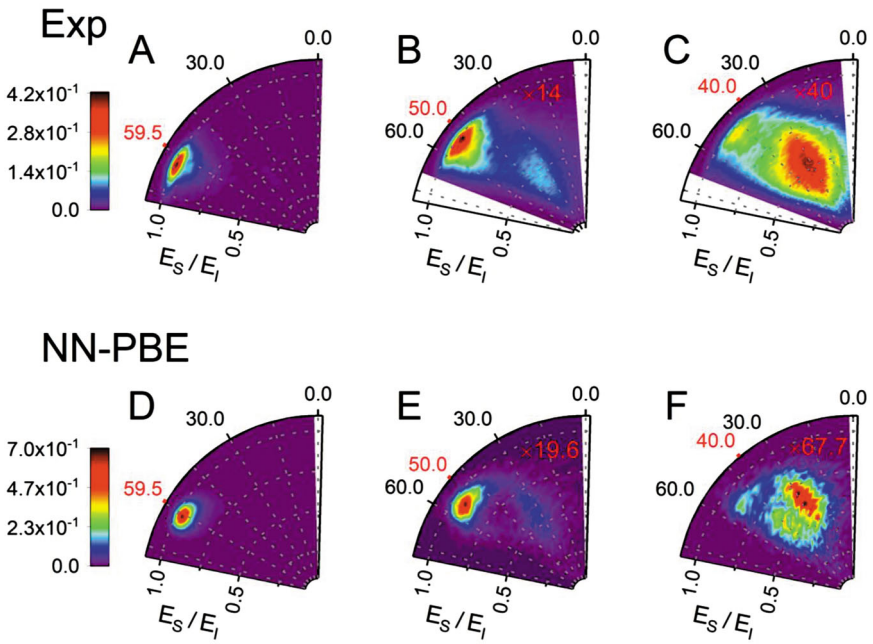

FIGURE 19 Comparison of experiment[328] (panels a–c) and theory[329] (d–f) for H atom scattering from graphene at a translational energy of incidence $E_i = 1.9$ eV. The experiments were done on graphene grown on Pt (111), while the theory is for free standing graphene. $E_n = E_i \cos^2(\theta_i)$, varied by changing the incidence angle, θ_i (indicated in red) is 0.49, 0.78, and 1.11 eV for panels a and d, b and e, and c and f, respectively. The polar plots give the scattered flux as a function of scattering angle and ratio of the energy of the scattered H atoms, E_S and E_i. The flux is multiplied by the factors shown in red in panels b, c, e, and f. Reprinted from Jiang HY, Kammler M, Ding FZ, et al. Imaging covalent bond formation by H atom scattering from graphene. Science. 2019;364(6438):379, Copyright 2021, with permission from AAAS

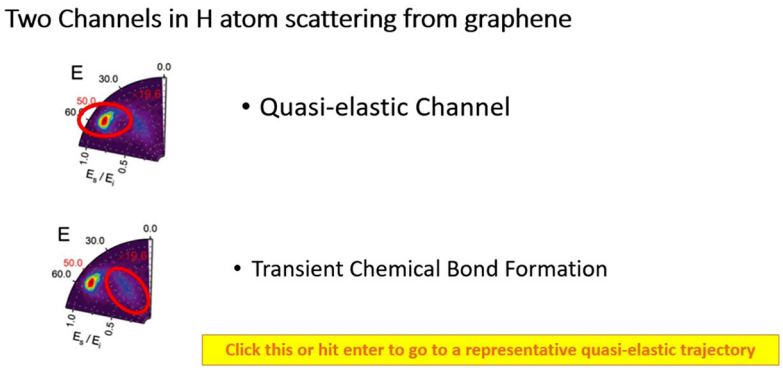

FIGURE 20 The trajectories found in molecular dynamics simulations of H scattering from graphene. Top and side views visible simultaneously

rotated from that of the quasi-elastic trajectory. The directional forces involved in the transient C-H bond formation are responsible for this.

From analysis of trajectories like this, a simple but perhaps unexpected picture emerges. For transient chemical bond formation, the H atom approach triggers an electronic change to the system within about 10 fs, where the attacked C-atom in the graphene experiences a partial electronic rehybridization from sp^2 to sp^3. Of course, this also affects the electronic bonding to its neighbors. The fastest response to this electronic change is to excite in plane C-C stretching. In fact, it is the next nearest neighbor C-atoms (and not the C-atom being attacked by the H atom) that begin moving first. Only later does the H-attacked C-atom begin to pucker out of plane, exerting a drag on the departing H atom. The transfer of energy to these four atoms accounts for most of the large energy loss observed in experiment.

It is worth noting that the energy loss seen here is actually much larger than anything seen for H atoms scattered from metals. The adiabatic (i.e., mechanical energy transfer) is so efficient due to the transient chemical bond formation that it is difficult to rule out (or in) the possibility of EHP excitation. It is also worth considering that the simulations have neglected the presence of the underlying substrate—the experiments were done with graphene grown on Pt(111). It would be very interesting to see how H atom inelastic scattering depends on variation of the substrate. Experimentally, one may grow graphene on a variety of materials. Theoretically, it would appear possible to extend neural networks and DFT to include the substrate in simulations.

The examples shown so far have been restricted to studies of inelastic scattering, but they have already brought some of the features of adsorption into focus. We now turn to a systematic presentation of the dynamics of adsorption and desorption.

ADSORPTION–DESORPTION

Basic definitions and concepts

Adsorption, and its reverse process desorption, are two of the dynamically simplest yet most important chemical reactions occurring at surfaces. Consider a gas-phase molecule AB, which can remain intact upon adsorption, $AB \rightarrow AB^*$, or it can break apart, $AB \rightarrow A^* + B^*$, called molecular and dissociative adsorption, respectively. Note, we use *s, throughout, to indicate adsorbed species. Reversing the direction of

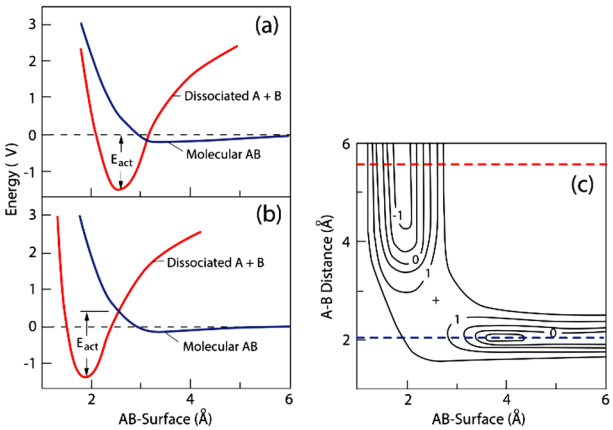

FIGURE 21 Lennard-Jones view of dissociative adsorption. Blue curves represent the potential energy of an intact AB molecule as it approaches the surface; red curves represent the potential energy of molecular fragments A and B. (a) Nonactivated adsorption: here, the energy of the crossing point (transition state) is lower than that of the gas-phase molecule. (b) Activated adsorption: here, the transition state is higher than the asymptotic energy. (c) A 2D PES makes the situation clearer

the arrows in these two reactions, a molecule can desorb intact—molecular desorption—or undergo "recombinative desorption."

In 1932, Lennard-Jones[330] presented a 1D picture of dissociative adsorption—see Figure 21(a) and (b). This view involves an undissociated *AB* molecule's potential (blue curves) and a potential for the dissociated fragments *A*· and *B*· (red curves). In fact, the blue and red curves do not intersect—a two-dimensional PES—Figure 21(c)—is needed to see that the transition state (+) is not located on either curve. These reactions are best described as concerted motion along a multidimensional PES, with many of the same issues arising that influence gas-phase dynamics: curvature of the reaction path, early or late transition states, distribution of energy among degrees of freedom, molecular orientation, and so forth. Many additional features not present in gas-phase reactions influence reactions at surfaces, including energy dissipation, surface corrugation, or surface defects, steps, and other special reaction sites. The rate of desorption is one of the most accessible kinetics measurements in surface chemistry. Temperature programmed desorption detects the rate of desorption as the temperature is ramped. The rate is measured from high to low adsorbate coverage, θ,

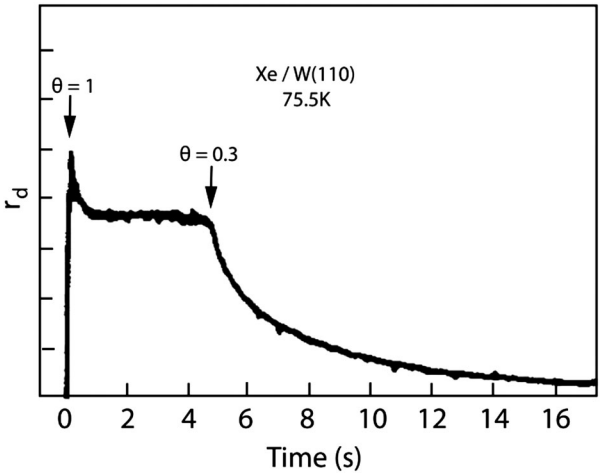

FIGURE 22 The isothermal desorption of a full monolayer of Xe from W(110) at 75.5 K. The rate of desorption is measured with a mass spectrometer after a rapid temperature jump with a slight overshoot. The rate is initially independent of coverage—0th order—indicating that desorption takes place from the edges of large islands. At this temperature, a phase transition occurs at a coverage of 0.3 monolayers and the islands evaporate into a "2 D gas." Ordinary first-order kinetics are then seen.[331,332] Reprinted from Opila R, Gomer R. Thermal-desorption of XE from the W(110) plane, Surf Sci. 1981;112(1-2):1-22, Copyright 2021, with permission from Elsevier

that is, the number of adsorbed molecules per unit area on the surface, which plays the role of concentration in gas-phase kinetics.

Influence of coverage on adsorption and desorption

The dependence of desorption rates on coverage can be complex and sometimes mystifying. Figure 22 shows a beautiful example, the isothermal desorption of Xe from W(110). The presence of attractive interactions between adsorbates can have striking effects on desorption rates. Here, there is a sharp change of slope in the rate which arises when a first-order two-dimensional phase transition occurs at $\theta = 0.3$.[332] The free energies of the two phases are continuous through the transition, but the enthalpies and entropies that control the rate of desorption can be very different.[332]

Influence of steps on desorption

Desorption can also take place from different surface sites, for example, from terraces and steps. The step desorption's pre-factor can be several orders of magnitude larger than that of terrace desorption.[333] This is an entropic effect where a step-bound adsorbate is constrained to live in a lower entropy 1D world compared to a terrace bound species. The reduced entropy of the adsorbate dramatically enhances the desorption rate.

Peculiar coverage dependencies can arise when adsorbates are able to diffuse to defects, which commonly bind molecules more strongly than do terraces.[334] Figure 23(a) and (b) shows the energetic landscape and the desorption measurements, respectively. In experiment, the initial rate of desorption is rapid—terrace desorption—until the terrace sites are empty and then desorption decelerates being limited by the rate of step to terrace diffusion.[335]

Detecting trapping/desorption

In the previous section, we have seen the results of many beautiful experiments that infer the nature of molecule–surface interactions from measurements of the quantum state, speed, and angular distributions of molecules undergoing direct scattering, conditions where the molecule has no time to reach equilibrium with the solid. Langmuir considered this process of molecular "reflection" already in 1917 and pointed out the importance of and difficulty associated with distinguishing "reflection" from condensation followed by evaporation.[336] With the experimental tools now available, this is readily accomplished. See Figure 24.

Using a molecular beam with a narrow velocity distribution, Xe atoms scattered from Pt(111) exhibit distinctly bimodal TOF distributions, the slower fraction trapping and then desorbing, while the faster fraction scatters directly.[337] The angular distribution of direct scattering is also much narrower than that of trapping/desorption. Naturally, the residence time and the speed distribution of trapping/desorption depends on T_S. Figure 24(e–j) shows vibrational state-to-state TOF experiments.[310] Here, CO($v = 2$) is prepared in a molecular beam just 0.5-mm before collision with a Au(111) surface. The returning CO molecules are state specifically detected about ~1-cm away from the surface by REMPI and their TOF recorded by scanning the delay between the two laser pulses. Just as for Xe on Pt(111), two contributions to the speed distribution are seen. As the residence time is similar to the vibrational relaxation lifetime of CO($v = 1, 2$) on Au(111),[199] the trapping/desorption component detected in vibrationally excited states of CO appears to increase with T_S. This system has also been studied by molecular dynamics on an HDNN PES.[338] Inspired by ideas developed in this work, it was possible to show that collisions of CO on Au(111) first pass through a metastable chemisorption well before partially equilibrating in a physisorption well, the lowest energy surface binding site.[310]

Detailed balance, or why the desorption rate depends on the sticking probability

The properties of thermal equilibrium can be used to great advantage when studying trapping and desorption. To see this, consider adsorption in the language of TST, where the flux through a "point of no return" dividing plane in the adsorption direction is:

$$F_{TST}(\theta, T) = \frac{k_B T}{h} Q_{2D} e^{\mu(\theta,T)/k_B T} \quad (3)$$

where k_B is Boltzmann's constant, $\mu(\theta, T)$ is the chemical potential of the gas, Q_{2D} is a simplified two-dimensional ideal gas partition function for a noninteracting adsorbate, and h is Planck's constant—see Ref. [339] and Figure 25.

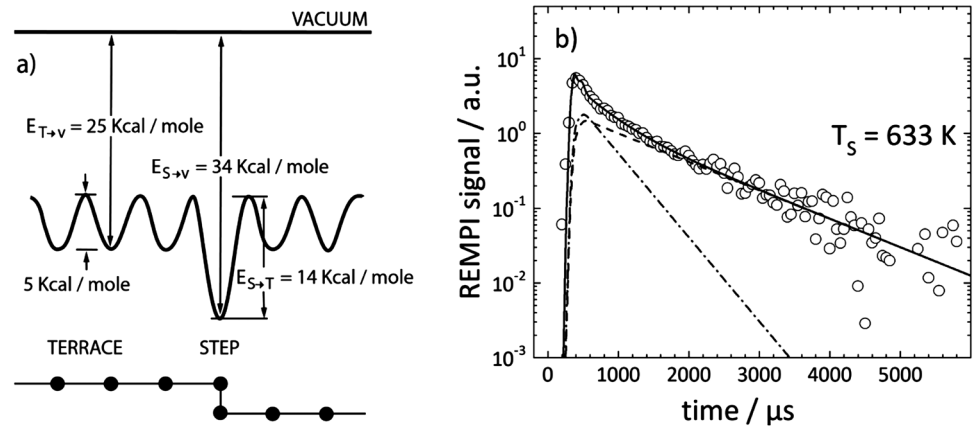

FIGURE 23 Desorption from steps and terraces. (a) Model of NO binding at steps and terraces of Pt(111) developed to describe: (1) thermal desorption from terraces and (2) thermal diffusion from steps to terraces followed by thermal desorption.[334] (b) Experimentally observed bi-exponential desorption predicted by this model of CO desorption from Pt(111).[335] The fast component is simple desorption from terraces, while the slow component is a sequential process involving thermal diffusion from steps to terraces followed by desorption from terraces

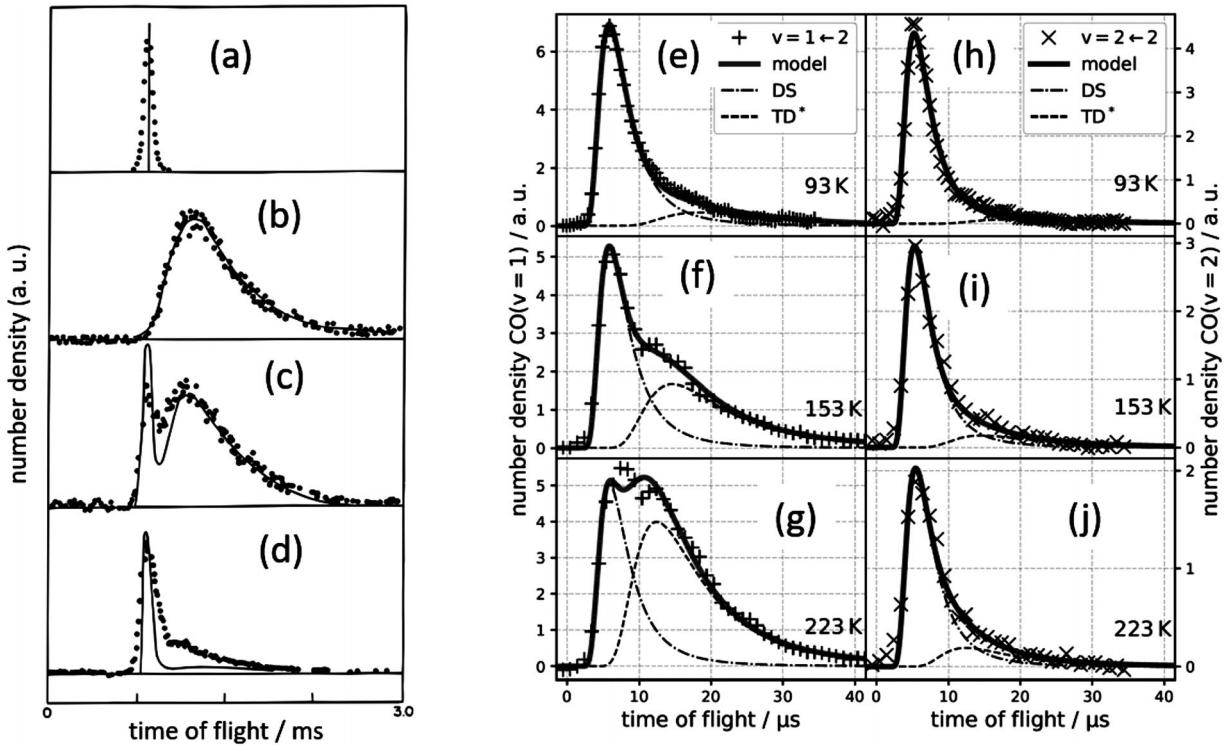

FIGURE 24 Distinguishing direct scattering from trapping/desorption. (a–d) TOF measurements of Xe scattering from Pt(111). (a) Xe beam incident at 75° from the surface normal with $E_i = 0.14$ eV; also shown are scattered Xe detected at: (b) 0°, (c) 45°, and (d) 75°. The fast feature is direct scattering, while the slow feature is trapping desorption.[337] The solid lines in (a–d) are MD simulations—the circles are from experiment.[10] (e–j) State-to-state TOF measurements of CO scattering from Au(111) (+). A pulsed beam of CO($v = 2$) collides with Au(111). REMPI detects specific vibrational states of scattered CO several cm from surface and the TOF is recorded. Both direct scattering and trapping desorption are seen, proving that CO($v = 2$) can survive a trapping desorption encounter with Au(111)[310]

Of course, some molecules that pass through the dividing plane may not trap, but instead bounce back from the surface introducing a recrossing correction that is the sticking probability, $P_S(\theta, T)$. The recrossing corrected TST rate of adsorption then becomes:

$$R_{ads} = P_S(\theta, T)\, F_{TST}(\theta, T) \tag{4}$$

Note that at equilibrium, the adsorption and desorption rates must balance.

$$R_{des} = R_{ads} = P_S(\theta, T)\, F_{TST}(\theta, T) \tag{5}$$

Remarkably, the rate of desorption is proportional to the sticking probability—this is, at first glance nonintuitive, but it expresses the

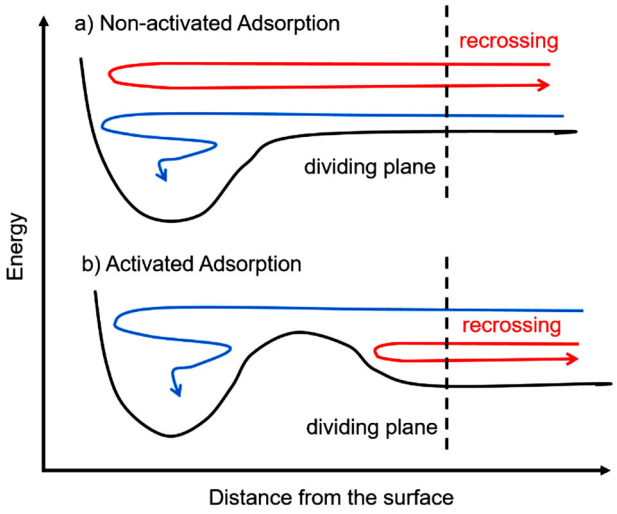

FIGURE 25 Transition state theory of adsorption and desorption. It is convenient to define the point of no return to be a plane parallel to the surface at large distance. When this is done, the thermal sticking coefficient can be used to correct the recrossing error in TST. (a) High-energy molecules are less likely to stick. This appears as a recrossing error in TST. Consequently, desorption rates are higher for low energy molecules and the translational temperature of desorbing molecules can be lower than T_S. (b) Low energy molecules are more likely to recross and energy distributions of desorbing molecules can be hyperthermal

principle of detailed balance. The nonequilibrium dynamics of desorption is encoded in the sticking probability's dependence on incidence conditions, coverage, and temperature.[340]

In fact, Equation (5) can be written in terms of the speed, s, angle, ϑ, and quantum state (v, J, M)-specific sticking probabilities.

$$P_S(\vartheta, s, v, J, M) F_{TST}(T) = R_{des}(\vartheta, s, v, J, M,) \quad (6)$$

Measurements of state-specific and velocity-resolved rates of desorption reliably predict their corresponding sticking probabilities.[341,342]

Application of detailed balance

The analysis of the velocity distribution of the trapping-desorption fraction for Ar scattered from hydrogen-covered W(100)[343] showed that at low T_S the mean energy of desorbed atoms was $2k_BT$, in accord with a Maxwellian distribution at the T_S. This is consistent with a near-unity trapping probability at low gas and surface temperature. At higher surface temperatures, the mean energy of the desorbed atoms was markedly lower than $2k_BT$, consistent with a decrease of the trapping probability at higher gas and surface temperatures. Furthermore, at low surface temperatures, the trapping-desorption fraction obeyed the $\cos\vartheta$ angular distribution required if the sticking probability were unity, but at higher surface temperature, the angular distribution was observed to be broader than $\cos\vartheta$. This indicates that the trapping probability depends more strongly on the component of gas momentum normal to the surface plane than parallel to it, resulting in a larger decrease of normal momentum than parallel. Molecular beam and computational studies of Ar scattered from Pt(111)[344] confirm that momentum in the normal direction is accommodated more rapidly than the parallel component, and that at higher surface temperatures for which the Ar residence time is less than 100 ps, atoms desorb prior to accommodating their parallel component of momentum.

Dissociative adsorption and recombinative desorption of molecules is more complicated and more interesting than that of intact adsorption/desorption. The sticking probability, in principle, can depend on not only the surface temperature and the initial translational energy and angle of approach of the molecule, but also on its initial electronic or spin-orbit state, the initial vibrational state, the initial rotational energy and polarization, and the initial orientation of the molecule. The design and fruition of extraordinary spectroscopic and molecular beam techniques, coupled with advanced computational modeling, has provided detailed and quantitative knowledge of the dynamics of molecular bond-breaking and making at surfaces.[345] Recently, detailed balance together with an elaborate microkinetic analysis has been used to show that adsorption to a physisorption well may be facilitated by transient chemisorption in a metastable well with stronger molecule surface interactions.[310]

DYNAMICS OF REACTIONS AT SURFACES

Even prior to the quantum revolution, Langmuir and others were thinking about atoms and molecules on surfaces.[346,347] Langmuir's brilliant interpretations of simple yet rigorous experiments led him to intuit key aspects of possible reaction mechanism at surfaces,[1] one where surfaces resemble a checkerboard[348] on which every square can be occupied by only one atom or molecule.[349] Through adsorption and diffusion, molecules and atoms end up on neighboring squares and react with one another. Reactions and desorption remove molecules from the surface creating empty spaces for subsequent adsorption to occur. The elementary steps (highlighted above in bold) of this so-called Langmuir–Hinshelwood (LH) mechanism have all become central topics in the study of reactions at surfaces.

An alternative to this mechanism is that of Eley and Rideal.[350] In this "ER" mechanism, a gas-phase atom or molecule collides at the binding site of a chemisorbed atom or molecule and reacts without coming into thermal equilibrium with the solid. Modern experimental methods readily distinguish LH from ER, since the energy available to the products is typically much higher for ER reactions than for LH[351]—less chemical energy is lost to the solid[351]—and ER reactions exhibit a "memory effect,"[352,353] where the speed, angle, or quantum state of the incident reactant influence the speed, angle, and quantum state of the product. This is obviously not the case for an LH reaction where the reactants equilibrate with the solid before reaction.

Intrinsic to LH is the idea that adsorbed reactants thermalize with the surface and that products form at a speed controlled by thermal reaction and diffusion. Nevertheless, LH reactions can produce

hyperthermal products—for example, when two adsorbed H atoms thermally desorb from a copper surface, they must overcome a substantial barrier; the H_2 formed at the barrier has no time to equilibrate with the solid and is ejected from the surface with a great deal of translational (and vibrational) energy.[354] These nonthermal effects lend themselves to state, speed, and angle-resolved experiments that are particularly sensitive to the PES of the reaction in the vicinity of the transition state, allowing the extension of the dynamical approach from the gas-phase to reactions at surfaces.

This section contains highlights of work on nonthermal ER reactions and direct dissociative adsorption, together with an exposition of the problems of measuring and predicting the rates of thermal reactions. Arguably, the most important goal of the dynamical approach for surface chemistry is to accurately predict thermal reaction rates—see, for example, Ref. [355]. Thermal surface reactions are by far the most common in nature and most required for practical use. Predicting thermal rates represents the true payout for a highly developed theoretical understanding. For this, we need detailed dynamical experiments capable of probing the key features of the PESs of elementary reaction steps, thereby testing the computational methods used to generate them. We also need means to determine reaction mechanisms—LH versus ER for example—but even more basic than that, we must find out which elementary reactions are important, and determine the active sites of those reactions.

Vibrational and translational promotion of surface reactions

H_2 on copper

One of the best understood systems is the reaction $H_{2(g)} \overset{Cu(111)}{\longleftrightarrow} 2H^*$, which has been studied in both directions and for different isotopologues and previously reviewed.[8] The reaction has served a similar role for the theoretical development of surface chemistry as the H_3 reaction has for gas-phase reactions. Experiments on dissociative adsorption and associative desorption show that there are two reaction mechanisms, an activated dissociation process that is promoted by both reactant vibration and translation[356] and another, still unexplained reaction inhibited by translational energy but promoted by vibration.[357,358]

The translationally activated reaction and corresponding measurements on the reverse process exemplify the principle of detailed balance.[342,359,360] Some of the best information on dissociative adsorption comes from the application of detailed balance to associative desorption in hydrogen permeation experiments, where recombining $H_{2(g)}$, $HD_{(g)}$, or $D_{2(g)}$ are state-specifically ionized with REMPI and by field free ion TOF, their velocities are obtained. The hydrogen molecule's motion depends on four quantities, $H_2(v, J, M, \vec{v})$—the quantum numbers for molecular vibration, rotation, alignment, and the velocity vector. Ro-vibrational state resolved reaction thresholds, $E_0(v, J)$, provide the magnitude of translational energy needed for each ro-vibrational state to react. These can be determined both experimentally[357] and theoretically[345] and agreement is good. Analogous work has extended this to include alignment effects, where $E_0(v, J, M)$ is measured[361,362]—H_2 with its bond-axis parallel to the surface requires less translational energy to react than molecules with another alignment. This confirms aspects of the transition state structure for the reaction, where the H – H bond lies parallel to the surface over a bridge site of Cu(111).[363] The reaction has also been studied in this way on stepped surfaces $2H^* \overset{Cu(211)}{\longrightarrow} H_{2(g)}$. Unlike many surface reactions, here steps are somewhat less reactive than terraces.[357]

Application of the dynamical approach to this reaction involves improving theory to reach agreement with data like that just described, in this case optimizing a Born–Oppenheimer PES, using a semi-empirical specific reaction parameter (SRP) functional.[363] The fact that this has proven possible is apparently due to the fact that the most important complications anticipated in moving from the gas phase to metal surfaces—the influence of phonons and EHPs—do not appear to affect this reaction greatly.[364]

HCl on gold and silver

The situation appears to be much more challenging for the reaction $HCl_{(g)} \overset{Au(111)}{\longleftrightarrow} H^* + Cl^*$. Inelastic scattering probabilities for collisions at Au[266] and Ag[264] were measured as a function of surface temperature and incidence energy of translation. These results suggest that hot EHPs excite H – Cl interatomic motion efficiently near the transition state for dissociative adsorption. The dissociative adsorption probability's dependence on vibrational and translational incidence energy was also measured with a hot-nozzle technique.[365] The experimentally derived reaction probabilities were much smaller than predicted by theories using a 6D Born–Oppenheimer PES with quantum wave packets.[366] Some improvement was found using a different functional.[367] Classical AIMD calculations that allow the surface atoms to move also failed to bridge the gap to experiment[368]; furthermore, the reaction path and barrier height depend strongly on choice of functional.[369] A new PES has been developed with a higher reaction barrier but agreement with experiment is still poor.[265]

In related work on the ER reaction: $H_{(g)} + Cl^* \overset{Au(111)}{\longrightarrow} HCl_{(g)}$, AIMD calculations produced HCl vibrational excitation far larger than that seen in experiment. By including LDFA friction, vibrational excitation was reduced[370] and trajectories showed H atoms lose energy before reacting with Cl^*, a plausible influence of electronic friction on reactivity. But the HCl vibrational distribution was still much hotter than seen experimentally—compare figure 18 of Ref. [352] with figure 2 of Ref. [370], possibly an indication of the limitations of the LDFA.

While the research on this reaction, so far, is no success story, it is without doubt one of the most interesting for future study. It has recently been suggested that for reactions where the difference between the surface' work function and the electron affinity of the adsorbate is smaller than 7 eV, DFT-GGA calculations of barrier heights may be unreliable.[371] As seen in Figure 15, it is precisely under these conditions that electronically nonadiabatic coupling between

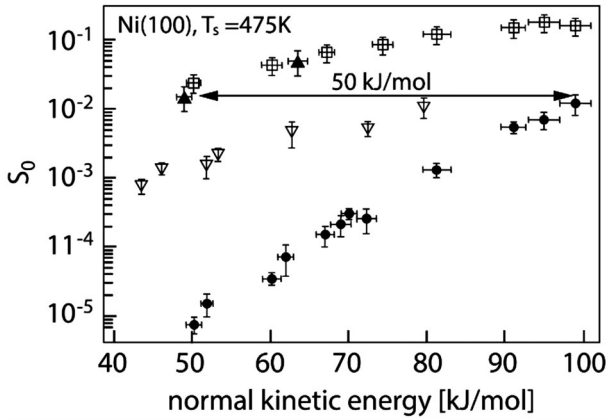

FIGURE 26 State-resolved sticking coefficients, S_0, for $CH_{4(g)}$ in the ν_1 (▲), $2\nu_3$ (□), ν_3 (∇), and ground (•) vibrational states on Ni(100) as a function of incident kinetic energy normal to the surface.[379] Reprinted with permission from Maroni P, Papageorgopoulos DC, Sacchi M, Dang TT, Beck RD, Rizzo TR. State-resolved gas-surface reactivity of methane in the symmetric C-H stretch vibration on Ni(100). Phys Rev Lett. 2005;94(24):246104, Copyright 2021 by the American Physical Society

adsorbate nuclear motion and the solids EHPs may become important. In fact, there is strong experimental evidence that this reaction[266] and the analogous reaction on Ag(111)[264] may be strongly influenced by such nonadiabatic coupling. Hence, this reaction presents a challenge to theory's ability to accurately calculate adiabatic electronic energies as well as nonadiabatic dynamics. Meeting those challenges will no doubt lead to better theoretical methods and deeper understanding.

Dissociation of polyatomic molecules on metal surfaces

Both theoretical and experimental studies of the vibrational and translational promotion of surface reactions have extended to those involving reactants with more than two atoms. Some of the reactions that have attracted attention include: $CH_{4(g)} \xrightarrow{Ni,Pt} CH_3^* + H^*$,[372–375] $H_2O_{(g)} \xrightarrow{Ni,Cu} OH^* + H^*$,[372] $NH_{3(g)} \xrightarrow{Ru} NH_2^* + H^*$,[376] $CO_{2(g)} \xrightarrow{Ni} CO^* + O^*$,[377] and $CH_3OH_{(g)} \xrightarrow{Cu} CH_3O^* + H^*$.[378]

The influence of vibrational excitation on dissociative adsorption was first seen by changing the beam source temperature and seed gas to thermally excite CH_4 vibrations.[380,381] This influence of vibration is more cleanly seen with laser pre-excitation of the molecule, where a molecular beam of methane with controlled translational energy is excited by a c. w. infrared laser with high power and coherence producing selected vibrational states. Auger electron or reflection absorption infrared spectroscopy (RAIRS) is then used to look for the buildup of reaction products on the surface.[375] Studies like this have demonstrated mode specificity[379,382,383]—see Figure 26—and bond selectivity[384] as well as steric effects[385] in chemisorption reactions, highlighting the nonstatistical and complex nature of gas–surface reaction dynamics.[373] These studies have also demonstrated that surface atom motion plays an important role in determining the ease with which the gas-phase molecule surmounts the reaction barrier.[386] It is even possible to reveal the dynamics of reaction at specific surface sites.[387]

While the many degrees of freedom of methane make full-dimensional quantum calculations challenging,[388] an approximate 15 DOF quantum method has been demonstrated using a reaction path Hamiltonian,[389] originally developed for gas-phase problems.[390] The "quantum reaction path" method provides an accurate description of the translational motion and nine internal molecular DOFs of methane, and while a vibrationally adiabatic basis set is used, all vibrationally nonadiabatic couplings are included. This method was the first to succeed in capturing mode-specific reactivity like that shown in Figure 26. It also avoids an artifact of classical mechanics, where zero point energy can flow within the molecule—such effects are difficult to avoid when using QCT and AIMD trajectories.[391]

Beyond this, the quantum reaction path method also helped reveal the influence of surface atom motion on the reaction, seen experimentally as a strong surface temperature dependence of the reaction probability.[392] DFT calculations show that the barrier to dissociation is modulated by the out-of-plane motion of the metal atom most intimately involved with the transition state.[393] For methane on Ni, the effect of this on the reaction probability was treated in an approximate way, using a lattice sudden model,[394,395] which effectively averages over the barrier height and momentum distributions along the reaction coordinate produced by thermal motion of the Ni atom.[396] More recently, this approximate scheme has been validated by 8D quantum dynamics calculations on a 14D PES.[397] This and the previous studies all conclude Ni-lattice motion is involved in the reaction.

Observing adsorbed reaction intermediates and products with surface-site specificity can be achieved using RAIRS to detect products, and preparing state-selected reactants in a molecular beam. Using CH_3D with either the C – H or C – D bond pre-excited, RAIRS can distinguish adsorbed products—CH_3^* or CDH_2^*—at different surface sites.[387,398] For reactions on Pt (211), at low incidence energies of translation and without vibrational pre-excitation, only dissociation at steps was observed, without isotopic selectivity. However, with vibrational pre-excitation of the C – H bond, only infrared absorption corresponding to CDH_2^* bound at steps could be seen at low incidence energies of translation. At higher translational energy, dissociation at terraces appeared and bonds without vibrational excitation became more reactive.[399] Note that under the conditions of these experiments, CH_3^* diffusion is believed to be unimportant. The authors concluded that the barrier to reaction at steps is at least 0.3 eV lower than at terraces[387]—DFT predicted barriers for dissociation at steps and terraces of 0.55 eV and 0.82, respectively, when using an SRP functional.[400]

The dissociation of water on metals has also attracted attention, inspired by vibrational state selected molecular beam measurements of dissociation probabilities for the reaction $D_2O_{(g)} \xrightarrow{Ni(111)} OD^* + D^*$.[401] Here, vibrational efficacy is larger than the translational, probably related to the late barrier to reaction[401]—see the Polanyi rules (Section 2.1).[48] The quantum reaction path method was also applied and after rescaling the barrier height, good agreement with experiment was found.[402] These calculations exhibited bond

selective dissociation for HOD and again, a strong influence of surface atom motion. A nine DOF PES was also produced and site specific reactivity could be studied[403]; a site averaging model was also tested.[404] Scientists have also begun to explore the properties of water dissociation on other surfaces, like Cu,[405,406] AgNi,[407] and Cu/Ni alloys.[408,409]

In contrast to these reactions, where the molecule travels over the dissociation barrier on a sub-picosecond time-scale, LH involves newly adsorbed reactants rapidly equilibrating with the solid. Does one then expect vibrational promotion of LH reactions? Recently, the vibrational relaxation lifetime of molecules bound by physisorption interactions has been measured to be ~50 ps,[199] more than an order of magnitude longer than vibrational relaxation for chemisorbed molecules.[190,410] This helps to explain why it is possible to observe the trapping followed by thermal desorption of a vibrationally excited molecule.[411] These observations suggest that while the LH mechanism involves thermalization of reactant translation and rotation, reactant vibration may relax more slowly and may live long enough to accelerate surface reactions prior to the vibrational energy being lost to the solid.

In an experiment similar to those described in Ref. [375], CH_4 dissociation probabilities on Ir(111) were obtained for selected vibrational states as a function of translational energy.[412] QCT simulations on a PES that had been fitted to 5000 DFT points were performed to obtain the sticking probability dependence on surface temperature as well as incidence translational and vibrational energy of CH_4. Remarkably good agreement with experiment was found.[412] Further analysis of the trajectories showed that at low incidence energy, adsorbed molecules with unrelaxed vibrational excitation could dissociate with higher efficiency than vibrationally cold molecules. TST rate calculations assuming the precursor-mediated mechanism suggested that vibrationally excited states might react at surface defect sites.[413] It is well known that while molecules initially adsorb to majority sites, diffusion to minority defect sites like steps is often much faster than desorption and reaction rates at these defects can be much higher than at majority sites. This intriguing work suggests the same might be true for vibrationally excited molecules physisorbed to catalytic surfaces.

The influence of nonadiabatic electronic effects on reaction probabilities

The question of how strongly Born–Oppenheimer failure influences surface chemical reactions remains unanswered at this time. One problem is that nearly all theoretical studies have so far been limited to modelling electronically nonadiabatic effects with electronic friction at the level of the LDFA.[293,414] In such calculations, electronic nonadiabaticity is typically small, for example, for $H_2O_{(g)} \xrightarrow{Pt} H_2O^*$,[415] $CH_{4(g)} \xrightarrow{Ni} CH_3^* + H^*$,[416] or $H_2O_{(g)} \xrightarrow{Ni} OH^* + H^*$[417] or for $H_{2(g)} \xrightarrow{Cu(111)} 2H^*$.[299]

It should not be surprising that friction-based calculations, which all rely on a weak coupling approximation, are limited in their ability to describe strong electronically nonadiabatic effects. Friction fails to describe electronically nonadiabatic multi-quantum vibrational excitation of NO in collisions with Au(111), whereas an IESH model involving strong coupling via an electron transfer reaction gave good agreement[249]—see Figure 12.

Other experimental evidence that tends to contradict the conclusions of LDFA-based friction studies comes from studies where observed chemicurrents,[418] which were attributed to the reaction of $2H^* \xrightarrow{Au(111)} H_{2(g)}$, and from permeation studies of the same reaction.[419] Further development of electronically nonadiabatic dynamical propagation algorithms is clearly needed, for example, ODF,[309] and methods beyond those involving a weak coupling approximation.[276,316] We also clearly need studies of a wider variety of reactions.

One example of recent progress in this direction deserves mention. Experiments and theory on the dissociative chemisorption,[420–422] inelastic scattering[423] and associative desorption[424,425] of N_2 on Ru(0001) have provided compelling evidence that energy dissipation via EHP excitations plays an important role in its reaction dynamics. For example, adiabatic molecular dynamics simulations predict vibrational energies of desorbed molecules to be much too high.[426] Friction coefficients obtained by FGR from DFT calculations show that friction can be an order of magnitude larger in the vicinity of the recombination transition state than in the chemisorption state.[427] This was attributed to the charge redistribution that accompanies the formation and breaking of chemical bonds.[427] Since then, using neural networks to fit DFT data, a full-dimensional PES has been produced.[428] This allowed study of the effect of surface atom motion on the reaction. The same PES was used to make a direct comparison between LDFA and ODF methods—this revealed that the latter achieves better agreement with experiment for reaction probabilities and vibrational energy distributions, although it slightly underestimates translational energy loss.[309] While dissociative adsorption of N_2 on Ru has proven a valuable testing ground for these new theories, we caution that the experimental dissociative adsorption probabilities being compared to exhibit large error bars.[420–422]

Thermal reaction rates

Molecular beams have long been used to measure surface reaction rates.[21] One of the most successful approaches is molecular beam relaxation spectrometry (MBRS)[436,437]—see Figure 27. For a simple reaction like first-order desorption, the molecular beam delivers and replenishes the adsorbate concentration and the time-dependent product signal is used to extract the desorption rate constant. Note that when the sticking probability is independent of coverage and temperature, the rate constant for desorption and the reaction probability are obtained by simply varying the beam modulation frequency and/or the surface temperature, while recording the phase shift. MBRS has been applied in this way to a large number of reactions, including hydrogen recombination, CO desorption, NO desorption, H_2, and CO oxidation.[436,437]

CO oxidation

Many consider CO oxidation on Pt and Pd the best-understood reactions in heterogeneous catalysis, yet a review of the results, even

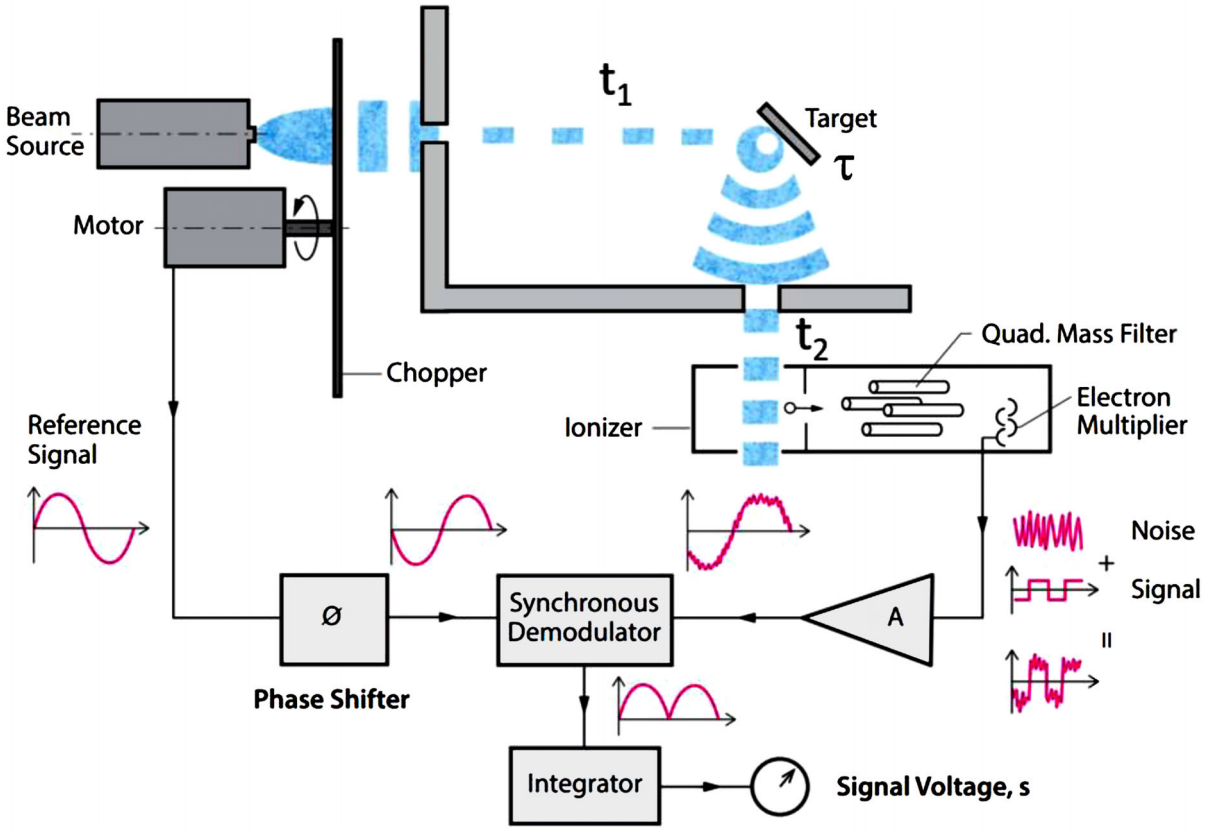

FIGURE 27 Molecular beam relaxation spectrometry (MBRS): By modulating a molecular beam with a chopping wheel, while a mass spectrometer detects the time-dependent reactant and product density. The observed signal depends on the flight-time of the reactant to the surface, t_1; the reaction time at the surface, τ, and the flight-time from the surface to the detector, t_2. One performs digital acquisition of the product waveforms (time domain) or phase-sensitive lock-in amplification (frequency domain),[429,430] a technique adapted from fluorescence lifetime[431] and chemical kinetics[432] and first used in a beam surface experiment to distinguish signal from background.[433–435] The phase-shift of products with respect to reactants reflects the reaction time at the surface. Reprinted from Schwarz JA, Madix RJ. Modulated beam relaxation spectrometry. Surf Sci. 1974;46(1):317-341, Copyright 2021, with permission from Elsevier

including those obtained with MBRS, illustrates the problems encountered in surface kinetics. Due to the ability of MBRS to directly probe the CO residence time and CO_2 formation rate, an LH (and not an ER) mechanism could be proven.[438–440] O_2 is activated by dissociation forming adsorbed O*, which recombines with diffusionally mobile CO* to form $CO_{2(g)}$ with release of energy.

$$O_{2(g)} \xrightarrow{\text{sticking}} 2O^* \quad \text{(R1)}$$

$$CO_{(g)} \xrightarrow{\text{sticking}} CO^* \quad \text{(R2)}$$

$$CO^* \xrightarrow{\text{diffusion}} CO^* \quad \text{(R3)}$$

$$CO^* + O^* \xrightarrow{\text{reaction}} CO_2^* \quad \text{(R4)}$$

$$CO_2^* \xrightarrow{\text{desorption}} CO_{2(g)} \quad \text{(R5)}$$

MBRS showed that reaction (R4) is thermally activated. It is also strongly exoergic as evidenced by the observation of $CO_{2(g)}$ with hyperthermal translational[441–443] and vibrational[444–446] energy. The large translational energy release is produced by a force directed normal to the surface and produces narrower angular distributions in the desorbing $CO_{2(g)}$ products than would be expected for a desorbing molecule that had been at thermal equilibrium with the surface.[439,443,447] Clearly, hyperthermal products form by passing over a high barrier to CO_2 formation and are ejected from the surface before they can transfer the energy imparted to them by the reaction back to the surface.

$$CO^* + O^* \xrightarrow{\text{reaction}} CO_{2(g)} \quad \text{(R6)}$$

Under other reaction conditions, desorbing $CO_{2(g)}$ appears to have first thermalized with the surface—here, translational energies are lower and infrared chemiluminescence is reduced.[448–451] These observations show that CO_2 formation proceeds over a barrier, releasing part of its exothermicity to product excitation. They also suggest that reactions (R4) and (R6) may involve different elementary reactions at different active sites.

An alternative view postulates that all products form by reaction over a single activation barrier at a single reaction site, but

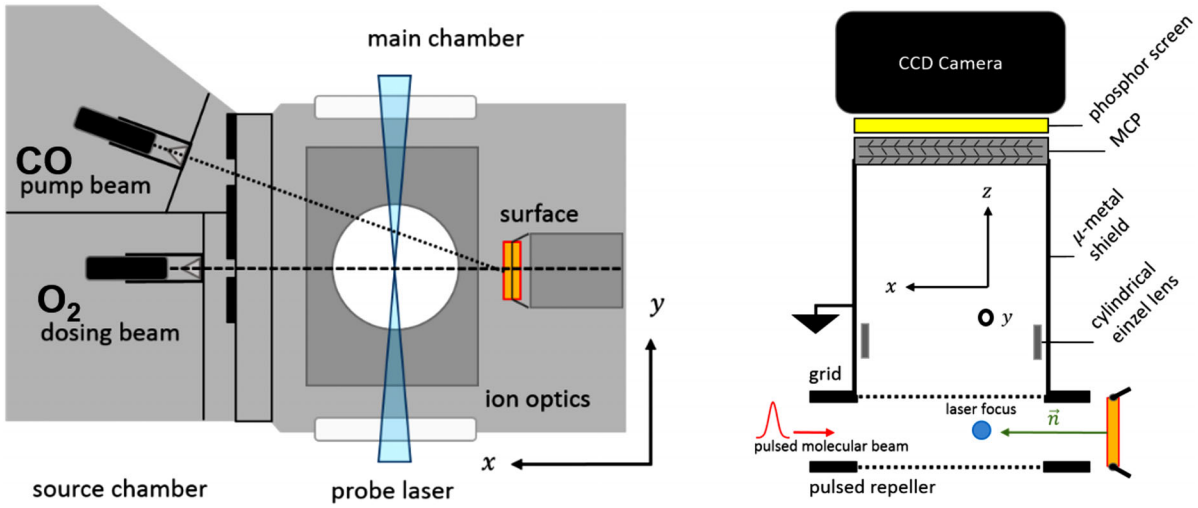

FIGURE 28 Velocity resolved kinetics: A beam of O_2 runs continuously to maintain a constant O* coverage. A short molecular beam pulse of CO initiates the reaction at the surface. Universal detection is achieved by nonresonant multiphoton absorption from a high power pulsed laser, leading to ionization of both CO and CO_2. The ions are recorded on a position sensitive detector that allows the speed to be obtained. The ion signal intensity is proportional to molecular density, which is multiplied by the recorded speed to give molecular flux. By scanning the delay between the CO pulse and the laser ionization pulse, the kinetic trace is obtained. The speed information is also used to correct for the product flight time from the surface to the ionization volume

due to the strong interactions between the product and the Pt surface, only a fraction desorb promptly with hyperthermal velocities, while the rest become trapped and thermalize with the surface before desorbing.[451]

A mechanism involving reaction sites at terraces and steps turns out to be important to this reaction. Even on (111) facets of single crystals, where step densities may be as low as 10^{-3}, reactions at steps can easily be 1000 × faster than at terraces. Furthermore, O* binds mainly at step sites[452,453] at low coverage and temperatures; furthermore, O_2 dissociates more rapidly at steps.[454,455]

The methods necessary to solve some of these problems became available only after the adaptation of slice ion-imaging to reactive surface scattering[456-458]—see Figure 28—providing numerous advantages for obtaining rates of elementary surface reactions.

The primary advantages of this method come from its ability to measure simultaneously the product density and speed, leading to the product flux, also called the *kinetic trace*. Consider a simple first-order reaction, CO desorption from a surface, $CO^* \xrightarrow{k_{des}(T)} CO_{(g)}$, governed by the following kinetic equation:

$$R_{des} \equiv \frac{d\left[CO_{(g)}\right]}{dt} = -\frac{d\left[CO^*\right]}{dt} = k_{des}\,(T)\left[CO^*\right]_t \qquad (7)$$

The reaction rate, R_{des}, has units of $cm^{-2}\ s^{-1}$—a flux. An experiment that automatically provides the flux of desorbing molecules is highly advantageous. Knowledge of the product's speed is also used to correct each ion signal for the time spent flying from the surface to the laser ionization volume, t_2 in Figure 27 for MBRS.[436]

A third advantage is that different reactions may produce the same product but with different speeds. Figure 29 shows the results of ion imaging applied to the CO oxidation reaction on Pt (111).[456] The ion image shown in panel a exhibits a bimodal velocity distribution, shown explicitly in panel b (speed distribution) and panel c (angular distributions). The kinetic trace can be obtained selectively—panel d—for the high-speed (red) and the low-speed (blue) velocity groups. This information immediately suggests a realistic kinetic model.

Motivated to more deeply understand the ion imaging experiments, AIMD trajectories showed that CO_2 formation at steps indeed leads to thermalized CO_2, while the terrace reaction produces hyperthermal CO_2.[459] Chemisorbed CO_2 may form at step sites, taking on a bent structure with a partial negative charge. CO_2 chemisorption is unimportant at Pt terraces.

Identifying the active site

Obviously, meaningful comparison of theory and experiment requires knowledge of the reaction site—it makes little sense to compare reaction rates measured at steps to those calculated with a reaction model involving terraces. Since the field's inception, identifying the active site in surface chemistry has been a bane. A catalytic surface inhabited by adsorbates may exhibit a complex phase diagram of equilibrium structures dependent upon the partial pressure of gases and temperature. For example, when *ab initio* thermodynamics is used for Ru(0001) in the presence of $O_{2(g)}$ and $CO_{(g)}$, four different surface structures are found.[460,461] Each surface structure offers a specific reaction geometry with its own transition state and barrier height.

Oxygen islands are a related example concerning CO and H_2 oxidation on Pt and Pd. At low temperature, scanning tunneling microscopy (STM) shows that CO* and O* segregate and reactions occur only at their borders[462]—just like oil and water, reactants need not mix in

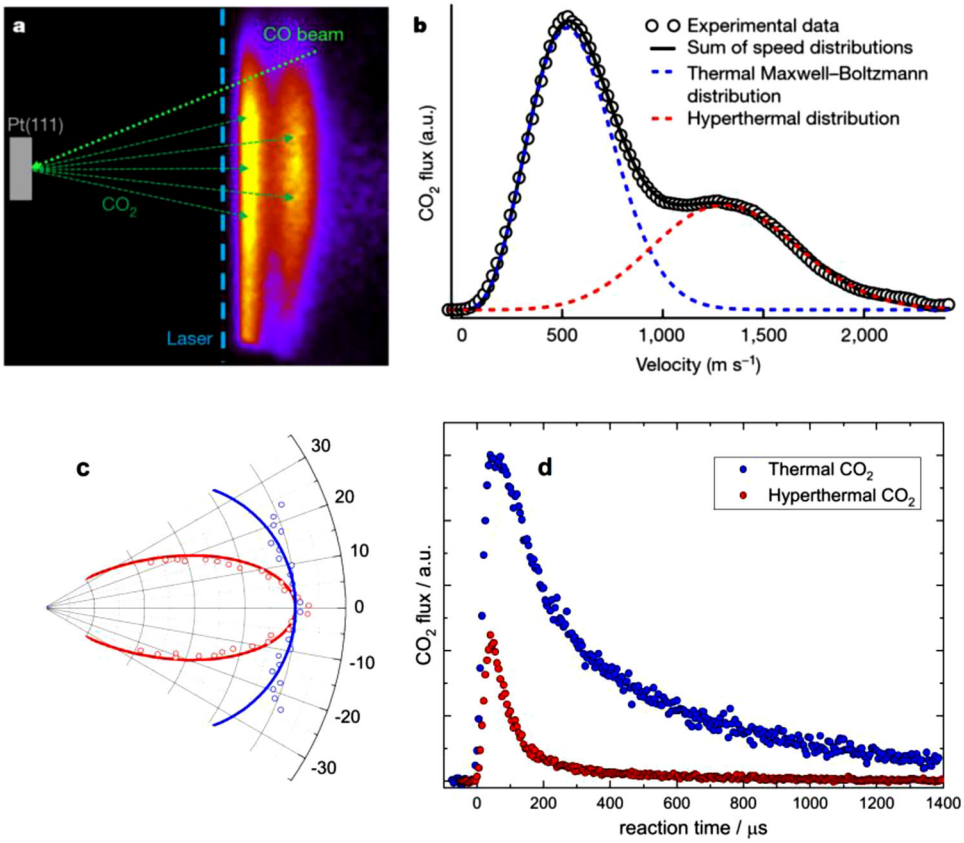

FIGURE 29 Ion imaging of chemical reaction products from CO oxidation on Pt(111). (a) Ion image of CO_2, (b) derived velocity distribution reveals the contribution of a thermal and a hyperthermal channel, (c) derived angular distributions, and (d) the total CO_2 flux of the thermal (blue) and hyperthermal (red) components. The densities have been converted to flux using the measured velocities, the intensities have been corrected for differences in angular distributions, and the time axis has been corrected for product flight time. Figure reproduced with permission from Ref. [456], Nature Publishing Group. The data shown here were obtained for a reaction proceeding as a surface temperature of $T_S = 593$ K

surface chemistry. Most theoretical calculations of CO oxidation barriers consider pairwise interactions between reactants: $CO^* \cdots O^*$. But even with submonolayer O^* coverages at relatively high temperatures, two or more phases may form, one packed in a 2×2 lattice in equilibrium with a second phase of uncondensed O^*. The O^*-island phase allows reactions within them or at their edges, obviously with different transition states. This concept was used to explain the observation that CO oxidation does not go to completion during a temperature programmed reaction cycle,[463] suggesting that the island structure of the O^* reactants limits reaction. These authors argued that the reaction proceeds by diffusion of adsorbed CO to the perimeters of the immobile adsorbed atomic oxygen islands.[463] Similar effects have been observed previously during temperature programmed reaction and titration studies of the $H_{2(g)} + \frac{1}{2}O_{2(g)} \overset{Pt(111)}{\longrightarrow} H_2O_{(g)}$.[464] Data supporting the idea of O^* islands are also available for reactions on Pt[462,465] and Pd.[466,467] When MBRS was applied to CO oxidation on Pd(111), the derived activation energies increased from low to high O^* coverage.[438] This was rationalized as having to do with the influence of islands at high coverage that became less important at low coverage.[438] The O^*-islands discussed so far exist at equilibrium, and phase diagrams of O^*-islands on Pt(111) have been calculated[468] from first principles using of $O^* - O^*$ interactions computed with DFT.[469]

O^*-islands can also form under kinetic control. Oxygen dissociation on Pt is precursor mediated: $O_{2(g)} \overset{Pt(111)}{\longrightarrow} O_2^* \overset{Pt(111)}{\longrightarrow} 2O^*$; furthermore, combining STM-experiments with theory, it could be shown that O_2^* dissociation proceeds on the upper side of Pt step edges.[454] STM also showed that O_2^* dissociation is more likely in the vicinity of O^*.[465,470] This set of observations reveals how dissociation kinetics can lead to highly nonequilibrium surface structures, resulting from a dynamic heterogeneity in the adsorption mechanism. In short, a kinetically determined ordering of the adsorbate.

Making measurements on the living catalyst

These studies point out that a catalyst is dynamic, generating active sites due to exposure to reactants, a "living catalyst."[471] This presents another experimental challenge. Since measuring rates of surface reactions requires signal averaging, the catalyst must return to its original state at the end of each measurement to allow for averaging. The dynamic catalyst may make this impossible.

Recently, velocity-resolved kinetics using high-repetition-rate pulsed laser ionization and high-speed ion imaging detection has been achieved.[472] This overcomes the time-consuming scanning of the delay

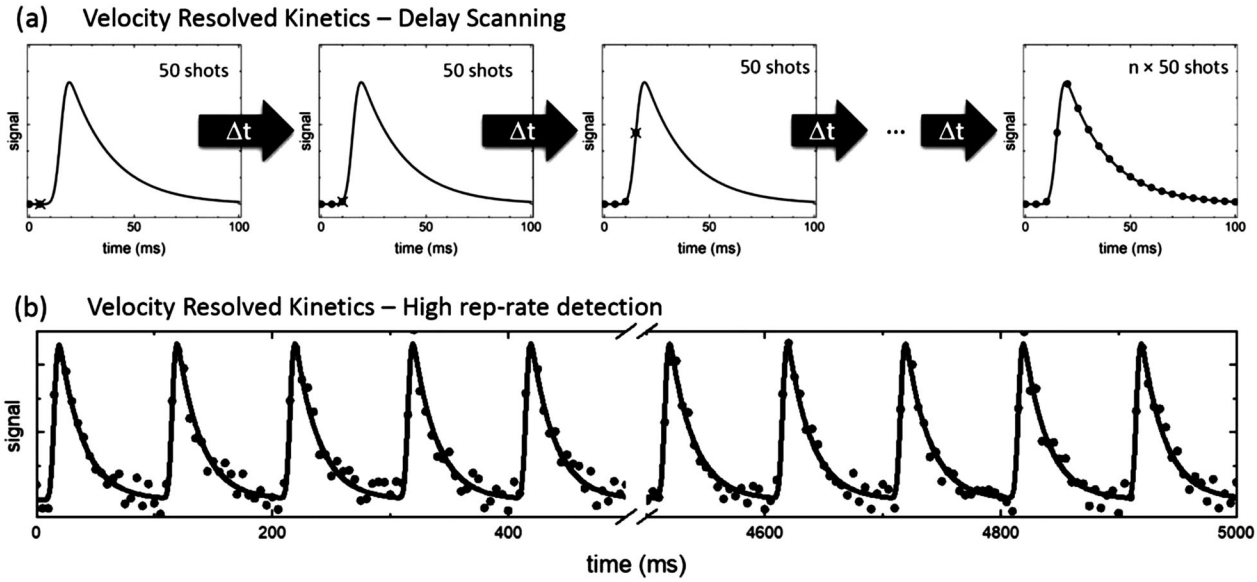

FIGURE 30 Comparison of delay scanning (a) versus high-rep-rate detection (b). In delay scanning, we average many ion images at each delay between the initiating molecular beam pulse and the ionizing laser pulse, generating the kinetic trace. For high rep-rate detection, we record many points in the kinetic trace for each molecular beam pulse, increasing the duty cycle by orders of magnitude, enabling measurements while the catalyst is changing.[472] Reprinted from Borodin D, Golibrzuch K, Schwarzer M, et al. Measuring transient reaction rates from nonstationary catalysts. ACS Catal. 2020;10:14056-14066

between the reaction initiating molecular beam pulse and the laser ionization pulse—Figure 30(a). In the new approach—Figure 30(b)—the reaction is initiated by a single molecular beam pulse and the product formation rate is observed by a sequence of pulses produced by a 1-kHz repetition-rate laser. This increases the data acquisition rate by up to a 1000 ×. With fiber lasers capable of running at 100 kHz or higher, another 100 × improvement is within reach. Thus, what once took hours to measure can now be done in seconds and soon much faster. In addition, this approach overcomes the diffusion problem arising in many molecular beam reactive scattering experiments.[473] To demonstrate the problem, consider that if one starts with an O*-saturated Pt surface and doses it with CO pulses; then, O* is removed more rapidly from the part of the surface where the center of the molecular beam is incident. As time passes, most CO_2 formed from CO that adsorbed near the center of the beam where O* is depleted, and diffused to the edges of the beam where O* is still present. Using high rep-rate velocity-resolved kinetics, the diffusional influence could be observed and quantitatively modeled.[472]

Exploiting our dynamical understanding of surface reactions to obtain a predictive theory of reaction rates remains yet an unfulfilled goal, as current limitations of the tools needed to make accurate measurements of reaction rates at well-characterized active sites have prevented meaningful tests of rate-theory. However, with experiments and theory both improving, we are increasingly benefitting from the fruitful interplay and we stand at the threshold of bringing this effort to fruition. Comparing to another subfield of complex chemistry provides some perspective. While surely not more complex, the study of heterogeneous catalysis has suffered from a structural deficit compared to enzymology. Methods to identify enzyme active sites—X-ray and electron diffraction—preceded by decades the theory of enzyme rates and dynamics at the transition state. Analogous methods to routinely identify surface active sites lay still in the future. In comparison to enzymology, we are still groping a bit to realize the structure function relationship. Nevertheless, as we learn more about active sites in heterogeneous catalysis through a fruitful interplay of experiment and theory, there is every reason to be optimistic that a predictive theory of rates will become available. After nearly a century, the dynamical approach is the gift that just keeps on giving, finding application to understand increasingly complex chemistry.

OUTLOOK

In this penultimate section, we wish to express our opinions regarding important directions for future research. This review has cited very little research on electronically inelastic scattering—there is very little. It should be noted that an instrument using a Stark decelerator for surface scattering has been reported[474] and used to investigate electronic quenching of CO $a^3\Pi$ on metals with and without adsorbates.[475] This is certainly an interesting direction for the future.

Perhaps of greatest concern to us is the need to compare theory and experiment on the level of rates of elementary reactions. Here, many more rates must be measured accurately and these must be compared to rates calculated from first principles theory. The experimental methods are now available to obtain accurate rates on simple model surfaces and these must be extended to more complex surfaces that reflect new phenomena present in real catalysts. It will only be with the development of predictive theoretical methods, validated by experiment, that we may one day achieve useful microkinetic models of real catalysts.

An important target is an experimental tool for routine use that can reveal the structure of active sites of surface reactions in real catalysts. Here, the combination of near-field infrared spectroscopy with scanning probe methods[476–478] may be of great importance; however, it will need to work at temperatures relevant to catalysis. Theory can also be crucially important here, for example, providing *ab initio* equilibrium structures present under realistic catalytic conditions.[479]

We also need new theoretical tools. DFT-GGA is still suspect when it comes to calculating reaction barriers. Accurate wave function-based electronic structure theory[480] perhaps employing self-consistent embedding methods[481–483] or quantum Monte Carlo[484] could at least provide benchmarks for methods. They also have the potential to offer accurate information on excited electronic states. The approximate methods must themselves also improve. Hybrid functionals applied to GGA densities is one promising direction.[371]

A nagging question is to what extent energy dissipation to the solid—for example, due to coupling to EHPs—influences the rates of surface reactions. The influence of friction on reaction rates in liquids and biological systems has been widely demonstrated and quantified, based on the pioneering theory of Kramers.[485] At surfaces, both phonon and EHP dissipation must be considered. For the latter, we require demonstrably correct theoretical methods for electronically nonadiabatic dynamics. Current friction approaches while improving[314] are unlikely to be sufficient as they rely on a weak coupling approximation and are likely not applicable to problems that exhibit strong and localized nonadiabaticity, such as electron transfer. IESH still represents a fruitful avenue of future study and improvement.[316] We also need measurements on a wider variety of systems. Systems for which $E_{v(v,\, r_{outer})} - \Phi$ is large and hence electron transfer is more likely (see Figure 15) are promising candidates for observing the influence of nonadiabatic electronic excitation on reaction rates.

The importance of quantum effects in surface chemistry needs much more effort. Recently, H atom beams have been produced at energies as low as 0.2 eV and with such narrow speed distributions, they could not be measured by Rydberg-atom tagging.[486] These could deliver a great deal of excellent quantitative scattering data capable of testing quantum mechanical theories of reaction dynamics. High-dimensional quantum calculations, for example, by unifying the power of multi-configuration time-dependent Hartree dynamics[487,488] with that of neural network PESs,[489] appear to be within reach. However, at least until quantum computers become widely accessible, fully quantum mechanical descriptions of catalytic systems are likely to remain intractable. Hence, accurate mixed quantum classical dynamics are extremely important.

Another interesting condensed phase quantum system is CO adsorbed to NaCl. In Section 5.1, we pointed out that CO vibrational relaxation is extremely inefficient. This allows high-resolution infrared emission spectroscopy to be carried out from which two orientation isomers have been identified.[490] Normally, CO adsorbs with the C-atom close to a Na^+ of the NaCl surface, but an "upside down" isomer has also been observed.[490] Remarkably, experiments reveal well-resolved line spectra. This problem has already drawn interest from theorists developing PESs[491,492] applying quantum dynamical methods.[493] The challenges are formidable, but this system offers a proving ground for testing quantum dynamical methods in the high dimensions of condensed phases, providing a blueprint for exciting experimental and theoretical advances that may lead to fascinating discoveries, and take us systematically toward the dream of predicting and watching the intricate motions of individual atoms during a catalytic reaction.

CLOSING REMARKS AND APOLOGIES

In this manuscript, we have not attempted a comprehensive review of the field of chemical dynamics. Rather, our aim has been to highlight the most important concepts and present selected examples from gas-phase dynamics that illustrate how successful the dynamical approach has been and to extend the discussion to encompass the complexity and richness of reactions at surfaces. We have attempted to draw a line from the discovery of quantum mechanics, which inspired chemical dynamics, to the time of this writing in the first days of 2021. This perhaps foolishly ambitious undertaking means we must apologize to all those who do not find their work reviewed here. Beyond limits of time and space, it is hardly possible to be aware of all the significant work occurring over nearly a century. We do hope that those dedicated to the approaches of gas-phase chemical dynamics see here the possibility to extend the reach of their expertise to complex problems in other branches of chemistry.

ACKNOWLEDGMENTS

The authors acknowledge all of the students, post-docs, and coworkers with whom they have been so fortunate to work over the years. Thanks also go to Prof. Igor Rahinov for carefully reading an early draft and providing many helpful comments. The authors also thank Mr. Hartmut Sebesse who prepared many of the figures. Finally, they thank Prof.s Joel Bowman and Arthur Suits for providing animations of roaming reactions and Dr. Alexander Kandratsenka for making movies of H scattering from graphene.

AUTHOR CONTRIBUTIONS

The manuscript was written through contributions of all authors. All authors have given approval to the final version of the manuscript.

TRANSPARENT PEER REVIEW

The peer review history for this article is available at https://publons.com/publon/10.1002/ntls.10005.

ORCID

Alec M. Wodtke https://orcid.org/0000-0002-6509-2183

REFERENCES

1. Langmuir I. Nobel lecture — surface chemistry. *Nobel Media AB*. 1932. https://www.nobelprize.org/prizes/chemistry/1932/langmuir/lecture/.
2. Herschbach DR. Molecular dynamics of elementary chemical reactions (Nobel Lecture). *Angew Chem Int Ed*. 1987;26(12):1221-1243.

3. Lee YT. Molecular beam studies of elementary chemical processes (Nobel Lecture). *Angew Chem Int Ed*. 1987;26(10):939-951.
4. Polanyi JC. Some concepts in reaction dynamics (Nobel lecture). *Angew Chem Int Ed*. 1987;26(10):952-971.
5. Ertl G. Reactions at surfaces: from atoms to complexity (Nobel Lecture). *Angew Chem Int Ed*. 2008;47(19):3524-3535.
6. Wodtke AM, Matsiev D, Auerbach DJ. Energy transfer and chemical dynamics at solid surfaces: the special role of charge transfer. *Prog Surf Sci*. 2008;83(3):167-214.
7. Rahinov I, Cooper R, Matsiev D, Bartels C, Auerbach DJ, Wodtke AM. Quantifying the breakdown of the Born–Oppenheimer approximation in surface chemistry. *PCCP*. 2011;13(28):12680-12692.
8. Golibrzuch K, Bartels N, Auerbach DJ, Wodtke AM. The dynamics of molecular interactions and chemical reactions at metal surfaces: testing the foundations of theory. *Annu Rev Phys Chem*. 2015; 66:399-425.
9. Park GB, Krüger BC, Borodin D, Kitsopoulos TN, Wodtke AM. Fundamental mechanisms for molecular energy conversion and chemical reactions at surfaces. *Rep Prog Phys*. 2019;82(9):096401.
10. Rettner CT, Auerbach DJ, Tully JC, Kleyn AW. Chemical dynamics at the gas—surface interface. *J Phys Chem*. 1996;100(31):13021-13033.
11. Tully JC. Chemical dynamics at metal surfaces. *Annu Rev Phys Chem*. 2000;51:153-178.
12. Schlögl R. Theory in heterogeneous catalysis — an experimentalist's view. *Cattech*. 2001;5(3):146-170.
13. Silva M, Jongma R, Field RW, Wodtke AM. The dynamics of "stretched molecules": experimental studies of highly vibrationally excited molecules with stimulated emission pumping. *Annu Rev Phys Chem*. 2001;52:811-852.
14. Zaera F. Probing catalytic reactions at surfaces. *Prog Surf Sci*. 2001;69(1-3):1-98.
15. Wodtke AM, Tully JC, Auerbach DJ. Electronically non-adiabatic interactions of molecules at metal surfaces: can we trust the Born–Oppenheimer approximation for surface chemistry? *Int Rev Phys Chem*. 2004;23(4):513-539.
16. Libuda J, Freund HJ. Molecular beam experiments on model catalysts. *Surf Sci Rep*. 2005;57(7-8):157-298.
17. Gleaves JT, Yablonsky G, Zheng XL, Fushimi R, Mills PL. Temporal analysis of products (TAP)—recent advances in technology for kinetic analysis of multi-component catalysts. *J Mol Catal A: Chem*. 2010;315(2):108-134.
18. Okada M. Surface chemical reactions induced by well-controlled molecular beams: translational energy and molecular orientation control. *J Phys-Cond Matter*. 2010;22(26):263003.
19. Wodtke AM. Electronically non-adiabatic influences in surface chemistry and dynamics. *Chem Soc Rev*. 2016;45(13):3641-3657.
20. Yang XM, Wodtke AM. Surface reaction dynamics. *Chem Soc Rev*. 2016;45(13):3573-3575.
21. Zaera F. Use of molecular beams for kinetic measurements of chemical reactions on solid surfaces. *Surf Sci Rep*. 2017;72(2):59-104.
22. Park GB, Kitsopoulos TN, Borodin D, et al. The kinetics of elementary thermal reactions in heterogeneous catalysis. *Nat Rev Chem*. 2019;3(12):723-732.
23. Kleyn AW. Molecular beams and chemical dynamics at surfaces. *Chem Soc Rev*. 2003;32(2):87-95.
24. Levine RD, Bernstein RB. *Molecular Reaction Dynamics and Chemical Reactivity*. Oxford University Press; 1987.
25. Houston PL. *Chemical Kinetics and Reaction Dynamics*. Courier Corporation; 2012.
26. Brouard M, Vallance C. *Tutorials in Molecular Reaction Dynamics*. Royal Society of Chemistry; 2015.
27. Somorjai GA. *Chemistry in Two Dimensions: Surfaces*. Cornell University Press; 1981.
28. Ertl G. *Reactions at Solid Surfaces*. John Wiley & Sons; 2010.
29. Born M, Heisenberg W, Jordan P. Quantum mechanics II. *Z Phys*. 1926;35(8/9):557-615.
30. Dirac PAM. Quantum mechanics of many-electron systems. *Proc R Soc London, Ser A*. 1929;123(792):714-733.
31. Born M, Oppenheimer R. Quantum theory of molecules. *Ann Phys-Berlin*. 1927;84(20):0457-0484.
32. Eyring H, Polanyi M. Concerning simple gas reactions. *Z Phys Chem B-Chem Elem Aufbau Mater*. 1931;12(4):279-311.
33. Eyring H, Polanyi M. On simple gas reactions. *Z Phys Chem*. 2013;227(9-11):1221-1245.
34. Eyring H. The theory of absolute reaction rates. *Trans Farad Soc*. 1938;34(1):0041-0048.
35. Urey H. Editorial. *J Chem Phys*. 1933;1(1):1-2.
36. Basco N, Norrish RGW. Vibrational disequilibrium in reactions between atoms and molecules. *Can J Chem*. 1960;38(10):1769-1779.
37. Schawlow AL, Townes CH. Infrared and optical masers. *Phys Rev*. 1958;112(6):1940-1949.
38. Maiman TH. Stimulated optical radiation in ruby. *Nature*. 1960;187(4736):493-494.
39. Herschbach D, Kwei GH, Norris JA. Reactive scattering in crossed molecular beams — K atoms with CH_3I and C_2H_5I. *J Chem Phys*. 1961;34(5):1842.
40. Wall FT, Hiller LA, Mazur J. Statistical computation of reaction probabilities. *J Chem Phys*. 1958;29(2):255-263.
41. Meinel AB. OH emission bands in the spectrum of the night sky. 1. *Astrophys J*. 1950;111(3):555.
42. McKinley JD, Garvin D, Boudart MJ. Production of excited hydroxyl radicals in the hydrogen atom-ozone reaction. *J Chem Phys*. 1955;23(5):784-786.
43. Lipscomb FJ, Norrish RGW, Thrush BA. The study of energy transfer by kinetic spectroscopy. 1. The production of vibrationally excited oxygen. *Proc R Soc London, Ser A*. 1956;233(1195):455-464.
44. McGrath WD, Norrish RGW. The flash photolysis of ozone. *Proc R Soc London, Ser A*. 1957;242(1230):265.
45. Kaufman F, Kelso JR. Vibrationally excited ground-state nitrogen in active nitrogen. *J Chem Phys*. 1958;28(3):510-511.
46. Cashion JK, Polanyi JC. Infrared chemiluminescence from the gaseous reaction atomic-H plus Cl_2. *J Chem Phys*. 1958;29(2):455-456.
47. Kasper JVV, Pimentel GC. HCl chemical laser. *Phys Rev Lett*. 1965;14(10):352.
48. Polanyi JC. Some concepts in reaction dynamics. *Acc Chem Res*. 1972;5(5):161.
49. Polanyi JC. Proposal for an infrared maser dependent on vibrational excitation. *J Chem Phys*. 1961;34(1):347.
50. Freemann WM. Developer of the laser calls it 'a solution seeking a problem'. *New York Times*, May 6, 1964.
51. Javan A, Herriott DR, Bennett WR. Population inversion and continuous optical maser oscillation in a gas discharge containing a HE-NE mixture. *Phys Rev Lett*. 1961;6(1):106.
52. White AD, Rigden JD. Continuous gas maser operation in visible. *Proc Inst Radio Eng*. 1962;50(7):1697.
53. Bridges WB. Laser oscillation in singly ionized argon in the visible spectrum. *Appl Phys Lett*. 1964;4(7):128.
54. Patel CKN. Continuous-wave laser action on vibrational-rotational transitions of CO_2. *Phys Rev A*. 1964;136(5A):1187.
55. Patel CKN. Selective excitation through vibrational energy transfer + optical maser action in N_2CO_2. *Phys Rev Lett*. 1964;13(21):617.
56. Zare RN. My life with LIF: a personal account of developing laser-induced fluorescence. *Annu Rev Anal Chem*. 2012;5:1-14.
57. Hocker LO, Kovacs MA, Rhodes CK, Flynn GW, Javan A. Vibrational relaxation measurements in CO_2 using an induced-fluorescence technique. *Phys Rev Lett*. 1966;17(5):233.
58. Yardley JT, Moore CB. Laser-excited vibrational fluorescence and energy transfer in methane. *J Chem Phys*. 1966;45(3):1066.

59. Ronn AM. Laser-induced infrared fluorescence. *J Chem Phys*. 1968;48(1):511.
60. Tango WJ, Link JK, Zare RN. Spectroscopy of K_2 using laser-induced fluorescence. *J Chem Phys*. 1968;49(10):4264.
61. Sakurai K, Broida HP. Spectral study of NO_2 fluorescence excited by 11 lines of argon and krypton ion lasers. *J Chem Phys*. 1969;50(6):2404.
62. Tango WJ, Zare RN. Radiative lifetime of $B^1\Pi_u$ state of K_2. *J Chem Phys*. 1970;53(8):3094.
63. Schäfer FP, Schmidt W, Volze J. Organic dye solution laser. *Appl Phys Lett*. 1966;9(8):306-309.
64. Sorokin PP, Lankard JR, Hammond EC, Moruzzi VL. Laser-pumped stimulated emission from organic dyes: experimental studies and analytical comparisons. *IBM J Res Dev*. 1967;11(2):130-148.
65. Schultz A, Zare RN, Cruse HW. Laser-induced fluorescence — method to measure internal state distribution of reaction products. *J Chem Phys*. 1972;57(3):1354.
66. Dagdigian PJ, Zare RN. Primitive angular-distribution studies of internal states in crossed-beam reactions using laser fluorescence detection. *J Chem Phys*. 1974;61(6):2464-2465.
67. Smith GP, Zare RN. Angular-distribution of product internal states using laser fluorescence detection —Ba+KCl reaction. *J Chem Phys*. 1976;64(6):2632-2640.
68. Hall JL, Robinson EJ, Branscomb LM. Laser double-quantum photodetachment of iminus. *Phys Rev Lett*. 1965;14(25):1013.
69. Fox RA, Kogan RM, Robinson EJ. Laser triple-quantum photoionization of cesium. *Phys Rev Lett*. 1971;26(23):1416.
70. Held B, Manus C, Mainfray G, Morellec J. Molecular cesium component in multiphoton ionization of a cesium atomic-beam by a Q-switched neodymium-glass laser at 1.06 mum. *Phys Rev Lett*. 1972;28(3):130.
71. Held B, Mainfray G, Manus C, Morellec J, Sanchez F. Resonant multiphoton ionization of a cesium atomic-beam by a tunable-wavelength Q-switched neodymium-glass laser. *Phys Rev Lett*. 1973;30(10):423-426.
72. Lineberger WC, Patterson TA. 2 photon photodetachment spectroscopy — C2 SIGMA-2 states. *Chem Phys Lett*. 1972;13(1):40.
73. Collins CB, Johnson BW, Popescu D, Musa G, Pascu ML, Popescu I. Multiphoton ionization of molecular cesium with a tunable dye laser. *Phys Rev A*. 1973;8(4):2197-2201.
74. Johnson PM, Berman MR, Zakheim D. Nonresonant multiphoton ionization spectroscopy — 4-photon ionization spectrum of nitric-oxide. *J Chem Phys*. 1975;62(6):2500-2502.
75. Petty G, Tai C, Dalby FW. Nonlinear resonant photoionization in molecular iodine. *Phys Rev Lett*. 1975;34(19):1207-1209.
76. Johnson PM. Multiphoton ionization spectrum of benzene. *J Chem Phys*. 1976;64(10):4143-4148.
77. Parker DH, Sheng SJ, Elsayed MA. Multiphoton ionization spectrum of trans-hexatriene in 6.2 eV region. *J Chem Phys*. 1976;65(12):5534-5535.
78. McDonald JD, Lebreton PR, Lee YT, Herschbach DR. Molecular beam kinetics: reactions of deuterium atoms with halogen molecules. *J Chem Phys*. 1972;56(2):769-788.
79. Herman Z, Kerstetter JD, Rose TL, Wolfgang R. Crossed-beam study of a simple ion-molecule reaction in energy range 0.70–25 eV. *J Chem Phys*. 1967;46(7):2844.
80. Gentry WR, Gislason EA, Lee YT, Mahan BH, Tsao CW. Product energy and angular distributions from reaction of N_2^+ with isotopic hydrogen molecules. *Disc Farad Soc*. 1967(44):137.
81. Lee YT, McDonald JD, Lebreton PR, Herschbach DR. Molecular beam reactive scattering apparatus with electron bombardment detector. *Rev Sci Instrum*. 1969;40(11):1402.
82. Neumark DM, Wodtke AM, Robinson GN, Hayden CC, Lee YT. Experimental investigation of resonances in reactive scattering — the $F+H_2$ reaction. *Phys Rev Lett*. 1984;53(3):226-229.
83. Parker DH, Bernstein RB. Oriented molecule beams via the electrostatic hexapole — preparation, characterization, and reactive scattering. *Annu Rev Phys Chem*. 1989;40:561-595.
84. Bethlem HL, Berden G, Meijer G. Decelerating neutral dipolar molecules. *Phys Rev Lett*. 1999;83(8):1558-1561.
85. van de Meerakker SYT, Bethlem HL, Vanhaecke N, Meijer G. Manipulation and control of molecular beams. *Chem Rev*. 2012;112(9):4828-4878.
86. De Jongh T, Besemer M, Shuai Q, et al. Imaging the onset of the resonance regime in low-energy NO-He collisions. *Science*. 2020;368(6491):626-630.
87. Feldman DL, Lengel RK, Zare RN. Multiphoton ionization — method for characterizing molecular-beams and beam reaction-products. *Chem Phys Lett*. 1977;52(3):413-417.
88. Heck AJR, Chandler DW. Imaging techniques for the study of chemical-reaction dynamics. *Annu Rev Phys Chem*. 1995;46:335-372.
89. Chandler DW, Houston PL. Two-dimensional imaging of state-selected photodissociation products detected by multiphoton ionization. *J Chem Phys*. 1987;87(2):1445-1447.
90. Buntine MA, Baldwin DP, Zare RN, Chandler DW. Application of ion imaging to the atom-molecule exchange-reaction — $H+HI = H_2+I$. *J Chem Phys*. 1991;94(6):4672-4675.
91. Kitsopoulos TN, Buntine MA, Baldwin DP, Zare RN, Chandler DW. Reaction-product imaging — the $H+D_2$ reaction. *Science*. 1993;260(5114):1605-1610.
92. Eppink A, Parker DH. Velocity map imaging of ions and electrons using electrostatic lenses: application in photoelectron and photofragment ion imaging of molecular oxygen. *Rev Sci Instrum*. 1997;68(9):3477-3484.
93. Gebhardt CR, Rakitzis TP, Samartzis PC, Ladopoulos V, Kitsopoulos TN. Slice imaging: a new approach to ion imaging and velocity mapping. *Rev Sci Instrum*. 2001;72(10):3848-3853.
94. Townsend D, Minitti MP, Suits AG. Direct current slice imaging. *Rev Sci Instrum*. 2003;74(4):2530-2539.
95. Lin JJ, Zhou JG, Shiu WC, Liu KP. Application of time-sliced ion velocity imaging to crossed molecular beam experiments. *Rev Sci Instrum*. 2003;74(4):2495-2500.
96. Ashfold MNR, Nahler NH, Orr-Ewing AJ, et al. Imaging the dynamics of gas phase reactions. *PCCP*. 2006;8(1):26-53.
97. Roothaan CCJ. New developments in molecular orbital theory. *Rev Mod Phys*. 1951;23(2):69-89.
98. Mulliken RS. Bonding power of electrons and theory of valence. *Chem Rev*. 1931;9(3):347-388.
99. Møller C, Plesset MS. Note on an approximation treatment for many-electron systems. *Phys Rev*. 1934;46(7):618-622.
100. Bartlett RJ. Many-body perturbation-theory and coupled cluster theory for electron correlation in molecules. *Annu Rev Phys Chem*. 1981;32:359-401.
101. Raghavachari K. Electron correlation techniques in quantum-chemistry — recent advances. *Annu Rev Phys Chem*. 1991;42:615-642.
102. Kohn W, Sham LJ. Self-consistent equations including exchange and correlation effects. *Phys Rev*. 1965;140(4A):A1133-A1138.
103. Behler J. Perspective: machine learning potentials for atomistic simulations. *J Chem Phys*. 2016;145(17):170901.
104. Blais NC, Bunker DL. Monte Carlo calculations. 2. Reactions of alkali atoms with methyl iodide. *J Chem Phys*. 1962;37(11):2713.
105. Karplus M, Sharma RD, Porter RN. Dynamics of reactive collisions — $H+H_2$ exchange reaction. *J Chem Phys*. 1964;40(7):2033.
106. Truhlar DG, Kuppermann A. Quantum mechanics of $H+H_2$ reaction — exact scattering probabilities for collinear collisions. *J Chem Phys*. 1970;52(7):3841.
107. Kuppermann A, Schatz GC. Quantum-mechanical reactive scattering — accurate 3-dimensional calculation. *J Chem Phys*. 1975;62(6):2502-2504.

108. McCullough EA, Wyatt RE. Dynamics of collinear H+H_2 reaction. 1. Probability density and flux. *J Chem Phys*. 1971;54(8):3578.
109. Heller EJ. Time-dependent approach to semiclassical dynamics. *J Chem Phys*. 1975;62(4):1544-1555.
110. Car R, Parrinello M. Unified approach for molecular dynamics and density-functional theory. *Phys Rev Lett*. 1985;55(22):2471-2474.
111. Ufimtsev IS, Martinez TJ. Quantum chemistry on graphical processing units. 3. Analytical energy gradients, geometry optimization, and first principles molecular dynamics. *J Chem Theo Comp*. 2009;5(10):2619-2628.
112. Hu W, Schatz GC. Theories of reactive scattering. *J Chem Phys*. 2006;125(13).
113. Truhlar DG, Wyatt RE. History of H-3 kinetics. *Annu Rev Phys Chem*. 1976;27:1-43.
114. Wall FT, Hiller LA, Mazur J. Statistical computation of reaction probabilities. 2. *J Chem Phys*. 1961;35(4):1284.
115. Datz S, Taylor EH. Atom-molecule reaction of hydrogen studied by molecular beams. *J Chem Phys*. 1963;39(7):1896.
116. Karplus M, Sharma RD. Exchange reactions with activation energy. I. Simple barrier potential for (H,H_2). *J Chem Phys*. 1965;43(9):3259.
117. Karplus M, Tang KT. Quantum-mechanical study of H+H_2 reactive scattering. *Disc Farad Soc*. 1967(44):56.
118. Elkowitz AB, Wyatt RE. Quantum-mechanical reaction cross-sections for 3-dimensional hydrogen-exchange reaction. *J Chem Phys*. 1975;62(6):2504-2506.
119. Schatz GC, Kuppermann A. Dynamical resonances in collinear, coplanar, and 3-dimensional quantum-mechanical reactive scattering. *Phys Rev Lett*. 1975;35(19):1266-1269.
120. Chatfield DC, Mielke SL, Allison TC, Truhlar DG. Quantized dynamical bottlenecks and transition state control of the reaction of D with H_2: effect of varying the total angular momentum. *J Chem Phys*. 2000;112(19):8387-8408.
121. Kwei GH, Lo VWS. Crossed beam studies of the hydrogen-exchange reaction — the reaction of H and D atoms with T_2 molecules. *J Chem Phys*. 1980;72(11):6265-6275.
122. Geddes J, Fite WL, Krause HF. Atom-molecule reaction D+H_2-HD+H studied by molecular-beams. *J Chem Phys*. 1972;56(7):3298.
123. Götting R, Mayne HR, Toennies JP. Molecular-beam measurements of differential cross-sections for the reaction D+H_2 → HD+H at E_{CM} = 1.0 eV. *J Chem Phys*. 1984;80(5):2230-2232.
124. Götting R, Mayne HR, Toennies JP. Molecular-beam scattering measurements of differential cross-sections for D+H_2 (v=0) → HD+H at E_{CM} = 1.5 eV. *J Chem Phys*. 1986;85(11):6396-6419.
125. Buntin SA, Giese CF, Gentry WR. State-resolved differential cross-sections for the reaction D+H_2 → HD+H. *J Chem Phys*. 1987;87(2):1443-1445.
126. Buntin SA, Giese CF, Gentry WR. The hydrogen-exchange reaction — discrepancies between experimental state-resolved differential cross-sections and 3-D quantum dynamics. *Chem Phys Lett*. 1990;168(6):513-517.
127. Continetti RE, Balko BA, Lee YT. Crossed molecular-beams study of the reaction D+H_2 → HD+H at collision energies of 0.53 and 1.01 eV. *J Chem Phys*. 1990;93(8):5719-5740.
128. Continetti RE, Zhang JZH, Miller WH. Resonance structure in the energy-dependence of state-to-state differential scattering cross-sections for the D+H_2(V,J) → HD(V,J)+H at E_{CM} reaction — comment. *J Chem Phys*. 1990;93(7):5356-5357.
129. Schnieder L, Seekamp-Rahn K, Borkowski J, et al. Experimental studies and theoretical predictions for the D+D_2 → HD+D reaction. *Science*. 1995;269(5221):207-210.
130. Schnieder L, Seekamp-Rahn K, Wrede E, Welge KH. Experimental determination of quantum state resolved differential cross sections for the hydrogen exchange reaction D+D_2 → HD+D. *J Chem Phys*. 1997;107(16):6175-6195.
131. Wrede E, Schnieder L, Welge KH, Aoiz FJ, Banares L, Herrero VJ. High resolution study of the D+D_2 → HD+D reaction dynamics at a collision energy of 2.2 eV. *Chem Phys Lett*. 1997;265(1-2):129-136.
132. Xie Y, Zhao H, Wang Y, et al. Quantum interference in H plus HD → H_2+D between direct abstraction and roaming insertion pathways. *Science*. 2020;368(6492):767.
133. Chao SD, Harich SA, Dai DX, Wang CC, Yang XM, Skodje RT. A fully state- and angle-resolved study of the H+HD → D+H_2 reaction: comparison of a molecular beam experiment to *ab initio* quantum reaction dynamics. *J Chem Phys*. 2002;117(18):8341-8361.
134. Harich SA, Dai DX, Wang CC, Yang XM, Chao SD, Skodje RT. Forward scattering due to slow-down of the intermediate in the H+HD → D+H_2 reaction. *Nature*. 2002;419(6904):281-284.
135. Berry MV. Quantal phase-factors accompanying adiabatic changes. *Proc R Soc London, Ser A*. 1984;392(1802):45-57.
136. Herzberg GL-H. H C. *Disc Farad Soc*. 1963;35:77.
137. Teller E. The crossing of potential energy surfaces. *J Phys Chem*. 1937;41:109-116.
138. Atchity GJ, Xantheas SS, Ruedenberg K. Potential-energy surfaces near intersections. *J Chem Phys*. 1991;95(3):1862-1876.
139. Yarkony DR. Diabolical conical intersections. *Rev Mod Phys*. 1996;68(4):985-1013.
140. Yuan D, Guan Y, Chen W, et al. Observation of the geometric phase effect in the H+HD → H_2+D reaction. *Science*. 2018;362(6420):1289.
141. Yuan D, Huang Y, Chen W, et al. Observation of the geometric phase effect in the H+HD → H_2+D reaction below the conical intersection. *Nat Commun*. 2020;11(1):3640.
142. Xu H, Shaferray NE, Merkt F, et al. Measurement of the state-specific differential cross-section for the D_2+H → HD(V' = 4, J' = 3)+D reaction at a collision energy of 2.2 eV. *J Chem Phys*. 1995;103(12):5157-5160.
143. Fernandez-Alonso F, Bean BD, Zare RN. Measurement of the HD(v' = 2, J' = 3) product differential cross section for the H+D_2 exchange reaction at 1.55 +/– 0.05 eV using the photoloc technique. *J Chem Phys*. 1999;111(3):1022-1034.
144. Fernandez-Alonso F, Bean BD, Zare RN. Differential cross sections for H+D_2 → HD(v(') = 1, J(') = 1,5,8)+D at 1.7 eV. *J Chem Phys*. 1999;111(3):1035-1042.
145. Fernandez-Alonso F, Bean BD, Zare RN. Differential cross sections for H+D_2 → HD (v ' = 2, J ' = 0,3,5)+D at 1.55 eV. *J Chem Phys*. 1999;111(6):2490-2498.
146. Bartlett NCM, Jankunas J, Goswami T, Zare RN, Bouakline F, Althorpe SC. Differential cross sections for H+D_2 → HD(v = 2, j ' = 0,3,6,9) + D at center-of-mass collision energies of 1.25, 1.61, and 1.97 eV. *PCCP*. 2011;13(18):8175-8179.
147. Jankunas J, Sneha M, Zare RN, Bouakline F, Althorpe SC. Disagreement between theory and experiment grows with increasing rotational excitation of HD(v', j') product for the H+D_2 reaction. *J Chem Phys*. 2013;138(9):094310.
148. Jankunas J, Sneha M, Zare RN, Bouakline F, Althorpe SC. Simultaneous measurement of reactive and inelastic scattering: differential cross section of the H plus HD → HD(v', j ') + H reaction. *Z Phys Chem*. 2013;227(9-11):1281-1299.
149. Gao H, Sneha M, Bouakline F, Althorpe SC, Zare RN. Differential cross sections for the H+D_2 → HD(v' = 3, j' = 4-10) + D reaction above the conical intersection. *J Phys Chem A*. 2015;119(50):12036-12042.
150. Jambrina PG, Herraez-Aguilar D, Aoiz FJ, Sneha M, Jankunas J, Zare RN. Quantum interference between H+D_2 quasiclassical reaction mechanisms. *Nat Chem*. 2015;7(8):661-667.
151. Sneha M, Gao H, Zare RN, Jambrina PG, Menendez M, Aoiz FJ. Multiple scattering mechanisms causing interference effects in the differential cross sections of H+D_2 → HD(v' = 4, j') + D at 3.26 eV collision energy. *J Chem Phys*. 2016;145(2):024308.

152. Yuan D, Yu S, Chen W, et al. Direct observation of forward-scattering oscillations in the H+D_2 → H_2+D reaction. *Nat Chem*. 2018;10(6):653-658.
153. Skodje RT, Skouteris D, Manolopoulos DE, Lee SH, Dong F, Liu KP. Resonance-mediated chemical reaction: F+HD → HF+D. *Phys Rev Lett*. 2000;85(6):1206-1209.
154. Townsend D, Lahankar SA, Lee SK, et al. The roaming atom: straying from the reaction path in formaldehyde decomposition. *Science*. 2004;306(5699):1158-1161.
155. Vanzee RD, Foltz MF, Moore CB. Evidence for a 2nd-molecular channel in the fragmentation of formaldehyde. *J Chem Phys*. 1993;99(3):1664-1673.
156. Preston RK, Tully JC. Effects of surface crossing in chemical reactions — H3+ system. *J Chem Phys*. 1971;54(10):4297.
157. Ochs G, Teloy E. Integral cross sections for reactions of H^+ with D_2; new measurements. *J Chem Phys*. 1974;61(11):4930-4931.
158. Tully JC, Preston RK. Trajectory surface hopping approach to nonadiabatic molecular collisions: the reaction of H^+ with D_2. *J Chem Phys*. 1971;55(2):562-572.
159. Krenos JR, Preston RK, Wolfgang R, Tully JC. Molecular-beam and trajectory studies of reactions of H^+ with H_2. *J Chem Phys*. 1974;60(4):1634-1659.
160. Stueckelberg EC. Theory of inelastic collisions between atoms. *Helv Phys Acta*. 1932;5:369.
161. Tully JC. Collisions of F($^2P_{1/2}$) with H_2. *J Chem Phys*. 1974;60(8):3042-3050.
162. McLachlan AD. Variational solution of time-dependent Schrodinger equation. *Mol Phys*. 1964;8(1):39.
163. Tully JC. Molecular-dynamics with electronic-transitions. *J Chem Phys*. 1990;93(2):1061-1071.
164. Bittner ER, Rossky PJ. Quantum decoherence in mixed quantum-classical systems — nonadiabatic processes. *J Chem Phys*. 1995;103(18):8130-8143.
165. Granucci G, Persico M, Zoccante A. Including quantum decoherence in surface hopping. *J Chem Phys*. 2010;133(13):134111.
166. Subotnik JE, Shenvi N. A new approach to decoherence and momentum rescaling in the surface hopping algorithm. *J Chem Phys*. 2011;134(2):024105.
167. Wang L, Akimov A, Prezhdo OV. Recent progress in surface hopping: 2011–2015. *JPCLett*. 2016;7(11):2100-2112.
168. Nielsen S, Kapral R, Ciccotti G. Mixed quantum-classical surface hopping dynamics. *J Chem Phys*. 2000;112(15):6543-6553.
169. Zhu C, Jasper AW, Truhlar DG. Non-Born–Oppenheimer trajectories with self-consistent decay of mixing. *J Chem Phys*. 2004;120(12):5543-5557.
170. Jain A, Alguire E, Subotnik JE. An efficient, augmented surface hopping algorithm that includes decoherence for use in large-scale simulations. *J Chem Theo Comp*. 2016;12(11):5256-5268.
171. Ben-Nun M, Martinez TJ. Nonadiabatic molecular dynamics: validation of the multiple spawning method for a multidimensional problem. *J Chem Phys*. 1998;108(17):7244-7257.
172. Ben-Nun M, Quenneville J, Martinez TJ. *Ab initio* multiple spawning: photochemistry from first principles quantum molecular dynamics. *J Phys Chem A*. 2000;104(22):5161-5175.
173. Meyer HD, Miller WH. Classical analog for electronic degrees of freedom in non-adiabatic collision processes. *J Chem Phys*. 1979;70(7):3214-3223.
174. Stock G, Thoss M. Semiclassical description of nonadiabatic quantum dynamics. *Phys Rev Lett*. 1997;78(4):578-581.
175. Meyer HD, Worth GA. Quantum molecular dynamics: propagating wavepackets and density operators using the multiconfiguration time-dependent Hartree method. *Theor Chem Acc*. 2003;109(5):251-267.
176. Lee SH, Liu KP. Effect of reagent rotation in O(^{1}D)+H_2 (v = 0,j): a sensitive probe of the accuracy of the *ab initio* excited surfaces? *J Chem Phys*. 1999;111(9):4351-4352.
177. Balucani N, Leonori F, Casavecchia P, Fu BN, Bowman JM. Crossed molecular beams and quasiclassical trajectory surface hopping studies of the multichannel nonadiabatic O(^{3}P) + ethylene reaction at high collision energy. *J Phys Chem A*. 2015;119(50):12498-12511.
178. Attar AR, Bhattacherjee A, Pemmaraju CD, et al. Femtosecond X-ray spectroscopy of an electrocyclic ring-opening reaction. *Science*. 2017;356(6333):54-58.
179. Fingerhut BP, Dorfman KE, Mukamel S. Monitoring nonadiabatic dynamics of the RNA base uracil by UV pump-IR probe spectroscopy. *JPCLett*. 2013;4(11):1933-1942.
180. Bao JL, Truhlar DG. Variational transition state theory: theoretical framework and recent developments. *Chem Soc Rev*. 2017;46(24):7548-7596.
181. Keck JC. *Variational Theory of Reaction Rates*. London: John Wiley and Sons; 1967.
182. Lester MI, Klippenstein SJ. Unimolecular decay of criegee intermediates to OH radical products: prompt and thermal decay processes. *Acc Chem Res*. 2018;51(4):978-985.
183. Klippenstein SJ. From theoretical reaction dynamics to chemical modeling of combustion. *Proc Combust Inst*. 2017;36(1):77-111.
184. Garcia-Viloca M, Gao J, Karplus M, Truhlar DG. How enzymes work: analysis by modern rate theory and computer simulations. *Science*. 2004;303(5655):186-195.
185. Perdew JP, Burke K, Ernzerhof M. Generalized gradient approximation made simple. *Phys Rev Lett*. 1996;77(18):3865-3868.
186. Berland K, Cooper VR, Lee K, et al. van der Waals forces in density functional theory: a review of the vdW-DF method. *Rep Prog Phys*. 2015;78(6):066501.
187. Chang HC, Ewing GE. Infrared fluorescence from a monolayer of CO on NACL(100). *Phys Rev Lett*. 1990;65(17):2125-2128.
188. Chen L, Lau JA, Schwarzer D, Meyer J, Verma VB, Wodtke AM. The Sommerfeld ground-wave limit for a molecule adsorbed at a surface. *Science*. 2019;363(6423):158-161.
189. Ryberg R. Vibrational line-shape of chemisorbed CO. *Phys Rev B*. 1985;32(4):2671-2673.
190. Beckerle JD, Cavanagh RR, Casassa MP, Heilweil EJ, Stephenson JC. Subpicosecond transient infrared spectroscopy of adsorbates. Vibrational dynamics of CO/Pt(111). *J Chem Phys*. 1991;95(7):5403.
191. Cavanagh RR, Germer TA, Heilweil EJ, Stephenson JC. Time-resolved measurements of substrate to adsorbate energy-transfer. *Faraday Discuss*. 1993;96:235-243.
192. Harris AL, Levinos NJ, Rothberg L, et al. Vibrational-energy transfer to metal-surfaces probed by sum generation — CO/Cu(100) and CH3S/AG(111). *J Electron Spectrosc Relat Phenom*. 1990;54:5-16.
193. Germer TA, Stephenson JC, Heilweil EJ, Cavanagh RR. Picosecond time-resolved adsorbate response to substrate heating — spectroscopy and dynamics of CO/Cu(100). *J Chem Phys*. 1994;101(2):1704-1716.
194. Persson M, Hellsing B. Electronic damping of adsorbate vibrations on metal-surfaces. *Phys Rev Lett*. 1982;49(9):662-665.
195. Hellsing B, Persson M. Electronic damping of atomic and molecular vibrations at metal-surfaces. *Phys Scripta*. 1984;29(4):360-371.
196. Rantala TT, Rosen A. Electronic damping of adsorbate motion — CO vibration on the Cu(100) surface. *Phys Rev B*. 1986;34(2):837-842.
197. Forsblom M, Persson M. Vibrational lifetimes of cyanide and carbon monoxide on noble and transition metal surfaces. *J Chem Phys*. 2007;127(15):154303.
198. Rittmeyer SP, Meyer J, Juaristi JI, Reuter K. Electronic friction-based vibrational lifetimes of molecular adsorbates: beyond the independent-atom approximation. *Phys Rev Lett*. 2015;115(4):046102.

199. Kumar S, Jiang HY, Schwarzer M, Kandratsenka A, Schwarzer D, Wodtke AM. Vibrational relaxation lifetime of a physisorbed molecule at a metal surface. *Phys Rev Lett*. 2019;123(15):156101.
200. Loncaric I, Alducin M, Juaristi JI, Novko D. CO stretch vibration lives long on Au(111). *JPCLett*. 2019;10(5):1043-1047.
201. Dombrowski E, Peterson E, Del Sesto D, Utz AL. Precursor-mediated reactivity of vibrationally hot molecules: methane activation on Ir(111). *Catal Today*. 2015;244:10-18.
202. Head-Gordon M, Tully JC. Molecular-orbital calculations of the lifetimes of the vibrational-modes of CO on Cu(100). *Phys Rev B*. 1992;46(3):1853-1856.
203. Head-Gordon M, Tully JC. Vibrational-relaxation on metal-surfaces — molecular-orbital theory and application to CO/Cu(100). *J Chem Phys*. 1992;96(5):3939-3949.
204. Tully JC, Gomez M, Head-Gordon M. Electronic and phonon mechanisms of vibrational-relaxation — CO on Cu(100). *J Vac Sci Technol A-Vac Surf Films*. 1993;11(4):1914-1920.
205. Saltsburg H, Smith JN. Molecular-beam scattering from (111) plane of silver. *J Chem Phys*. 1966;45(6):2175.
206. Romney MJ, Anderson JB. Scattering of 0.05–5-eV argon from the (111) plane of silver. *J Chem Phys*. 1969;51(6):2490-2496.
207. Stoll AG, Smith DL, Merrill RP. Scattering of rare gases (He, Ne, Ar, Kr, and Xe) from platinum (111) surfaces. *J Chem Phys*. 1971;54(1):163.
208. Logan RM, Stickney RE. Simple classical model for the scattering of gas atoms from a solid surface. *J Chem Phys*. 1966;44(1):195-201.
209. Logan RM. Classical theory for the interaction of gas atoms with solid surfaces. *J Chem Phys*. 1968;49(2):860.
210. McClure JD. Atomic and molecular scattering from solids. II. comparison of classical scattering models in relation to experiment. *J Chem Phys*. 1969;51(5):1687.
211. Trilling L, Hurkmans A. The scattering of ions from a clean solid surface in the 1 to 10 eV range. *Surf Sci*. 1976;59(2):361-372.
212. Auerbach D, Becker C, Cowin J, Wharton L. Energy accommodation and reactivity of O_2 on tungsten. *Appl Phys*. 1977;14(2):141-147.
213. Auerbach DJ, Becker CA, Cowin JP, Wharton L. UHV application of spring-loaded Teflon seals. *Rev Sci Instrum*. 1978;49(11):1518-1519.
214. Hurst JE, Wharton L, Janda KC, Auerbach DJ. Direct inelastic scattering Ar from Pt(111). *J Chem Phys*. 1983;78(3):1559-1581.
215. Goodman FO, Wachman HY. *Dynamics of Gas-Surface Scattering*. New York, San Francisco, London: Academic Press; 1976.
216. Benedek G, Toennies JP. *Atomic Scale Dynamics at Surfaces*. Springer; 2018.
217. Tully JC. Dynamics of gas surface interactions — thermal-desorption of AR and XE from platinum. *Surf Sci*. 1981;111(3):461-478.
218. Tully JC. Dynamics of gas–surface interactions — 3D generalized Langevin model applied to fcc and bcc surfaces. *J Chem Phys*. 1980;73(4):1975-1985.
219. Arumainayagam CR, Madix RJ, McMaster MC, Suzawa VM, Tully JC. Trapping dynamics of xenon on PT(111). *Surf Sci*. 1990;226(1-2):180-190.
220. Smith RJ, Kara A, Holloway S. A molecular-dynamics study for the trapping and scattering of Ar/Pt(111). *Surf Sci*. 1993;281(3):296-308.
221. Kulginov D, Persson M, Rettner CT, Bethune DS. An empirical interaction potential for the Ar/Pt(111) system. *J Phys Chem*. 1996;100(19):7919-7927.
222. Frenkel F, Hager J, Krieger W, et al. Rotationally inelastic gas-surface scattering investigated by laser-induced fluorescence. *Phys Rev Lett*. 1981;46(2):152-155.
223. McClelland GM, Kubiak GD, Rennagel HG, Zare RN. Determination of internal-state distributions of surface scattered molecules: incomplete rotational accommodation of NO on Ag(111). *Phys Rev Lett*. 1981;46(13):831-834.
224. Kleyn AW, Luntz AC, Auerbach DJ. Rotational energy-transfer in direct inelastic surface scattering — NO on Ag(111). *Phys Rev Lett*. 1981;47(16):1169-1172.
225. Kimman J, Rettner CT, Auerbach DJ, Barker JA, Tully JC. Correlation between kinetic-energy transfer to rotation and to phonons in gas–surface collisions of NO with Ag(111). *Phys Rev Lett*. 1986;57(16):2053-2056.
226. Rahinov I, Cooper R, Yuan C, Yang XM, Auerbach DJ, Wodtke AM. Efficient vibrational and translational excitations of a solid metal surface: state-to-state time-of-flight measurements of HCl(v = 2,J = 1) scattering from Au(111). *J Chem Phys*. 2008;129(21):214708.
227. Golibrzuch K, Shirhatti PR, Rahinov I, Auerbach DJ, Wodtke AM, Bartels C. Incidence energy dependent state-to-state time-of-flight measurements of NO(v = 3) collisions with Au(111): the fate of incidence vibrational and translational energy. *PCCP*. 2014;16(16):7602-7610.
228. Kleyn AW, Horn TCM. Rainbow scattering from solid surfaces. *Phys Rep*. 1991;199(4):191-230.
229. Muhlhausen CW, Williams LR, Tully JC. Dynamics of gas–surface interactions — scattering and desorption of No from Ag(111) and Pt(111). *J Chem Phys*. 1985;83(5):2594-2606.
230. Barker JA, Kleyn AW, Auerbach DJ. Rotational energy distributions in molecule surface scattering: model calculations for NO/Ag(111). *Chem Phys Lett*. 1983;97(1):9-13.
231. Cavanagh RR, King DS. Rotational- and spin-state distributions: NO thermally desorbed from Ru(001). *Phys Rev Lett*. 1981;47(25):1829-1832.
232. Schinke R. Rotational rainbows in diatom(solid) surface scattering. *J Chem Phys*. 1982;76(5):2352.
233. Lin MC, Ertl G. Laser probing of molecules desorbing and scattering from solid surfaces. *Annu Rev Phys Chem*. 1986;37(1):587-615.
234. Coltrin ME, Kay BD. Quasiclassical trajectory study of rotational energy transfer in the scattering of NH3 from a flat, rigid gold surface. *J Chem Phys*. 1988;89(1):551-561.
235. Jacobs DC, Zare RN. Simplified trajectory method for modeling gas–surface scattering: the NO/Pt(111) system. *J Chem Phys*. 1989;91(5):3196-3207.
236. Geuzebroek FH, Wiskerke AE, Tenner MG, Kleyn AW, Stolte S, Namiki A. Rotational-excitation of oriented molecules as a probe of molecule surface interaction. *J Phys Chem*. 1991;95(21):8409-8421.
237. Hines MA, Zare RN. The interaction of CO with Ni(111): rainbows and rotational trapping. *J Phys Chem*. 1993;98(11):9134.
238. Krüger BC, Bartels N, Wodtke AM, Schäfer T. Final rotational state distributions from NO(v_i = 11) in collisions with Au(111): the magnitude of vibrational energy transfer depends on orientation in molecule–surface collisions. *PCCP*. 2016;18(22):14976-14979.
239. Park GB, Krüger BC, Meyer S, Kandratsenka A, Wodtke AM, Schäfer T. An axis-specific rotational rainbow in the direct scatter of formaldehyde from Au(111) and its influence on trapping probability. *PCCP*. 2017;19(30):19904-19915.
240. Rettner CT, Kimman J, Auerbach DJ. Inelastic-scattering of NO from Ag(111) — internal state, angle, and velocity resolved measurements. *J Chem Phys*. 1991;94(1):734-750.
241. Golibrzuch K, Baraban JH, Shirhatti PR, Werdecker J, Bartels C, Wodtke AM. Observation of translation-to-vibration excitation in acetylene scattering from Au(111): a REMPI based approach. *Z Phys Chem*. 2015;229(10-12):1929-1949.
242. Kay BD, Raymond TD, Coltrin ME. Observation of direct multiquantum vibrational excitation in gas-surface scattering: NH_3 on Au(111). *Phys Rev Lett*. 1987;59(24):2792-2794.
243. Rettner CT, Fabre F, Kimman J, Auerbach DJ. Observation of direct vibrational excitation in gas–surface collisions: NO on Ag(111). *Phys Rev Lett*. 1985;55(18):1904-1907.
244. Rettner CT, Kimman J, Fabre F, Auerbach DJ, Morawitz H. Direct vibrational excitation in gas–surface collisions of NO with Ag(111). *Surf Sci*. 1987;192(1):107-130.
245. Ran Q, Matsiev D, Auerbach DJ, Wodtke AM. Observation of a change of vibrational excitation mechanism with surface temperature: HCl collisions with Au(111). *Phys Rev Lett*. 2007;98(23):237601.

246. Shirhatti PR, Werdecker J, Golibrzuch K, Wodtke AM, Bartels C. Electron hole pair mediated vibrational excitation in CO scattering from Au(111): incidence energy and surface temperature dependence. *J Chem Phys*. 2014;141(12):124704.
247. Wagner RJV, Krüger BC, Park GB, Wallrabe M, Wodtke AM, Schäfer T. Electron transfer mediates vibrational relaxation of CO in collisions with Ag(111). *PCCP*. 2019;21(4):1650-1655.
248. Golibrzuch K, Kandratsenka A, Rahinov I, et al. Experimental and theoretical study of multi-quantum vibrational excitation: NO(v = 0 → 1,2,3) in collisions with Au(111). *J Phys Chem A*. 2013;117(32):7091-7101.
249. Cooper R, Bartels C, Kandratsenka A, et al. Multiquantum vibrational excitation of NO scattered from Au(111): quantitative comparison of benchmark data to *ab initio* theories of nonadiabatic molecule–surface interactions. *Angew Chem Int Ed*. 2012;51(20):4954-4958.
250. Cooper R, Rahinov I, Yuan C, Yang XM, Auerbach DJ, Wodtke AM. Efficient translational excitation of a solid metal surface: state-to-state translational energy distributions of vibrational ground state HCl scattering from Au(111). *J Vac Sci Technol, A*. 2009;27(4):907-912.
251. Golibrzuch K, Shirhatti PR, Altschaffel J, et al. State-to-state time-of-flight measurements of NO scattering from Au(111): direct observation of translation-to-vibration coupling in electronically nonadiabatic energy transfer. *J Phys Chem A*. 2013;117(36):8750-8760.
252. Yang X, Wodtke AM. Efficient state-specific preparation of highly vibrationally excited NO($X\,^2\Pi$). *J Chem Phys*. 1990;92(1):116-120.
253. Field RW, Bradford RS, Broida HP, Harris DO. Excited-state microwave spectroscopy on a $^1\Sigma$ state of BaO. *J Chem Phys*. 1972;57(5):2209.
254. Field RW, Broida HP, Bradford RS, Harris DO. Microwave optical double-resonance spectroscopy of BaO. *J Chem Phys*. 1972;56(9):4712.
255. Field RW, English AD, Tanaka T, Harris DO, Jennings DA. Microwave optical double-resonance spectroscopy with a CW dye laser — BaO $X^1\Sigma$ and $A^1\Sigma$. *J Chem Phys*. 1973;59(5):2191-2203.
256. Harris DO, Field RW, Broida HP. Microwave optical double-resonance spectroscopy of metal-oxides. *Ber Bunsen-Ges Phys Chem*. 1974;78(2):146-153.
257. Tanaka T, Field RW, Harris DO. Microwave optical double resonance and continuous wave dye laser excitation spectroscopy of NO_2. *J Mol Spectrosc*. 1975;56(2):188-199.
258. Gottscho RA, Field RW, Bacis R, Silvers SJ. Simultaneous measurement of rotational and translational relaxation by sub-Doppler optical-optical double-resonance spectroscopy — BaO($A^1\Sigma^+$)-Ar and BaO($A^1\Sigma^+$)-CO_2. *J Chem Phys*. 1980;73(2):599-611.
259. Gottscho RA, Weiss PS, Field RW, Pruett JG. Sub-Doppler optical-optical double-resonance spectroscopy of BaO — electronic-structure in the 4-eV region. *J Mol Spectrosc*. 1980;82(2):283-309.
260. Kittrell C, Abramson E, Kinsey JL, et al. Selective vibrational-excitation by stimulated-emission pumping. *J Chem Phys*. 1981;75(5):2056-2059.
261. Huang YH, Rettner CT, Auerbach DJ, Wodtke AM. Vibrational promotion of electron transfer. *Science*. 2000;290(5489):111-114.
262. Bartels N, Krüger BC, Meyer S, Wodtke AM, Schäfer T. Suppression of spontaneous emission in the optical pumping of molecules: pump-dump-sweep-probe. *JPCLett*. 2013;4(14):2367-2370.
263. Bartels N, Schäfer T, Huhnert J, Field RW, Wodtke AM. Production of a beam of highly vibrationally excited CO using perturbations. *J Chem Phys*. 2012;136(21):214201.
264. Geweke J, Wodtke AM. Vibrationally inelastic scattering of HCl from Ag(111). *J Chem Phys*. 2020;153(16):164703.
265. Gerrits N, Geweke J, Smeets EWF, Voss J, Wodtke AM, Kroes GJ. Closing the gap between experiment and theory: reactive scattering of HCl from Au(111). *J Phys Chem C*. 2020;124(29):15944-15960.
266. Geweke J, Shirhatti PR, Rahinov I, Bartels C, Wodtke AM. Vibrational energy transfer near a dissociative adsorption transition state: state-to-state study of HCl collisions at Au(111). *J Chem Phys*. 2016;145(5):054709.
267. Krüger BC, Bartels N, Bartels C, et al. NO vibrational energy transfer on a metal surface: still a challenge to first-principles theory. *J Phys Chem C*. 2015;119(6):3268-3272.
268. Schäfer T, Bartels N, Golibrzuch K, et al. Observation of direct vibrational excitation in gas–surface collisions of CO with Au(111): a new model system for surface dynamics. *PCCP*. 2013;15(6):1863-1867.
269. Bartels N, Golibrzuch K, Bartels C, et al. Dynamical steering in an electron transfer surface reaction: oriented NO(v = 3, 0.08 < E-i < 0.89 eV) relaxation in collisions with a Au(111) surface. *J Chem Phys*. 2014;140(5):054710.
270. Wagner RJV, Henning N, Krüger BC, et al. Vibrational relaxation of highly vibrationally excited CO scattered from Au(111): evidence for CO-formation. *JPCLett*. 2017;8(19):4887-4892.
271. Krüger BC, Meyer S, Kandratsenka A, Wodtke AM, Schäfer T. Vibrational inelasticity of highly vibrationally excited NO on Ag(111). *JPCLett*. 2016;7(3):441-446.
272. Steinsiek C, Shirhatti PR, Geweke J, Bartels C, Wodtke AM. Work function dependence of vibrational relaxation probabilities: NO(v = 2) scattering from ultrathin metallic films of Ag/Au(111). *J Phys Chem C*. 2018;122(18):10027-10033.
273. Schäfer T, Bartels N, Hocke N, Yang XM, Wodtke AM. Orienting polar molecules without hexapoles: optical state selection with adiabatic orientation. *Chem Phys Lett*. 2012;535:1-11.
274. Bartels N, Golibrzuch K, Bartels C, et al. Observation of orientation-dependent electron transfer in molecule–surface collisions. *PNAS*. 2013;110(44):17738-17743.
275. Bartels N, Krüger BC, Auerbach DJ, Wodtke AM, Schäfer T. Controlling an electron-transfer reaction at a metal surface by manipulating reactant motion and orientation. *Angew Chem Int Ed*. 2014;53(50):13690.
276. Shenvi N, Roy S, Tully JC. Dynamical steering and electronic excitation in NO scattering from a gold surface. *Science*. 2009;326(5954):829-832.
277. White JD, Chen J, Matsiev D, Auerbach DJ, Wodtke AM. Conversion of large-amplitude vibration to electron excitation at a metal surface. *Nature*. 2005;433(7025):503-505.
278. Nahler NH, White JD, Larue J, Auerbach DJ, Wodtke AM. Inverse velocity dependence of vibrationally promoted electron emission from a metal surface. *Science*. 2008;321(5893):1191-1194.
279. LaRue JL, White JD, Nahler NH, et al. The work function of submonolayer cesium-covered gold: a photoelectron spectroscopy study. *J Chem Phys*. 2008;129(2):024709.
280. LaRue J, Schäfer T, Matsiev D, et al. Vibrationally promoted electron emission at a metal surface: electron kinetic energy distributions. *PCCP*. 2011;13(1):97-99.
281. LaRue JL, Schäfer T, Matsiev D, et al. Electron kinetic energies from vibrationally promoted surface exoemission: evidence for a vibrational autodetachment mechanism. *J Phys Chem A*. 2011;115(50):14306-14314.
282. Fermi E, Teller E. The capture of negative mesotrons in matter. *Phys Rev*. 1947;72(5):399-408.
283. Ritchie RH. Interaction of charged particles with a degenerate fermi-dirac electron gas. *Phys Rev*. 1959;114(3):644-654.
284. Echenique PM, Nieminen RM, Ritchie RH. Density functional calculation of stopping power of an electron-gas for slow ions. *Solid State Commun*. 1981;37(10):779-781.
285. Echenique PM, Nieminen RM, Ashley JC, Ritchie RH. Nonlinear stopping power of an electron-gas for slow ions. *Phys Rev A*. 1986;33(2):897-904.

286. Puska MJ, Nieminen RM. Atoms embedded in an electron-gas — phase-shifts and cross-sections. *Phys Rev B*. 1983;27(10):6121-6128.
287. Schaich WL. Brownian-motion model of surface chemical-reactions — derivation in large mass limit. *J Chem Phys*. 1974;60(3):1087-1093.
288. Dagliano EG, Kumar P, Schaich W, Suhl H. Brownian-motion model of interactions between chemical species and metallic electrons — bootstrap derivation and parameter evaluation. *Phys Rev B*. 1975;11(6):2122-2143.
289. Li YG, Wahnstrom G. Nonadiabatic effects in hydrogen diffusion in metals. *Phys Rev Lett*. 1992;68(23):3444-3447.
290. Dou W, Subotnik JE. Universality of electronic friction: equivalence of von Oppen's nonequilibrium Green's function approach and the Head–Gordon–Tully model at equilibrium. *Phys Rev B*. 2017;96(10).
291. Trail JR, Bird DM, Persson M, Holloway S. Electron–hole pair creation by atoms incident on a metal surface. *J Chem Phys*. 2003;119(8):4539-4549.
292. Blanco-Rey M, Juaristi JI, Díez Muiño R, Busnengo HF, Kroes GJ, Alducin M. Electronic friction dominates hydrogen hot-atom relaxation on Pd(100). *Phys Rev Lett*. 2014;112(10):103203.
293. Novko D, Blanco-Rey M, Alducin M, Juaristi JI. Surface electron density models for accurate ab initiomolecular dynamics with electronic friction. *Phys Rev B*. 2016;93(24):245435.
294. Füchsel G, Schimka S, Saalfrank P. On the role of electronic friction for dissociative adsorption and scattering of hydrogen molecules at a Ru(0001) surface. *J Phys Chem A*. 2013;117(36):8761-8769.
295. Janke SM, Auerbach DJ, Wodtke AM, Kandratsenka A. An accurate full-dimensional potential energy surface for H-Au(111): importance of nonadiabatic electronic excitation in energy transfer and adsorption. *J Chem Phys*. 2015;143(12):124708.
296. Dorenkamp Y, Jiang HY, Kockert H, et al. Hydrogen collisions with transition metal surfaces: universal electronically nonadiabatic adsorption. *J Chem Phys*. 2018;148(3):034706.
297. Kandratsenka A, Jiang HY, Dorenkamp Y, et al. Unified description of H-atom-induced chemicurrents and inelastic scattering. *PNAS*. 2018;115(4):680-684.
298. Bunermann O, Jiang HY, Dorenkamp Y, et al. Electron–hole pair excitation determines the mechanism of hydrogen atom adsorption. *Science*. 2015;350(6266):1346-1349.
299. Juaristi JI, Alducin M, Muiño RD, Busnengo HF, Salin A. Role of electron–hole pair excitations in the dissociative adsorption of diatomic molecules on metal surfaces. *Phys Rev Lett*. 2008;100(11):116102.
300. Novko D, Blanco-Rey M, Juaristi JI, Alducin M. *Ab initio* molecular dynamics with simultaneous electron and phonon excitations: application to the relaxation of hot atoms and molecules on metal surfaces. *Phys Rev B*. 2015;92(20):201411.
301. Luntz AC, Makkonen I, Persson M, Holloway S, Bird DM, Mizielinski MS. Comment on "Role of electron–hole pair excitations in the dissociative adsorption of diatomic molecules on metal surfaces. *Phys Rev Lett*. 2009;102(10):109601.
302. Juaristi JI, Alducin M, Muino RD, Busnengo HF, Salin A. Comment on "Role of electron–hole pair excitations in the dissociative adsorption of diatomic molecules on metal surfaces" Juaristi et al. reply. *Phys Rev Lett*. 2009;102(10):109602.
303. Isborn CM, Li XS, Tully JC. Time-dependent density functional theory Ehrenfest dynamics: collisions between atomic oxygen and graphite clusters. *J Chem Phys*. 2007;126(13).
304. Moss CL, Isborn CM, Li XS. Ehrenfest dynamics with a time-dependent density-functional-theory calculation of lifetimes and resonant widths of charge-transfer states of Li^+ near an aluminum cluster surface. *Phys Rev A*. 2009;80(2).
305. Head-Gordon M, Tully JC. Molecular-dynamics with electronic frictions. *J Chem Phys*. 1995;103(23):10137-10145.
306. Kubo R. Fluctuation-dissipation theorem. *Rep Prog Phys*. 1966;29:255.
307. Askerka M, Maurer RJ, Batista VS, Tully JC. Role of tensorial electronic friction in energy transfer at metal surfaces. *Phys Rev Lett*. 2016;116(21):217601.
308. Maurer RJ, Askerka M, Batista VS, Tully JC. *Ab initio* tensorial electronic friction for molecules on metal surfaces: nonadiabatic vibrational relaxation. *Phys Rev B*. 2016;94(11):115432.
309. Spiering P, Shakouri K, Behler J, Kroes G-J, Meyer J. Orbital-dependent electronic friction significantly affects the description of reactive scattering of N_2 from Ru(0001). *JPCLett*. 2019;10(11):2957-2962.
310. Borodin D, Rahinov I, Shirhatti PR, et al. Following the microscopic pathway to adsorption through chemisorption and physisorption wells. *Science*. 2020;369(6510):1461-1465.
311. Maurer RJ, Jiang B, Guo H, Tully JC. Mode specific electronic friction in dissociative chemisorption on metal surfaces: H_2 on Ag(111). *Phys Rev Lett*. 2017;118(25):256001.
312. Maurer RJ, Zhang YL, Guo H, Jiang B. Hot electron effects during reactive scattering of H_2 from Ag(111): assessing the sensitivity to initial conditions, coupling magnitude, and electronic temperature. *Faraday Discuss*. 2019;214:105-121.
313. Zhang YL, Maurer RJ, Guo H, Jiang B. Hot-electron effects during reactive scattering of H_2 from Ag(111): the interplay between mode-specific electronic friction and the potential energy landscape. *Chem Sci*. 2019;10(4):1089-1097.
314. Zhang YL, Maurer RJ, Jiang B. Symmetry-adapted high dimensional neural network representation of electronic friction tensor of adsorbates on metals. *J Phys Chem C*. 2020;124(1):186-195.
315. Monturet S, Saalfrank P. Role of electronic friction during the scattering of vibrationally excited nitric oxide molecules from Au(111). *Phys Rev B*. 2010;82(7):075404.
316. Shenvi N, Roy S, Tully JC. Nonadiabatic dynamics at metal surfaces: independent-electron surface hopping. *J Chem Phys*. 2009;130(17).
317. Roy S, Shenvi NA, Tully JC. Model Hamiltonian for the interaction of NO with the Au(111) surface. *J Chem Phys*. 2009;130(17):174716.
318. Golibrzuch K, Shirhatti PR, Rahinov I, et al. The importance of accurate adiabatic interaction potentials for the correct description of electronically nonadiabatic vibrational energy transfer: a combined experimental and theoretical study of NO(v = 3) collisions with a Au(111) surface. *J Chem Phys*. 2014;140(4).
319. Box CL, Zhang Y, Yin R, Jiang B, Maurer RJ. Determining the effect of hot electron dissipation on molecular scattering experiments at metal surfaces. *JACS Au*. 2021;1:164-173.
320. Yin R, Zhang Y, Jiang B. Strong vibrational relaxation of NO scattered from Au(111): importance of the adiabatic potential energy surface. *JPCLett*. 2019;10(19):5969-5974.
321. Bunermann O, Jiang HY, Dorenkamp Y, Auerbach DJ, Wodtke AM. An ultrahigh vacuum apparatus for H atom scattering from surfaces. *Rev Sci Instrum*. 2018;89(9):094101.
322. Nørskov JK, Lundqvist BI. Correlation between sticking probability and adsorbate-induced electron structure. *Surf Sci*. 1979;89(1-3):251-261.
323. Pavanello M, Auerbach DJ, Wodtke AM, Blanco-Rey M, Alducin M, Kroes GJ. Adiabatic energy loss in hyperthermal H atom collisions with Cu and Au: a basis for testing the importance of nonadiabatic energy loss. *JPCLett*. 2013;4(21):3735-3740.
324. Kammler M, Janke SM, Kandratsenka A, Wodtke AM. Genetic algorithm approach to global optimization of the full-dimensional potential energy surface for hydrogen atom at fcc-metal surfaces. *Chem Phys Lett*. 2017;683:286-290.
325. Dorenkamp Y, Jiang HY, Kockert H, et al. Hydrogen collisions with transition metal surfaces: universal electronically nonadiabatic adsorption (vol 148, 034706, 2018). *J Chem Phys*. 2019;150(9):1.

326. Jeloaica L, Sidis V. DFT investigation of the adsorption of atomic hydrogen on a cluster-model graphite surface. *Chem Phys Lett*. 1999;300(1):157-162.
327. Zecho T, Güttler A, Sha X, Jackson B, Küppers J. Adsorption of hydrogen and deuterium atoms on the (0001) graphite surface. *J Chem Phys*. 2002;117(18):8486-8492.
328. Jiang HY, Kammler M, Ding FZ, et al. Imaging covalent bond formation by H atom scattering from graphene. *Science*. 2019;364(6438):379.
329. Wille S, Jiang H, Bünermann O, Wodtke AM, Behler J, Kandratsenka A. An experimentally validated neural-network potential energy surface for H-atom on free-standing graphene in full dimensionality. *PCCP*. 2020;22(45):26113-26120.
330. Lennard-Jones JE. Processes of adsorption and diffusion on solid surfaces. *Trans Farad Soc*. 1932;28:333-358.
331. Opila R, Gomer R. Thermal-desorption of XE from the W(110) plane. *Surf Sci*. 1981;112(1-2):1-22.
332. Estrup PJ, Greene EF, Cardillo MJ, Tully JC. Influence of surface phase-transitions on desorption-kinetics — the compensation effect. *J Phys Chem*. 1986;90(17):4099-4104.
333. Starr DE, Campbell CT. Large entropy difference between terrace and step sites on surfaces. *J Am Chem Soc*. 2008;130(23):7321-7327.
334. Serri JA, Tully JC, Cardillo MJ. The influence of steps on the desorption-kinetics of NO from Pt(111). *J Chem Phys*. 1983;79(3):1530-1540.
335. Golibrzuch K, Shirhatti PR, Geweke J, et al. CO desorption from a catalytic surface: elucidation of the role of steps by velocity-selected residence time measurements. *J Am Chem Soc*. 2015;137(4):1465-1475.
336. Langmuir I. The condensation and evaporation of gas molecules. *PNAS*. 1917;3(3):141-147.
337. Hurst JE, Becker CA, Cowin JP, Janda KC, Wharton L, Auerbach DJ. Observation of direct inelastic-scattering in the presence of trapping-desorption scattering — Xe on Pt(111). *Phys Rev Lett*. 1979;43(16):1175-1177.
338. Huang M, Zhou X, Zhang Y, et al. Adiabatic and nonadiabatic energy dissipation during scattering of vibrationally excited CO from Au(111). *Phys Rev B*. 2019;100(20).
339. Adamson AW, Gast AP. *Physical Chemistry of Surfaces*. John Wiley and Sons; 1997.
340. Tully JC. The dynamics of adsorption and desorption. *Surf Sci*. 1994;299-300:667-677.
341. Michelsen HA, Auerbach DJ. A critical-examination of data on the dissociative adsorption and associative desorption of hydrogen at copper surfaces. *J Chem Phys*. 1991;94(11):7502-7520.
342. Michelsen HA, Rettner CT, Auerbach DJ, Zare RN. Effect of rotation on the translational and vibrational energy dependence of the dissociative adsorption of D_2 on Cu(111). *J Chem Phys*. 1993;98(10):8294.
343. Rettner CT, Schweizer EK, Mullins CB. Desorption and trapping of argon at a 2H-W(100) surface and a test of the applicability of detailed balance to a nonequilibrium system. *J Chem Phys*. 1989;90(7):3800-3813.
344. Head-Gordon M, Tully JC, Rettner CT, Mullins CB, Auerbach DJ. On the nature of trapping and desorption at high surface temperatures — theory and experiments for the Ar-Pt(111) system. *J Chem Phys*. 1991;94(2):1516-1527.
345. Nattino F, Genova A, Guijt M, et al. Dissociation and recombination of D_2 on Cu(111): *ab initio* molecular dynamics calculations and improved analysis of desorption experiments. *J Chem Phys*. 2014;141(12):124705.
346. Langmuir I. The dissociation of water vapor and carbon dioxide at high temperatures. *J Am Chem Soc*. 1906;28(10):1357-1379.
347. Langmuir I. Über partielle Wiedervereinigung dissociierter Gase in Verlauf einer Abkühlung [Ph.D.]. Göttingen: Chemie, Georg-Augusts-Universität zu Göttingen; 1906.
348. Langmuir I. The dissociation of hydrogen into atoms. III. The mechanism of the reaction. *J Am Chem Soc*. 1916;38(6):1145-1156.
349. Langmuir I. The adsorption of gases on plane surfaces of glass, mica and platinum. *J Am Chem Soc*. 1918;40(9):1361-1403.
350. Rideal EK. A note on a simple molecular mechanism for heterogeneous catalytic reactions. *Math Proc Camb Philos Soc*. 1939;35(1):130-132.
351. Rettner CT, Auerbach DJ. Dynamics of the Eley–Rideal reaction of D-atoms with H-atoms adsorbed on Cu(111) — vibrational and rotational state distributions of the HD product. *Phys Rev Lett*. 1995;74(22):4551-4554.
352. Rettner CT. Reaction of an H-atom beam with Cl/Au(111): dynamics of concurrent Eley–Rideal and Langmuir–Hinshelwood mechanisms. *J Chem Phys*. 1994;101(2):1529-1546.
353. Rettner CT, Auerbach DJ. Distinguishing the direct and indirect products of a gas-surface reaction. *Science*. 1994;263(5145):365-367.
354. Comsa G, David R, Schumacher B-J. Fast deuterium molecules desorbing from metals. *Surf Sci Lett*. 1980;95(1):L210-L216.
355. Jørgensen M, Grönbeck H. First-principles microkinetic modeling of methane oxidation over Pd(100) and Pd(111). *ACS Catal*. 2016;6(10):6730-6738.
356. Rettner CT, Auerbach DJ, Michelsen HA. Role of vibrational and translational energy in the activated dissociative adsorption of D_2 on Cu(111). *Phys Rev Lett*. 1992;68(8):1164-1167.
357. Kaufmann S, Shuai Q, Auerbach DJ, Schwarzer D, Wodtke AM. Associative desorption of hydrogen isotopologues from copper surfaces: characterization of two reaction mechanisms. *J Chem Phys*. 2018;148(19).
358. Murphy MJ, Hodgson A. Adsorption and desorption dynamics of H_2 and D_2 on Cu(111): the role of surface temperature and evidence for corrugation of the dissociation barrier. *J Chem Phys*. 1998;108(10):4199-4211.
359. Rettner CT, Michelsen HA, Auerbach DJ. Quantum-state-specific dynamics of the dissociative adsorption and associative desorption of H_2 at a Cu(111) surface. *J Chem Phys*. 1995;102(11):4625.
360. Rettner CT, Michelsen HA, Auerbach DJ. From quantum-state-specific dynamics to reaction rates: the dominant role of translational energy in promoting the dissociation of D_2 on Cu(111) under equilibrium conditions. *Faraday Discuss*. 1993;96:17.
361. Gulding SJ, Wodtke AM, Hou H, Rettner CT, Michelsen HA, Auerbach DJ. Alignment of D_2(v,J) desorbed from Cu(111): low sensitivity of activated dissociative chemisorption to approach geometry. *J Chem Phys*. 1996;105(21):9702-9705.
362. Hou H, Gulding SJ, Rettner CT, Wodtke AM, Auerbach DJ. The stereodynamics of a gas-surface reaction. *Science*. 1997;277(5322):80-82.
363. Diaz C, Pijper E, Olsen RA, Busnengo HF, Auerbach DJ, Kroes GJ. Chemically accurate simulation of a prototypical surface reaction: H_2 dissociation on Cu(111). *Science*. 2009;326(5954):832-834.
364. Kroes G-J, Díaz C. Quantum and classical dynamics of reactive scattering of H_2 from metal surfaces. *Chem Soc Rev*. 2016;45(13):3658-3700.
365. Shirhatti PR, Geweke J, Steinsiek C, et al. Activated dissociation of HCl on Au(111). *JPCLett*. 2016;7(7):1346-1350.
366. Liu T, Fu B, Zhang DH. Six-dimensional quantum dynamics study for the dissociative adsorption of HCl on Au(111) surface. *J Chem Phys*. 2013;139(18):184705.
367. Füchsel G, Del Cueto M, Díaz C, Kroes G-J. Enigmatic HCl + Au(111) reaction: a puzzle for theory and experiment. *J Phys Chem C*. 2016;120:25760-25779.
368. Kolb B, Guo H. Communication: Energy transfer and reaction dynamics for DCl scattering on Au(111): an *ab initio* molecular dynamics study. *J Chem Phys*. 2016;145(1):011102.
369. Liu T, Fu B, Zhang DH. Six-dimensional potential energy surfaces of the dissociative chemisorption of HCl on Ag(111) with three density functionals. *J Chem Phys*. 2018;149(5):054702.

370. Zhou LS, Zhou XY, Alducin M, Zhang L, Jiang B, Guo H. *Ab initio* molecular dynamics study of the Eley–Rideal reaction of H + Cl-Au(111) → HCl + Au(111): impact of energy dissipation to surface phonons and electron–hole pairs. *J Chem Phys*. 2018;148(1):014702.
371. Gerrits N, Smeets EWF, Vuckovic S, Powell AD, Doblhoff-Dier K, Kroes G-J. Density functional theory for molecule–metal surface reactions: when does the generalized gradient approximation get it right, and what to do if it does not. *JPCLett*. 2020;11:10552-10560.
372. Roy S, Nayanthara KJ, Tiwari N, Tiwari AK. Energetics and dynamics of CH_4 and H_2O dissociation on metal surfaces. *Int Rev Phys Chem*. 2020;39(3):267-318.
373. Chadwick H, Beck RD. Quantum state–resolved studies of chemisorption reactions. *Annu Rev Phys Chem*. 2017;68(1):39-61.
374. Luntz AC, Beck RD. Review Article: Dynamics of methane dissociation on transition metals. *J Vac Sci Technol, A*. 2017;35(5):05C201.
375. Chadwick H, Beck RD. Quantum state resolved gas–surface reaction dynamics experiments: a tutorial review. *Chem Soc Rev*. 2016;45(13):3576-3594.
376. Hu X, Yang M, Xie D, Guo H. Vibrational enhancement in the dynamics of ammonia dissociative chemisorption on Ru(0001). *J Chem Phys*. 2018;149(4):044703.
377. Luo X, Zhou X, Jiang B. Effects of surface motion and electron–hole pair excitations in CO_2 dissociation and scattering on Ni(100). *J Chem Phys*. 2018;148(17):174702.
378. Chen J, Zhou X, Zhang Y, Jiang B. Vibrational control of selective bond cleavage in dissociative chemisorption of methanol on Cu(111). *Nat Commun*. 2018;9(1):1038.
379. Maroni P, Papageorgopoulos DC, Sacchi M, Dang TT, Beck RD, Rizzo TR. State-resolved gas-surface reactivity of methane in the symmetric C-H stretch vibration on Ni(100). *Phys Rev Lett*. 2005;94(24):246104.
380. Rettner CT, Pfnür HE, Auerbach DJ. On the role of vibrational energy in the activated dissociative chemisorption of methane on tungsten and rhodium. *J Chem Phys*. 1986;84(8):4163-4167.
381. Lee MB, Yang QY, Ceyer ST. Dynamics of the activated dissociative chemisorption of CH_4 and implication for the pressure gap in catalysis — a molecular-beam high-resolution electron-energy loss study. *J Chem Phys*. 1987;87(5):2724-2741.
382. Utz AL. Mode selective chemistry at surfaces. *Curr Opin Solid State Mater Sci*. 2009;13(1-2):4-12.
383. Beck RD, Maroni P, Papageorgopoulos DC, Dang TT, Schmid MP, Rizzo TR. Vibrational mode-specific reaction of methane on a nickel surface. *Science*. 2003;302(5642):98-100.
384. Killelea DR, Campbell VL, Shuman NS, Utz AL. Bond-selective control of a heterogeneously catalyzed reaction. *Science*. 2008;319(5864):790-793.
385. Yoder BL, Bisson R, Beck RD. Steric effects in the chemisorption of vibrationally excited methane on Ni(100). *Science*. 2010;329(5991):553-556.
386. Jackson B, Nave S. The dissociative chemisorption of methane on Ni(111): the effects of molecular vibration and lattice motion. *J Chem Phys*. 2013;138(17):174705.
387. Chadwick H, Guo H, Gutiérrez-González A, Menzel JP, Jackson B, Beck RD. Methane dissociation on the steps and terraces of Pt(211) resolved by quantum state and impact site. *J Chem Phys*. 2018;148(1):014701.
388. Jiang B, Yang MH, Xie DQ, Guo H. Quantum dynamics of polyatomic dissociative chemisorption on transition metal surfaces: mode specificity and bond selectivity. *Chem Soc Rev*. 2016;45(13):3621-3640.
389. Nave S, Tiwari AK, Jackson B. Dissociative chemisorption of methane on Ni and Pt surfaces: mode-specific chemistry and the effects of lattice motion. *J Phys Chem A*. 2014;118(41):9615-9631.
390. Miller WH, Handy NC, Adams JE. Reaction-path Hamiltonian for polyatomic-molecules. *J Chem Phys*. 1980;72(1):99-112.
391. Mastromatteo M, Jackson B. The dissociative chemisorption of methane on Ni(100) and Ni(111): classical and quantum studies based on the reaction path Hamiltonian. *J Chem Phys*. 2013;139(19):194701.
392. Campbell VL, Chen N, Guo H, Jackson B, Utz AL. Substrate vibrations as promoters of chemical reactivity on metal surfaces. *J Phys Chem A*. 2015;119(50):12434-12441.
393. Nave S, Tiwari AK, Jackson B. Methane dissociation and adsorption on Ni(111), Pt(111), Ni(100), Pt(100), and Pt(110)-(1×2): energetic study. *J Chem Phys*. 2010;132(5):054705.
394. Nave S, Jackson B. Methane dissociation on Ni(111): the role of lattice reconstruction. *Phys Rev Lett*. 2007;98(17):173003.
395. Tiwari AK, Nave S, Jackson B. Methane dissociation on Ni(111): a new understanding of the lattice effect. *Phys Rev Lett*. 2009;103(25):253201.
396. Guo H, Farjamnia A, Jackson B. Effects of lattice motion on dissociative chemisorption: toward a rigorous comparison of theory with molecular beam experiments. *JPCLett*. 2016;7:4576-4584.
397. Shen X, Zhang Z, Zhang DH. CH_4 dissociation on Ni(111): a quantum dynamics study of lattice thermal motion. *PCCP*. 2015;17(38):25499-25504.
398. Gutiérrez-González A, Torio ME, Busnengo HF, Beck RD. Site selective detection of methane dissociation on stepped Pt surfaces. *Top Catal*. 2019;62:859-873.
399. Gutierrez-Gonzalez A, Crim FF, Beck RD. Bond selective dissociation of methane (CH_3D) on the steps and terraces of Pt(211). *J Chem Phys*. 2018;149(7).
400. Migliorini D, Chadwick H, Nattino F, et al. Surface reaction barriometry: methane dissociation on flat and stepped transition-metal surfaces. *JPCLett*. 2017;8(17):4177-4182.
401. Hundt PM, Jiang B, van Reijzen ME, Guo H, Beck RD. Vibrationally promoted dissociation of water on Ni(111). *Science*. 2014;344(6183):504-507.
402. Farjamnia A, Jackson B. The dissociative chemisorption of water on Ni(111): mode- and bond-selective chemistry on metal surfaces. *J Chem Phys*. 2015;142(23):234705.
403. Jiang B, Guo H. Dynamics of water dissociative chemisorption on Ni(111): effects of impact sites and incident angles. *Phys Rev Lett*. 2015;114(16):166101.
404. Jiang B, Guo H. Quantum and classical dynamics of water dissociation on Ni(111): a test of the site-averaging model in dissociative chemisorption of polyatomic molecules. *J Chem Phys*. 2015;143(16):164705.
405. Liu T, Zhang Z, Fu B, Yang X, Zhang D. Mode specificity for the dissociative chemisorption of H_2O on Cu(111): a quantum dynamics study on an accurately fitted potential energy surface. *Phys Chem Chem Phys*. 2016;18:8537.
406. Shen XJ, Zhang DH. Recent advances in quantum dynamics studies of gas-surface reactions. *Adv Chem Phys*. 2018;163:77-116.
407. Ghosh S, Tiwari AK. Multifold enhancement in water dissociation with Ag/Ni bimetallic alloy surfaces. *Surf Sci*. 2020;701:9.
408. Ghosh S, Ray D, Tiwari AK. Effects of alloying on mode-selectivity in H_2O dissociation on Cu/Ni bimetallic surfaces. *J Chem Phys*. 2019;150(11):114702.
409. Ray D, Ghosh S, Tiwari AK. Controlling heterogeneous catalysis of water dissociation using Cu–Ni bimetallic alloy surfaces: a quantum dynamics study. *J Phys Chem A*. 2018;122:5698-5709.
410. Morin M, Levinos NJ, Harris AL. Vibrational energy transfer of CO/Cu(100): nonadiabatic vibration/electron coupling. *J Chem Phys*. 1992;96(5):3950-3956.
411. Shirhatti PR, Rahinov I, Golibrzuch K, et al. Observation of the adsorption and desorption of vibrationally excited molecules on a metal surface. *Nat Chem*. 2018;10(6):592-598.

412. Moiraghi R, Lozano A, Peterson E, Utz A, Dong W, Busnengo HF. Non-thermalized precursor-mediated dissociative chemisorption at high catalysis temperatures. *JPCLett*. 2020;11(6):2211-2218.
413. Jackson B. Direct and trapping-mediated pathways to dissociative chemisorption: CH_4 dissociation on Ir(111) with step defects. *J Chem Phys*. 2020;153(3):034704.
414. Alducin M, Díez Muiño R, Juaristi JI. Non-adiabatic effects in elementary reaction processes at metal surfaces. *Prog Surf Sci*. 2017;92(4):317-340.
415. Hu C, Zhang Y, Jiang B. Dynamics of H_2O adsorption on Pt(110)-(1 × 2) based on a neural network potential energy surface. *J Phys Chem C*. 2020;124(42):23190-23199.
416. Luo X, Jiang B, Juaristi JI, Alducin M, Guo H. Electron–hole pair effects in methane dissociative chemisorption on Ni(111). *J Chem Phys*. 2016;145(4):044704.
417. Jiang B, Alducin M, Guo H. Electron–hole pair effects in polyatomic dissociative chemisorption: water on Ni(111). *JPCLett*. 2016;7(2):327–331.
418. Schindler B, Diesing D, Hasselbrink E. Electronic excitations induced by hydrogen surface chemical reactions on gold. *J Chem Phys*. 2011;134(3):034705.
419. Shuai Q, Kaufmann S, Auerbach DJ, Schwarzer D, Wodtke AM. Evidence for electron–hole pair excitation in the associative desorption of H_2 and D_2 from Au(111). *JPCLett*. 2017;8(7):1657-1663.
420. Romm L, Katz G, Kosloff R, Asscher M. Dissociative chemisorption of N_2 on Ru(001) enhanced by vibrational and kinetic energy: molecular beam experiments and quantum mechanical calculations. *J Phys Chem B*. 1997;101(12):2213-2217.
421. Egeberg RC, Larsen JH, Chorkendorff I. Molecular beam study of N_2 dissociation on Ru(0001). *PCCP*. 2001;3(11):2007-2011.
422. Diekhöner L, Mortensen H, Baurichter A, Jensen E, Petrunin VV, Luntz AC. N_2 dissociative adsorption on Ru(0001): the role of energy loss. *J Chem Phys*. 2001;115(19):9028-9035.
423. Mortensen H, Jensen E, Diekhöner L, Baurichter A, Luntz AC, Petrunin VV. State resolved inelastic scattering of N_2 from Ru(0001). *J Chem Phys*. 2003;118(24):11200-11209.
424. Murphy MJ, Skelly JF, Hodgson A, Hammer B. Inverted vibrational distributions from N_2 recombination at Ru(001): evidence for a metastable molecular chemisorption well. *J Chem Phys*. 1999;110(14):6954-6962.
425. Diekhöner L, Hornekær L, Mortensen H, et al. Indirect evidence for strong nonadiabatic coupling in N_2 associative desorption from and dissociative adsorption on Ru(0001). *J Chem Phys*. 2002;117(10):5018-5030.
426. Díaz C, Perrier A, Kroes GJ. Associative desorption of N_2 from Ru(0001): a computational study. *Chem Phys Lett*. 2007;434(4-6):231-236.
427. Luntz AC, Persson M. How adiabatic is activated adsorption/associative desorption? *J Chem Phys*. 2005;123(7):074704.
428. Shakouri K, Behler J, Meyer J, Kroes G-J. Accurate neural network description of surface phonons in reactive gas–surface dynamics: N_2 + Ru(0001). *JPCLett*. 2017;8(10):2131-2136.
429. Schwarz J. Reactive scattering from solid surfaces. Treatment of lock-in detector signals from modulated molecular beams. *J Catal*. 1968;12(2):140-144.
430. Schwarz JA, Madix RJ. Modulated beam relaxation spectrometry. *Surf Sci*. 1974;46(1):317-341.
431. Gaviola E. Ein Fluorometer. Apparat zur Messung von Fluoreszensabklingzeiten. *Z Phys*. 1927;42:853.
432. Eigen M. Methods for investigation of ionic reactions in aqueous solutions with half-times as short as 10^{-9} sec. Application to neutralization and hydrolysis reactions. *Disc Farad Soc*. 1954;17:194.
433. Smith JN, Fite WL. Reflection and dissociation of H_2 on tungsten. *J Chem Phys*. 1962;37(4):898-904.
434. Fite WL, Datz S. Chemical research with molecular beams. *Annu Rev Phys Chem*. 1963;14:61.
435. Fite WL, Brackmann RT. Collisions of electrons with hydrogen atoms. I. Ionization. *Phys Rev*. 1958;112(4):1141-1151.
436. D'Evelyn MP, Madix RJ. Reactive scattering from solid surfaces. *Surf Sci Rep*. 1983;3(8):413-495.
437. Arumainayagam CR, Madix RJ. Molecular beam studies of gas–surface collision dynamics. *Prog Surf Sci*. 1991;38(1):1-102.
438. Engel T, Ertl G. A molecular beam investigation of the catalytic oxidation of CO on Pd (111). *J Chem Phys*. 1978;69(3):1267.
439. Campbell CT, Ertl G, Kuipers H, Segner J. A molecular-beam study of the catalytic-oxidation of CO on a Pt(111) surface. *J Chem Phys*. 1980;73(11):5862-5873.
440. Fair JA, Madix RJ. A molecular beam investigation of the oxidation of CO on Pt[9(111)×(100)]. *J Chem Phys*. 1980;73(7):3486.
441. Becker CA, Cowin JP, Wharton L, Auerbach DJ. CO_2 product velocity distributions for CO oxidation on platinum. *J Chem Phys*. 1977;67(7):3394.
442. Mullins CB, Rettner CT, Auerbach DJ. Dynamics of the oxidation of CO on Pt(111) by an atomic oxygen beam. *J Chem Phys*. 1991;95(11):8649-8651.
443. Cao GY, Moula MG, Ohno Y, Matsushima T. Dynamics on individual reaction sites in steady-state carbon monoxide oxidation on stepped platinum(113). *J Phys Chem B*. 1999;103(16):3235-3241.
444. Bernasek SL, Leone SR. Direct detection of vibrational excitation in the CO_2 product of the oxidation of CO on a platinum surface. *Chem Phys Lett*. 1981;84(2):401-404.
445. Coulston GW, Haller GL. The dynamics of CO oxidation on Pd, Rh, and Pt studied by high-resolution infrared chemiluminescence spectroscopy. *J Chem Phys*. 1991;95(9):6932.
446. Mantell DA, Ryali SB, Halpern BL, Haller GL, Fenn JB. The exciting oxidation of CO on Pt. *Chem Phys Lett*. 1981;81(2):185-187.
447. Palmer RL, Smith JNJ. Molecular beam study of CO oxidation on a (111) platinum surface. *J Chem Phys*. 1974;60(4):1453.
448. Poehlmann E, Schmitt M, Hoinkes H, Wilsch H. Velocity distributions of carbondioxide molecules from the oxidation of CO on Pt(111). *Surf Sci*. 1993;287:269-272.
449. Poehlmann E, Schmitt M, Hoinkes H, Wilsch H. Bimodal angular and velocity distributions of CO_2 desorbing after oxidation of CO on Pt(111). *Surf Rev Lett*. 1995;2(6):741-758.
450. Allers KH, Pfnur H, Feulner P, Menzel D. Fast reaction-products from the oxidation of CO on Pt(111) — angular and velocity distributions of the CO_2 product molecules. *J Chem Phys*. 1994;100(5):3985-3998.
451. Segner J, Campbell CT, Doyen G, Ertl G. Catalytic-oxidation of CO on Pt(111) — the influence of surface-defects and composition on the reaction dynamics. *Surf Sci*. 1984;138(2-3):505-523.
452. Jinnouchi R, Kodama K, Morimoto Y. DFT calculations on H, OH and O adsorbate formations on Pt(111) and Pt(332) electrodes. *J Electroanal Chem*. 2014;716:31-44.
453. Nagoya A, Jinnouchi R, Kodama K, Morimoto Y. DFT calculations on H, OH and O adsorbate formations on Pt(322) electrode. *J Electroanal Chem*. 2015;757:116-127.
454. Gambardella P, Šljivančanin Ž, Hammer B, Blanc M, Kuhnke K, Kern K. Oxygen dissociation at Pt steps. *Phys Rev Lett*. 2001;87(5):056103.
455. Badan C, Farber RG, Heyrich Y, Koper MTM, Killelea DR, Juurlink LBF. Step-type selective oxidation of platinum surfaces. *J Phys Chem C*. 2016;120(40):22927-22935.
456. Neugebohren J, Borodin D, Hahn HW, et al. Velocity-resolved kinetics of site-specific carbon monoxide oxidation on platinum surfaces. *Nature*. 2018;558(7709):280.
457. Harding DJ, Neugebohren J, Auerbach DJ, Kitsopoulos TN, Wodtke AM. Using ion imaging to measure velocity distributions in surface scattering experiments. *J Phys Chem A*. 2015;119(50):12255-12262.

458. Harding DJ, Neugebohren J, Hahn H, Auerbach DJ, Kitsopoulos TN, Wodtke AM. Ion and velocity map imaging for surface dynamics and kinetics. *J Chem Phys*. 2017;147(1).
459. Zhou L, Kandratsenka A, Campbell CT, Wodtke A, Guo H. Origin of thermal and hyperthermal CO_2 from CO oxidation on platinum surfaces: the role of post-transition-state dynamics, active sites, and chemisorbed CO_2. *Angew Chem Int Ed*. 2019;58:6916-6920.
460. Reuter K, Scheffler M. Composition, structure, and stability of RuO_2(110) as a function of oxygen pressure. *Phys Rev B*. 2002;65(3):035406.
461. Reuter K, Scheffler M. First-principles atomistic thermodynamics for oxidation catalysis: surface phase diagrams and catalytically interesting regions. *Phys Rev Lett*. 2003;90(4):046103.
462. Wintterlin J, Volkening S, Janssens TVW, Zambelli T, Ertl G. Atomic and macroscopic reaction rates of a surface-catalyzed reaction. *Science*. 1997;278(5345):1931-1934.
463. Gland JL, Kollin EB. Carbon monoxide oxidation on the Pt(111) surface: temperature programmed reaction of coadsorbed atomic oxygen and carbon monoxide. *J Chem Phys*. 1983;78(2):963.
464. Gland J. The hydrogen-oxygen reaction over the Pt(111) surface: transient titration of adsorbed oxygen with hydrogen. *J Catal*. 1982;77(1):263-278.
465. Zambelli T, Barth JV, Wintterlin J, Ertl G. Complex pathways in dissociative adsorption of oxygen on platinum. *Nature*. 1997;390(6659):495-497.
466. Conrad H, Ertl G, Kuppers J. Interactions between oxygen and carbon-monoxide on a Pd(111) surface. *Surf Sci*. 1978;76(2):323-342.
467. Stuve EM, Madix RJ, Brundle CR. CO oxidation on Pd(100): a study of the coadsorption of oxygen and carbon monoxide. *Surf Sci*. 1984;146(1):155-178.
468. Tang H, Van Der Ven A, Trout BL. Phase diagram of oxygen adsorbed on platinum (111) by first-principles investigation. *Phys Rev B*. 2004;70(4):045420.
469. Tang HR, Van der Ven A, Trout BL. Lateral interactions between oxygen atoms adsorbed on platinum (111) by first principles. *Mol Phys*. 2004;102(3):273-279.
470. Stipe BC, Rezaei MA, Ho W. Atomistic studies of O_2 dissociation on Pt(111) induced by photons, electrons, and by heating. *J Chem Phys*. 1997;107(16):6443-6447.
471. Freund HJ, Meijer G, Scheffler M, Schlogl R, Wolf M. CO oxidation as a prototypical reaction for heterogeneous processes. *Angew Chem Int Ed*. 2011;50(43):10064-10094.
472. Borodin D, Golibrzuch K, Schwarzer M, et al. Measuring transient reaction rates from nonstationary catalysts. *ACS Catal*. 2020;10:14056-14066.
473. Olander DR. Heterogeneous chemical kinetics by modulated molecular beam mass spectrometry. *J Colloid Interface Sci*. 1977;58(1):169-183.
474. Engelhart DP, Gratz F, Wagner RJV, et al. A new Stark decelerator based surface scattering instrument for studying energy transfer at the gas–surface interface. *Rev Sci Instrum*. 2015;86(4).
475. Engelhart DP, Wagner RJV, Johnsen PC, Wodtke AM, Schafer T. Adsorbate enhancement of electron emission during the quenching of metastable CO at metal surfaces. *PCCP*. 2015;17(17):11540-11545.
476. Hillenbrand R, Taubner T, Keilmann F. Phonon-enhanced light–matter interaction at the nanometre scale. *Nature*. 2002;418(6894):159-162.
477. Qazilbash MM, Brehm M, Chae BG, et al. Mott transition in VO_2 revealed by infrared spectroscopy and nano-imaging. *Science*. 2007;318(5857):1750-1753.
478. Knoll B, Keilmann F. Near-field probing of vibrational absorption for chemical microscopy. *Nature*. 1999;399(6732):134-137.
479. Michaelides A, Bocquet ML, Sautet P, Alavi A, King DA. Structures and thermodynamic phase transitions for oxygen and silver oxide phases on Ag{1 1 1}. *Chem Phys Lett*. 2003;367(3-4):344-350.
480. Zhang IY, Grüneis A. Coupled cluster theory in materials science. *Front Mater*. 2019;6:123.
481. Sun QN, Chan GKL. Quantum embedding theories. *Acc Chem Res*. 2016;49(12):2705-2712.
482. Libisch F, Huang C, Liao PL, Pavone M, Carter EA. Origin of the energy barrier to chemical reactions of O-2 on Al(111): evidence for charge transfer, not spin selection. *Phys Rev Lett*. 2012;109(19):198303.
483. Fornace ME, Lee J, Miyamoto K, Manby FR, Miller TF. Embedded mean-field theory. *J Chem Theo Comp*. 2015;11(2):568-580.
484. Powell AD, Kroes G-J, Doblhoff-Dier K. Quantum Monte Carlo calculations on dissociative chemisorption of H_2 + Al(110): minimum barrier heights and their comparison to DFT values. *J Chem Phys*. 2020;153(22):224701.
485. Kramers HA. Brownian motion in a field of force and the diffusion model of chemical reactions. *Physica*. 1940;7(4):284-304.
486. Bünermann O, Kandratsenka A, Wodtke AM. Inelastic scattering of H atoms from surfaces. *J Phys Chem A*. 2021;125(15):3059-3076.
487. Worth GA, Meyer HD, Koppel H, Cederbaum LS, Burghardt I. Using the MCTDH wavepacket propagation method to describe multimode non-adiabatic dynamics. *Int Rev Phys Chem*. 2008;27(3):569-606.
488. Meyer HD. Studying molecular quantum dynamics with the multiconfiguration time-dependent Hartree method. *Wiley Interdisc Rev-Comput Mol Sci*. 2012;2(2):351-374.
489. Brown A, Pradhan E. Fitting potential energy surfaces to sum-of-products form with neural networks using exponential neurons. *J Theor Comput Chem*. 2017;16(5):24.
490. Lau JA, Choudhury A, Li C, Schwarzer D, Verma VB, Wodtke AM. Observation of an isomerizing double-well quantum system in the condensed phase. *Science*. 2020;367(6474):175.
491. Chen J, Li J, Bowman JM, Guo H. Energy transfer between vibrationally excited carbon monoxide based on a highly accurate six-dimensional potential energy surface. *J Chem Phys*. 2020;153(5):054310.
492. Chen J, Hariharan S, Meyer J, Guo H. Potential energy landscape of CO adsorbates on NaCl(100) and implications in isomerization of vibrationally excited CO. *J Phys Chem C*. 2020;124(35):19146-19156.
493. Sinha S, Saalfrank P. "Inverted" CO molecules on NaCl(100): a quantum mechanical study. *Phys Chem Chem Phys*. 2021;23:7860.

How to cite this article: Auerbach DJ, Tully JC, Wodtke AM. Chemical dynamics from the gas-phase to surfaces. *Nat Sci*. 2021;1:e10005. https://doi.org/10.1002/ntls.10005